Electronic Supplementary Material (ESI) for Dalton Transactions.

Supporting Information

A Dianionic C_3-Symmetric Scorpionate: Synthesis and Coordination Chemistry

Serhii Tretiakov,[a] *Johannes A. M. Damen,*[a] *Martin Lutz,*[b] *Marc-Etienne Moret**[,a]

*E-Mail: M.Moret@uu.nl

[a] Utrecht University, Organic Chemistry & Catalysis, Debye Institute for Nanomaterials Science, Faculty of Science, 3584 CG Utrecht, The Netherlands

[b] Utrecht University, Crystal and Structural Chemistry, Bijvoet Center for Biomolecular Research, Faculty of Science, 3584 CH Utrecht, The Netherlands

Contents[*]

S1 General remarks 3

S2 Synthesis and characterization 5

S2.1 Syntheses towards TSMPK$_2$ (1) 5

***N*-Boc-3-methylindole (3)** 5

tris-(*N*-Boc-3-methylindol-2-yl)phosphine (4) 5

tris-(*N*-Boc-3-methylindol-2-yl)methylphosphonium iodide (5) 6

tris-(1*H*-3-methylindol-2-yl)methylphosphonium chloride (7) 7

TSMPK$_2$ (1) 7

S2.2 Metal complexes 8

{[(TSMP)Cu]K}$_4$ (8) 8

Generation and characterization of [(TSMP)CuP(OEt)$_3$]K (9a) *in situ* 9

[(TSMP)CuP(OEt)$_3$][K(18-crown-6)·CH$_3$CN] (9b) 10

(TSMP)Fe(Py)$_3$ (10) 11

(TSMP)Ni(Py)$_3$ (11) 12

Generation and characterization of crude [(TSMP)$_2$Fe]K$_2$ (12a) 12

[(TSMP)$_2$Fe][K(benzo-15-crown-5)$_2$]$_2$ (12b) 13

S3 X-ray crystal structure determinations 15

TSMPK$_2$ (1) 15

{[(TSMP)Cu]K}$_4$ (8) 17

[(TSMP)CuP(OEt)$_3$][K(18-crown-6)·CH$_3$CN] (9b) 18

(TSMP)Fe(Py)$_3$ (10) 23

(TSMP)Ni(Py)$_3$ (11) 24

[(TSMP)$_2$Fe][K(benzo-15-crown-5)$_2$]$_2$ (12b) 26

S4 Peripheral discussions 28

S4.1 NMR of tris-(*N*-Boc-3-methylindol-2-yl)methylphosphonium iodide (5) 28

S4.2 gCOSY and NOESY NMR of {[(TSMP)Cu]K}$_4$ (8) 30

S4.3 ^{1}H NMR of {[(TSMP)Cu]K}$_4$ (8) before and after addition of P(OEt)$_3$ 31

S4.4 NOE spectra of [(TSMP)CuP(OEt)$_3$]K (9a) 31

S4.5 Variable-temperature NMR studies of [(TSMP)$_2$Fe][K(benzo-15-crown-5)$_2$]$_2$ (12b) 32

S5 Literature references 34

S6 Spectra 36

---

[*] For the reader's convenience, this document is enhanced with hyperlinks. Clicking on any mention of a section/title/figure in the text will bring the reader to the object that was referred to.

S1 General remarks

All reactions involving air-sensitive compounds were conducted under a nitrogen atmosphere by using standard glovebox or Schlenk techniques.

Acetonitrile, diethyl ether and *n*-hexane were dried with an MBRAUN MB SPS-79 system. Acetonitrile was additionally dried by passing through a column of activated alumina after being kept over ca. 5 vol.% of 3Å molecular sieves over 48h. THF and dioxane were distilled from benzophenone/Na. Pyridine and DCM were distilled from CaH_2. Other solvents were used as supplied. Dried solvents were degassed by sparging with dry nitrogen for 30 min and stored in a glovebox under nitrogen atmosphere and over molecular sieves, except for acetonitrile which was stored without the sieves. THF-d_8 was purchased from ABCR, other deuterated solvents were acquired from Cambridge Isotope Laboratories, Inc. Chloroform-*d* and methylene chloride-d_2 were used as supplied, all other deuterated solvents were dried as indicated above for their proteo-analogues. Dried deuterated solvents were degassed by four freeze-pump-thaw cycles and stored in a glovebox over molecular sieves, except for acetonitrile-d_3 which was stored without the sieves. Phosphorus trichloride, trifluoroacetic acid and methyl iodide were purchased from Acros. All other chemicals were purchased from Sigma-Aldrich. Potassium hydride was supplied as a 30 wt.% suspension in mineral oil and was washed with dry and degassed *n*-hexane prior to use. $FeCl_2$ and CuCl were purchased in an anhydrous form. All commercially obtained chemicals were used as received, except for 18-crown-6, which was dried according to the literature procedure.[1]

All NMR measurements were performed at 298K on a Varian VNMRS400 or Varian MRF400 spectrometer, chemicals shifts are reported relative to TMS with the residual solvent signal as internal standard.[2] In case of paramagnetic Fe- and Ni-complexes **10** and **11**, TMS was used as an internal standard. All NMR experiments involving air-sensitive compounds were conducted in J. Young NMR tubes under an N_2 atmosphere. Peak multiplicity was quoted as s (singlet), d (doublet), t (triplet) and so on. In cases of unresolved couplings that strongly affect the line shape of individual components of an otherwise well-defined multiplet, the apparent multiplicity was quoted as 's' ('singlet'), 'd' ('doublet'), 't' ('triplet') and so on. ASAPHMQC experiments were conducted using the corresponding pulse sequence[3] as implemented in the VnmrJ 4.2 software.[4]

Effective magnetic moments in were obtained by the Evans method[5,6] using J. Young NMR tubes with a coaxial capillary insert as a reference. The latter was filled with a deuterated solvent with ~1% of TMS. The outer space contained the solution of the paramagnetic complex (5-10 mg/ml) in a deuterated solvent with the same concentration of TMS. Molar magnetic susceptibility was calculated from the difference between the chemical shifts of TMS signals in the capillary and the outer solution (Δδ in Hz) using the following equation:

$$\chi_M = \frac{\Delta\delta M}{\nu_0 S_f c} - \chi_M^{dia},$$

where M – molecular weight of the studied compound (g/mol); ν_0 – frequency of the spectrometer (Hz); S_f – shape factor of the magnet (4π/3); c – concentration of the paramagnetic complex (mg/ml); χ_M^{dia} – molar diamagnetic contribution to the paramagnetic susceptibility calculated using Pascal's constants.[7]

The effective magnetic moment was calculated as follows:

$$\mu_{eff} = \sqrt{8\chi_M T},$$

where T is temperature.

IR spectra were recorded on a Perkin-Elmer Spectrum Two FT-IR spectrometer. The bands were classified by an absorption intensity as: very weak (VW; 0-10% of the most intense absorption in the spectrum), weak (W; 10-30%), medium (M; 30-60%), strong (S; 60-90%), very strong (VS; 90-100%).

UV-Vis spectra were measured on a PerkinElmer Lambda 35 spectrometer. ESI-MS measurements were performed on a Waters LCT Premier XE KE317 spectrometer. Elemental analysis was conducted by Medac Ltd.

S2 Synthesis and characterization

S2.1 Syntheses towards TSMPK$_2$ (1)

The syntheses of compounds **3**, **5** and **7** were conducted in air. While the synthesis of **4** was done with the exclusion of air and moisture, the work-up was performed at ambient conditions since the product is not air-sensitive. All other procedures, due to both highly reactive starting materials and products, required inert atmosphere and rigorously dried and degassed solvents.

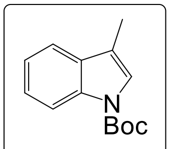

3

***N*-Boc-3-methylindole (3)**. The compound was synthesized using an adapted version of a procedure by Grehn and Ragnarsson.[8]

To a stirred solution of 3-methylindole **2** (18.87 g, 143.9 mmol, 1.000 equiv.) in CH$_3$CN (170 mL) were added DMAP (1.76 g, 14.4 mmol, 0.100 equiv.) and Boc$_2$O (37.68 g, 172.6 mmol, 1.200 equiv.) at room temperature. Evolution of gas commenced, and, after a few minutes, a clear solution formed. The reaction mixture was left to stir for 16h. After this, all 3-methylindole was consumed (as indicated by TLC), and the reaction was kept at 50 °C for 2h in order to decompose excess Boc$_2$O. Afterwards, the solvent was removed *in vacuo* and replaced with an equal volume of THF. The solution was filtered through a layer of silica, and the solvent was removed *in vacuo* to yield the product as a light-yellow free-flowing oil (98.5%, 32.86 g).

NMR spectra correspond to those published in the literature.[8] **^{1}H NMR** (400 MHz, chloroform-*d*) δ 8.13 (d, $J_{H,H}$ = 8.0 Hz, 1H, Ar-H), 7.49 (ddd, $J_{H,H}$ = 7.7, 1.4, 0.7 Hz, 1H, Ar-H), 7.36 (s, 1H, Ar-H), 7.31 (ddd, $J_{H,H}$ = 8.5, 7.2, 1.4 Hz, 1H, Ar-H), 7.24 (td, $J_{H,H}$ = 7.6, 1.1 Hz, 1H, Ar-H), 2.26 (s, 3H, Ar-CH$_3$), 1.66 (s, 9H, ^{t}Bu). **^{13}C NMR** (101 MHz, Chloroform-*d*) δ 149.8 (C=O^{Boc}), 135.5, 131.5, 124.2, 122.8, 122.3, 118.9, 116.3, 115.1, 83.2 (qC$^{t\text{-Bu}}$), 28.3 (CH$_3^{t\text{-Bu}}$), 9.6 (Ar-CH$_3$). **ATR-FTIR** (neat) ṽ (cm^{-1}): 422 (W). 531 (W), 557(W), 594 (W), 741 (M), 768 (W), 857 (W), 1018 (M), 1084 (S), 1151 (S), 1156 (S), 1224 (M), 1250 (S), 1307 (M), 1347 (S), 1350 (S), 1368 (S), 1388 (S), 1451 (S), 1726 (VS), 2921 (W), 2933 (W), 2978 (W).

<u>Appended spectra:</u> NMR in chloroform-*d*: ^{1}H (*Figure S18*), ^{13}C{^{1}H} (*Figure S19*); ATR-FTIR (neat, *Figure S20*).

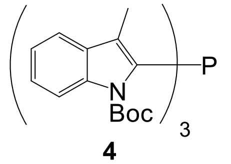

4

tris-(*N*-Boc-3-methylindol-2-yl)phosphine (4). A suspension of LDA (18.03 g, 168.3 mmol, 1.100 equiv.) in THF (200 ml) was added to a stirred at -78°C solution of *N*-Boc-3-methylindole **3** (35.39 g, 153.0 mmol, 1.000 equiv.) in THF (300 ml) over 1h. The reaction was allowed to stir over 4h at -78°C. Phosphorus trichloride (4.46 ml, 51.0 mmol, 0.330 equiv.) was added to the resulting salmon-pink reaction mixture over 1h using a syringe pump, resulting in a dark-orange coloration. The reaction mixture was allowed to warm up to room temperature over 16h. Saturated aqueous NH$_4$Cl (200 ml) was then added in air. The organic layer was separated, dried over Na$_2$SO$_4$ and passed through a layer of silica. The filtrate was freed from solvent *in vacuo*, and the resulting solid was recrystallized from THF/methanol 1:1 mixture at -35 °C overnight. Filtration and drying *in vacuo* yielded colorless cubic crystals (34.2%, 12.58 g).

^{1}H NMR (400 MHz, dichloromethane-d_2) δ 8.14 (d, $J_{H,H}$ = 8.4 Hz, 1H, Ar-H), 7.45 (d, $J_{H,H}$ = 7.7 Hz, 1H, Ar-H), 7.31 (ddd, $J_{H,H}$ = 8.4, 7.1, 1.3 Hz, 1H, Ar-H), 7.22 (ddd, $J_{H,H}$ = 8.0, 7.2, 1.0 Hz, 1H, Ar-H), 1.87 (d, $J_{H,P}$ = 0.9 Hz, 3H, Ar-CH$_3$), 1.38 (s, 9H, ^{t}Bu). **^{13}C NMR** (101 MHz, dichloromethane-d_2) δ 151.0 (d, $J_{C,P}$ = 2.7 Hz, C=O^{Boc}), 137.62, 137.60, 132.2, 131.4, 131.2, 126.11, 126.09, 125.2, 122.8, 118.9, 115.8, 84.8 (qC$^{t\text{-Bu}}$), 28.2 (CH$_3^{t\text{-Bu}}$), 9.8 (Ar-CH$_3$). **^{31}P NMR** (162 MHz, dichloromethane-d_2) δ -48.6. **ATR-FTIR (neat)** ṽ (cm^{-1}): 417 (VW), 461 (VW), 543 (VW), 603 (W), 613 (W), 652 (W), 656 (W), 744 (M), 756 (M), 817 (W), 869 (W), 996 (W), 1099 (S), 1127 (M), 1151 (S), 1158 (M), 1230 (M), 1247 (M), 1293 (M), 1319 (S), 1330 (S), 1354 (S), 1448 (M), 1475 (W), 1721 (VS), 2931 (W), 2971 (W), 2982 (W). **ESI-TOF-MS** in CH$_3$CN: found 722.3336 [*M*+H]$^+$, 744.3158 [*M*+Na]$^+$, 1465.6705 [2*M*+Na]$^+$ (calcd. 722.3359 [*M*+H]$^+$, 744.3179 [*M*+Na]$^+$, 1465.6459 [2*M*+Na]$^+$).

Appended spectra: NMR in dichloromethane-d_2: ^{1}H (*Figure S21*), ^{13}C{^{1}H} (*Figure S22*), ^{31}P (*Figure S23*); ATR-FTIR (neat, *Figure S24*).

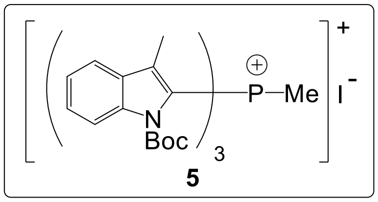

5

tris-(*N*-Boc-3-methylindol-2-yl)methylphosphonium iodide (5). Phosphine **4** (2.00 g, 2.77 mmol, 1.00 equiv.) was dissolved in THF (10.0 ml), and the reaction flask was placed into an ice bath. Methyl iodide (0.35 ml, 5.5 mmol, 2.0 equiv.) was added dropwise over a minute with vigorous stirring. The reaction was allowed to warm up to room temperature, which was accompanied by formation of a white suspension. After 16h of stirring, the suspension was filtered and the solid was washed with three small portions of cold Et$_2$O. Upon washing, some additional material that precipitated from the filtrate was collected by filtration and washed with cold Et$_2$O. The solids were combined and dried *in vacuo* to yield a fine white powder (89.6%, 2.00 g).

In dichloromethane-d_2 solution, the compound exists as a ~1:0.15 mixture of rotamers. ^{1}H NMR signals from the major rotamer are labeled with an asterisk. **^{1}H NMR** (400 MHz, dichloromethane-d_2) δ 8.18 (d, $J_{H,H}$ = 8.7 Hz, 0.05H, Ar-H), 8.11* (d, $J_{H,H}$ = 8.6 Hz, 1H, Ar-H), 8.05 (d, $J_{H,H}$ = 8.9 Hz, 0.05H, Ar-H), 7.86 (d, $J_{H,H}$ = 8.8 Hz, 0.05H, Ar-H), 7.68* (d, $J_{H,H}$ = 8.0 Hz, 1H, Ar-H), 7.63* (t, $J_{H,H}$ = 7.9 Hz, 1H, Ar-H), 7.44* (t, $J_{H,H}$ = 7.6 Hz, 1H, Ar-H), 2.87 (d, $J_{H,P}$ = 13.9 Hz, 0.15H, P-CH$_3$), 2.75* (d, $J_{H,P}$ = 15.1 Hz, 1H, P$^+$-CH$_3$), 2.37 (s, 0.15H, Ar-CH$_3$), 2.15 (s, 0.15H, Ar-CH$_3$), 2.04 (s, 0.15H, Ar-CH$_3$), 1.97* (d, $J_{H,P}$ = 2.1 Hz, 3H, Ar-CH$_3$), 1.66 (s, 0.45H, ^{t}Bu), 1.54* (s, 9H, ^{t}Bu), 1.48 (s, 0.45H, ^{t}Bu), 1.15 (s, 0.45H, ^{t}Bu). **^{13}C NMR** (101 MHz, dichloromethane-d_2) δ 151.1 (C=O^{Boc}), 137.2 (d, $J_{C,P}$ = 5.6 Hz, indole-C9 or C8, or C3), 136.5 (d, $J_{C,P}$ = 12.2 Hz, indole-C8 or C9, or C3), 131.2 (d, $J_{C,P}$ = 14.5 Hz, indole-C3 or C8, or C9), 129.7 (C^{Ar}-H), 124.7 (C^{Ar}-H), 121.0 (C^{Ar}-H), 116.6 (C^{Ar}-H), 116.5 (d, $J_{C,P}$ = 128.8 Hz, indole-C2), 87.9 (qC$^{t\text{-Bu}}$), 28.0 (CH$_3^{t\text{-Bu}}$), 24.8 (d, $J_{C,P}$ = 80.8 Hz, P$^+$-CH$_3$), 10.2 (Ar-CH$_3$). **^{31}P NMR** (162 MHz, dichloromethane-d_2) δ -2.2 (q, $J_{P,H}$ = 15.2 Hz, carbon satellites: $J_{P,C}$ = 128.9, 80.7 Hz, 1H), -3.9 (br.s., 0.15H). **ESI-TOF-MS** spectra in CH$_3$CN recorded in a positive mode contain signals from the original phosphonium cation and products of partial Boc-deprotection: 736.3525 [*M*]$^+$, 636.3006 [*M*-Boc+H]$^+$, 536.2492 [*M*-2Boc+2H]$^+$ (calcd. 736.3516 [*M*]$^+$, 636.2991[*M*-Boc+H]$^+$, 536.2467 [*M*-2Boc+2H]$^+$).

Appended spectra: NMR in dichloromethane-d_2: ^{1}H (*Figure S25*), ^{1}H NOESY (*Figure S26*), ^{13}C{^{1}H} (*Figure S27*), ^{31}P{^{1}H} (*Figure S28*), ^{31}P (*Figure S29*), ^{1}H-^{31}P ASAPHMQC (*Figure S30*).

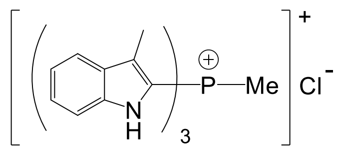

7

tris-(1*H*-3-methylindol-2-yl)methylphosphonium chloride (7). Phosphonium iodide **5** (10.00 g, 11.57 mmol) was dissolved in DCM (30.0 ml) in a round-bottom flask equipped with a stirring bar. Trifluoroacetic acid (30 ml) was added dropwise over a minute with vigorous stirring. The reaction mixture was left to stir over 16 h. After this, both DCM and trifluoroacetic acid were removed *in vacuo* to yield a sticky brown solid. In order to azeotropically remove trifluoroacetic acid trapped in the solid, it was three times redissolved in small portions of DCM (10.0 ml) followed by vacuum drying. This resulted into formation of a dark-yellow amorphous spongy mass that was turned into fine yellow powder by trituration with Et_2O. The powder was redissolved in 40.0 ml of CH_3CN/MeOH 1:1 and passed through a column of the chloride form of Amberlite® IRA-400 prewashed with two volumes of the same mixture of solvents. The elute was partially freed from solvent until crystallization commenced. The mixture was left to stand at room temperature overnight. In the morning, a white crystalline precipitate was collected, dried *in vacuo* to yield the target phosphonium chloride as white crystalline powder (80.0%, 4.37 g).

^{1}H NMR (400 MHz, DMSO-d_6) δ 12.34 (s, 1H, NH), 7.74 (d, $J_{\mathrm{H,H}}$ = 8.2 Hz, 1H, Ar-H), 7.59 (d, $J_{\mathrm{H,H}}$ = 8.4 Hz, 1H, Ar-H), 7.41 (t, $J_{\mathrm{H,H}}$ = 7.5 Hz, 1H, Ar-H), 7.20 (ddd, $J_{\mathrm{H,H}}$ = 8.0, 6.9, 0.9 Hz, 1H, Ar-H), 3.27 (d, $J_{\mathrm{H,P}}$ = 14.7 Hz, 1H, P^{+}-CH_3), 1.92 (d, $J_{\mathrm{H,P}}$ = 1.8 Hz, 3H, Ar-CH_3). **^{13}C NMR** (101 MHz, DMSO-d_6) δ 139.7 (d, $J_{\mathrm{C,P}}$ = 11.4 Hz, indole-C8), 128.0 (d, $J_{\mathrm{C,P}}$ = 13.0 Hz, indole C9 or C3), 126.9 (d, $J_{\mathrm{C,P}}$ = 15.8 Hz, indole C3 or C9), 126.2 (C^{Ar}-H), 120.4 (C^{Ar}-H), 120.3 (C^{Ar}-H), 112.6 (C^{Ar}-H), 108.6 (d, $J_{\mathrm{C,P}}$ = 120.0 Hz, indole-C2), 12.5 (d, J = 59.6 Hz, P^{+}-CH_3), 8.3 (Ar-CH_3). **^{31}P NMR** (162 MHz, DMSO-d_6) δ -14.0 (q, $J_{\mathrm{P,H}}$ = 14.7 Hz, carbon satellites: $J_{\mathrm{P,C}}$ = 120.2, 58.7, 11.9 Hz). **ATR-FTIR (neat)** ṽ (cm^{-1}): 427 (M), 460 (M), 516 (VW), 560 (W), 613 (W), 639 (W), 745 (VS), 805 (M), 908 (S), 1041 (M), 1099 (M), 1130 (M), 1151 (M), 1200 (M), 1238 (M), 1294 (W), 1332 (S), 1431 (W), 1515 (M), 1578 (W), 1617 (W), 2851 (M), 2914 (M), 2975 (S), 3024 (M), 3061 (M), 3437 (W). **ESI-TOF-MS** in CH_3CN: found 436.1916 $[M]^{+}$ (calcd. 436.1943 $[M^{+}]$).

<u>Appended spectra:</u> NMR in DMSO-d_6: ^{1}H (*Figure S31*), ^{13}C{^{1}H} (*Figure S32*), ^{31}P{^{1}H} (*Figure S33),* ^{31}P (*Figure S34*); ATR-FTIR (neat, *Figure S35*).

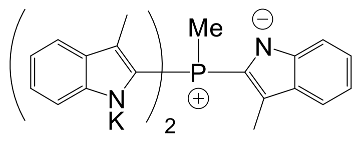

1

TSMPK$_2$ (1). Depending on the base, compound **1** can be prepared according to either of the two following procedures.

Procedure A (using KHMDS). A solution of KHMDS (0.041 g, 0.20 mmol, 3.0 equiv.) in THF (2.0 ml) was added to a stirred solution of chloride **7** (0.030 g, 0.068 mmol, 1.0 equiv.) in THF (2.0 ml). After stirring for 20 min, the solvent was removed *in vacuo*. After an hour of drying, the amorphous white residue was washed with hexane (3 x 4.0 ml) and dried *in vacuo* for another hour, after which both the solid and hexane washings were analyzed by NMR. ^{31}P spectra of the hexane washings showed no traces of phosphorus, whereas ^{1}H and ^{31}P spectra of the solid showed quantitative conversion of the starting material into **1**.

Procedure B (using KH). To a stirred solution of chloride **7** (0.050 g, 0.11 mmol, 1.0 equiv.) in THF (15.0 ml) was added a suspension of potassium hydride (0.014 g, 0.35 mmol, 3.3 equiv.) in 5.0 ml of THF (5.0 ml). The reaction was stirred for 2h, filtered, the solvent was removed *in vacuo* to yield an air-sensitive white amorphous solid. The residual THF content of 21.5 wt.% was determined using quantitative ^{1}H NMR measurements. With the product mass of 0.072 g this gives a quantitative yield. Crystals suitable for X-ray diffraction analysis were grown by vapor diffusion of diethyl ether into a solution of **1** in acetonitrile at room temperature.

Regardless of the procedure used, the final products show identical NMR spectra. **^{1}H NMR** (400 MHz, acetonitrile-*d*$_3$) δ 7.44 (d, $J_{H,H}$ = 8.0 Hz, 1H, Ar-H), 7.31 (d, $J_{H,H}$ = 8.3 Hz, 1H, Ar-H), 6.86 ('t', $J_{H,H}$ = 7.3 Hz, 1H, Ar-H), 6.76 ('t', $J_{H,H}$ = 7.2 Hz, 1H, Ar-H), 2.62 (d, $J_{H,P}$ = 13.8 Hz, 1H, P^{+}-CH_3), 2.10 (d, $J_{H,P}$ = 1.5 Hz, 3H, Ar-CH_3). **^{13}C NMR** (101 MHz, acetonitrile-*d*$_3$) δ 149.7 (d, $J_{C,P}$ = 24.3 Hz, indole-C8), 132.3 (d, $J_{C,P}$ = 10.9 Hz, indole-C9 or C3), 128.7 (d, $J_{C,P}$ = 117.8 Hz, indole-C2), 119.4 (C^{Ar}-H), 119.06 (C^{Ar}-H), 118.7 (C^{Ar}-H), 117.3 (d, $J_{C,P}$ = 26.4 Hz, indole-C3 or C9), 116.1 (C^{Ar}-H), 14.6 (d, $J_{C,P}$ = 63.5 Hz, P^{+}-CH_3), 10.4 (Ar-CH_3). **^{31}P NMR** (162 MHz, acetonitrile-*d*$_3$) δ -7.8 (q, $J_{P,H}$ = 13.7 Hz, carbon satellites: $J_{P,C}$ = 117.8, 63.6, 25.7, 10.9 Hz). No satisfactory elemental analysis could be obtained due to the high reactivity of **1** as well as solvation of the potassium cations, which results into the compound retaining an unknown amount of solvent.

<u>Appended spectra:</u> NMR in acetonitrile-*d*$_3$: ^{1}H (*Figure S36*), ^{13}C{^{1}H} (*Figure S37*), ^{31}P{^{1}H} (*Figure S38*), ^{31}P (*Figure S39*).

S2.2 Metal complexes

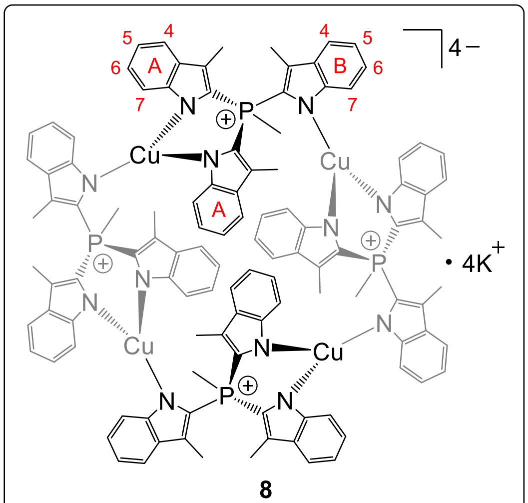

8

{[(TSMP)Cu]K}$_4$ (8). A solution of anhydrous CuCl (0.076 g, 0.77 mmol, 1.0 equiv.) in pyridine (6.0 ml) was added dropwise to dipotassium salt **1** (contains 21.5 wt% of THF, 0.500 g, 0.768 mmol, 1.00 equiv.) in pyridine (12.0 ml) over a minute. The clear red-orange solution was stirred for 3h, after which the solvent was evaporated *in vacuo*. The yellow solid was taken up in dry THF (20.0 ml), the resulting suspension was filtered, and the solid was washed with more THF until all color was extracted into the solution. The volume of combined filtrate and washings was reduced by evaporation in vacuo until yellow crystals started to form. Immediately after, the mixture was cooled down to -35 °C and kept so for 48h until the crystal formation stopped. The crystals were collected by vacuum filtration, washed with ~2 ml of cold THF and dried in vacuo to yield an air-sensitive fine yellow powder (95.4%, 0.393 g). Crystals suitable for X-ray diffraction analysis were grown by vapor diffusion of hexane into a pyridine solution of **8** at room temperature.

The ^{1}H NMR spectrum in acetonitrile-*d$_3$* is dominated by one species, chemical shifts and integral intensities of which are consistent with the solid-state structure of **8** derived from X-ray diffraction.

Additionally, gCOSY spectra clearly show the presence of two aromatic spin systems in a ratio of 2:1. Nevertheless, there are some minor signals that, according to NOESY spectra, are connected with the major species *via* chemical exchange. NMR data below are shown only for the major species. **^{1}H NMR** (400 MHz, acetonitrile-*d*$_3$) δ 7.83 (d, $J_{H,H}$ = 8.2 Hz, 1H, H^7_B), 7.64 (d, $J_{H,H}$ = 7.8 Hz, 1H, H^4_B), 7.33 – 7.24 (m, 2H, H^7_A), 7.20 – 7.13 (m, 2H, H^3_A), 6.99 ('t', $J_{H,H}$ = 7.3 Hz, 1H, H^5_B), 6.93 (ddd, $J_{H,H}$ = 7.8, 6.6, 1.1 Hz, 1H, H^6_B), 6.61 – 6.49 (m, 4H, H^6_A+H^5_A), 2.73 (d, $J_{H,P}$ = 13.9 Hz, 3H, P^+-CH_3), 2.18 (d, $J_{H,P}$ = 1.5 Hz, 3H, $CH_3^{Ar_B}$), 1.71 (d, $J_{H,P}$ = 1.5 Hz, 6H, $CH_3^{Ar_B}$). **^{13}C NMR** (101 MHz, acetonitrile-*d*$_3$) δ 150.3 (d, $J_{C,P}$ = 19.0 Hz, indole-C8^A), 148.8 (d, $J_{C,P}$ = 19.9 Hz, indole-C8^B), 131.9 (d, $J_{C,P}$ = 11.4 Hz, indole-C9^B or C3^B), 130.7 (d, $J_{C,P}$ = 12.8 Hz, indole-C9^A or C3^A), 125.4 (d, $J_{C,P}$ = 117.9 Hz, indole-C2^A), 122.7 (d, $J_{C,P}$ = 117.2 Hz, indole-C2^B), 120.3, 120.2, 120.2, 120.1, 119.6, 119.4, 119.1, 119.0, 118.8, 118.6, 118.6, 117.0, 116.2, 17.3 (d, $J_{C,P}$ = 61.9 Hz), 10.9 (d, $J_{C,P}$ = 2.0 Hz), 10.1. **^{31}P NMR** (162 MHz, acetonitrile-*d*$_3$) δ -16.9 (q, $J_{P,H}$ = 13.6 Hz, carbon satellites: $J_{P,C}$ = 117.5, 23.3, 19.0, 12.1 Hz). **UV-Vis** (acetonitrile): λ_{max} (ε)=307 ($8.4\cdot10^4$), 238 nm ($2.0\cdot10^5$ $cm^{-1}M^{-1}$). No satisfactory elemental analysis could be obtained due to high reactivity of **8** as well as solvation of the potassium cations, due to which the compound retains an unknown amount of solvent.

Appended spectra: NMR in acetonitrile-*d*$_3$: ^{1}H (*Figure S40*), gCOSY (*Figure S41*), NOESY (*Figure S42*, *Figure S43*), ^{13}C{^{1}H} (*Figure S44*), ^{1}H-^{13}C ASAPHMQC (*Figure S45*), ^{31}P{^{1}H} (*Figure S46*), ^{31}P (*Figure S47*); UV-Vis in acetonitrile (*Figure S48*).

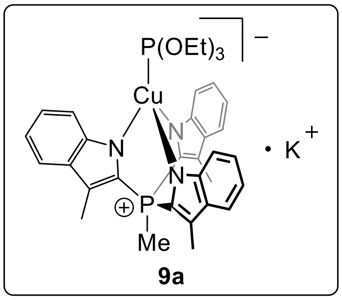

9a

Generation and characterization of [(TSMP)CuP(OEt)$_3$]K (9a) *in situ*. Complex **8** (0.016 g, 0.030 mmol, 1.0 equiv.) was suspended in 0.7 ml of acetonitrile-*d*$_3$ in a J. Young NMR tube. This was followed by an addition of P(OEt)$_3$ (5 µl, 0.03 mmol, 4 equiv.). The NMR tube was sealed under N_2 atmosphere, and the mixture was stirred until a clear white solution formed. The complex could not be purified by means of crystallization and, hence, was analysed in a crude form using NMR spectroscopy. However, isolation of a crystalline 18-crown-6 adduct **9b** was successful (see the synthesis below), which allowed for an X-ray diffraction study. Except for 18-crown-6 signals in **9b**, ^{1}H and ^{31}P NMR spectra of both **9a** and **9b** in acetonitrile-*d*$_3$ are virtually identical.

^{1}H NMR (400 MHz, acetonitrile-*d*$_3$) δ 7.65 (d, $J_{H,H}$ = 8.4 Hz, 1H, Ar-H^7), 7.43 ('d', $J_{H,H}$ = 8.0 Hz, 1H, Ar-H^4), 6.93 (t, $J_{H,H}$ = 7.5 Hz, 1H, Ar-H^6), 6.77 ('t', $J_{H,H}$ = 7.3 Hz, 1H, Ar-H^5), 4.25 (p, $J_{H,H}$ = $J_{H,P}$ = 7.2 Hz, 2H, $PO\underline{CH_2}CH_3$), 3.01 (d, $J_{H,P}$ = 14.6 Hz, 1H, P^+-CH_3), 2.48 (s, 3H, Ar-CH_3), 1.34 (t, $J_{H,H}$ = 7.0 Hz, 3H, $POCH_2\underline{CH_3}$). **^{13}C NMR** (101 MHz, acetonitrile-*d*$_3$) δ 149.3 (d, $J_{C,P}$ = 18.6 Hz, indole-C8), 130.8 (d, $J_{C,P}$ = 13.3 Hz, indole-C9 or C3), 127.0 (d, $J_{C,P}$ = 118.3 Hz, indole-C2), 120.1 (indole-C6), 119.2 (indole-C4), 118.0 (indole-C7), 116.5 (indole-C5), 115.6 (d, $J_{C,P}$ = 24.6 Hz, indole-C3 or C9), 60.6 (d, $J_{C,P}$ = 6.9 Hz, $PO\underline{CH_2}CH_3$), 17.0 (d, $J_{C,P}$ = 7.1 Hz, $POCH_2\underline{CH_3}$), 10.7 (Ar-CH_3), 8.9 (d, $J_{C,P}$ = 57.1 Hz, P^+-CH_3). **^{31}P NMR** (162 MHz, acetonitrile-*d*$_3$) δ 130.7 (br. s., 1P), -14.3 (q, $J_{P,H}$ = 14.4 Hz, 1P, carbon satellites: $J_{P,C}$ = 117.7, 56.9, 24.2, 18.4, 13.2 Hz). No satisfactory elemental analysis could be obtained due to a number of impurities in crude **9a** combined with its high reactivity as well as solvation of potassium cations, due to which the compound retains an unknown amount of solvent.

Appended spectra: NMR in acetonitrile-*d*$_3$: ^{1}H (*Figure S49*), ^{1}H{^{31}P} (*Figure S50*) ^{1}H DQF-COSY (*Figure S51*), ^{1}H NOE (*Figure S52*, *Figure S53*), ^{13}C{^{1}H} DEPTQ-135 (*Figure S54*), ^{1}H-^{13}C ASAPHMQC (*Figure S55*), ^{31}P{^{1}H} (*Figure S56*), ^{31}P (*Figure S57*).

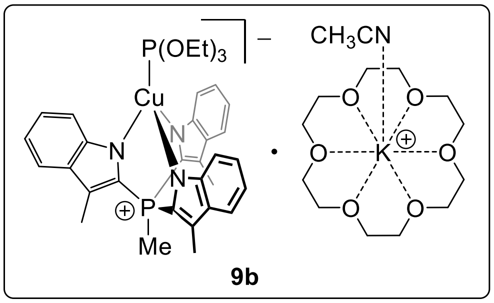

9b

[(TSMP)CuP(OEt)$_3$][K(18-crown-6)·CH$_3$CN] (9b). Depending on the starting material, compound **9b** can be prepared following either of the two procedures below.

Procedure A (preparation from 8). Complex **8** (0.100 g, 0.187 mmol, 1.00 equiv.) was suspended in 8.0 ml of acetonitrile. This was followed by dropwise addition of a mixture of P(OEt)$_3$ (32 µl, 0.19 mmol, 4.0 equiv.) and 18-crown-6 (0.049 g, 0.19 mmol, 1.0 equiv.) in acetonitrile (12.0 ml) over 30 sec. During the addition, the yellow suspension became a clear colorless solution. The volume of the latter was reduced *in vacuo* to ~2 ml, which resulted into ample crystal formation. After crystallization stopped at room temperature, the mixture was transferred into a freezer at -35 °C for 24h. After that time, the crystals were collected by vacuum filtration, washed with ~1.5 ml of cold acetonitrile in small portions and dried *in vacuo*. The above manipulations yielded air-sensitive white colorless needles in 65.3% (0.123 g) yield.

Procedure B (preparation from CuCl). Dipotassium salt **1** (contains 21.5 wt% of THF, 0.500 g, 0.768 mmol, 1.00 equiv.) in acetonitrile (12.0 ml) was added to a solution of anhydrous CuCl (0.076 g, 0.77 mmol, 1.0 equiv.) and P(OEt)$_3$ (132 µl, 0.768 mmol, 1.00 equiv.) in acetonitrile (6.0 ml). The resulting white suspension was stirred over an hour followed by addition of 18-crown-6 (0.203 g, 0.768 mmol, 1.00 equiv.) in acetonitrile (5.0 ml). Immediately after this, the suspension was filtered and the solid was washed with acetonitrile (2 x 25.0 ml). The volume of combined filtrate and washings was reduced *in vacuo* to ~5 ml, which resulted into ample crystal formation. After crystallization stopped at room temperature, the mixture was transferred into a freezer at -35 °C for 24h. After that time, the crystals were collected by vacuum filtration, washed with ~3 ml of cold acetonitrile in small portions and dried *in vacuo*. The above manipulations yielded air-sensitive white colorless needles in 69.9% (0.541 g) yield. Purity >95% according to NMR spectroscopy. Crystals suitable for X-ray diffraction analysis were grown by vapor diffusion of diethyl ether into an acetonitrile solution of **9b** at room temperature

^{1}H NMR (400 MHz, acetonitrile-*d*$_3$) δ 7.63 (d, $J_{H,H}$ = 8.4 Hz, 1H, Ar-H^7), 7.40 (d, $J_{H,H}$ = 8.0 Hz, 1H, Ar-H^4), 6.89 (‘t’, $J_{H,H}$ = 7.3 Hz, 1H, Ar-H^6), 6.74 (‘t’, $J_{H,H}$ = 7.3 Hz, 1H, Ar-H^5), 4.23 (p, $J_{H,H}$ = $J_{H,P}$ = 7.2 Hz, 2H, PO$\underline{CH_2}$CH$_3$), 3.53 (s, 8H, CH$_2$ of 18-crown-6), 2.99 (d, $J_{H,P}$ = 14.6 Hz, 1H, P$^+$-CH$_3$), 2.46 (d, $J_{H,P}$ = 1.6 Hz, 3H, Ar-CH$_3$), 1.31 (t, $J_{H,H}$ = 7.1 Hz, 3H, POCH$_2\underline{CH_3}$). **^{13}C NMR** (101 MHz, acetonitrile-*d*$_3$) δ 148.3 (d, $J_{C,P}$ = 18.6 Hz, indole-C8), 129.7 (d, $J_{C,P}$ = 13.4 Hz, indole-C9 or C3), 126.1 (d, $J_{C,P}$ = 117.7 Hz, indole-C2), 119.0 (indole-C6), 118.2 (indole-C4), 117.1 (indole-C7), 115.5 (indole-C5), 114.3 (d, $J_{C,P}$ = 24.3 Hz, indole-C3 or C9), 69.9 (CH$_2$ of 18-crown-6), 59.6 (d, $J_{C,P}$ = 7.4 Hz, PO$\underline{CH_2}$CH$_3$), 16.0 (d, $J_{C,P}$ = 7.2 Hz, POCH$_2\underline{CH_3}$), 9.7 (Ar-CH$_3$), 7.8 (d, $J_{C,P}$ = 57.0 Hz, P$^+$-CH$_3$). **^{31}P NMR** (162 MHz, acetonitrile-*d*$_3$) δ 131.3 (br. s., 1P), -14.4 (q, $J_{P,H}$ = 14.4 Hz, 1P, carbon satellites: $J_{P,C}$ = 117.6, 24.2, 18.4, 13.2 Hz). **UV-Vis** (acetonitrile): λ_{max} (ε)=ca. 349 (shoulder) (1.2·10^4), 316 (2.2·10^4), 246 ($4.2\cdot10^4$), 214 nm ($2.8\cdot10^4$ cm^{-1}M^{-1}). **ESI-TOF-MS** in CH_3CN: anionic unit: 662.2196 [*M*]$^-$ (calcd. 662.1763 [*M*]$^-$). No satisfactory elemental analysis could be obtained due to high reactivity of **9b**.

Appended spectra: NMR in acetonitrile-*d*$_3$: ^{1}H (*Figure S58*), ^{1}H DQF-COSY (*Figure S59*), ^{1}H NOE (Figure S60, *Figure S61*), ^{13}C{^{1}H} DEPTQ-135 (*Figure S62*), ^{1}H-^{13}C ASAPHMQC (*Figure S63*), ^{31}P{^{1}H} (*Figure S64*), ^{31}P (*Figure S65*); UV-Vis in acetonitrile (*Figure S66*).

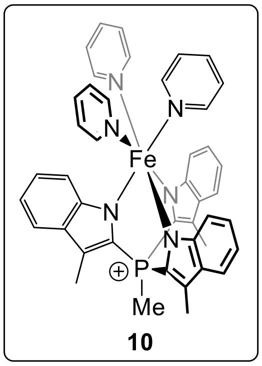
10

(TSMP)Fe(Py)$_3$ (10). Dry pyridine (30.0 ml) was added to a mixture of solid dipotassium salt **1** (contains 21.5 wt% of THF, 0.500 g, 0.768 mmol, 1.00 equiv.) and anhydrous $FeCl_2$ (0.097 g, 0.77 mmol, 1.00 equiv.). After 12h of stirring, the reaction mixture turned clear and acquired deep orange coloration. Subsequently, the solvent was removed *in vacuo* to give a bright-yellow solid. The latter was suspended in THF (25.0 ml) with 8 drops of pyridine (in order to improve solubility of the complex). The suspension was filtered, and the solid residue was washed with more THF until all color was extracted into the solution. Combined filtrate and washings were freed of solvent *in vacuo*. After this, the solid was redissolved in a minimal amount of pyridine, layered with an equal volume of hexane and left at room temperature for a week. Clear orange blocky crystals were collected, washed with a small volume of pyridine/hexane (1:1 (v/v)) solvent mixture and dried on a vacuum line for 30 min (prolonged drying results into a color change from orange to yellow and decreased solubility). Yield: 30.0% (0.167 g) of air-sensitive solid. Crystals suitable for X-ray diffraction analysis were grown by vapor diffusion of hexane into a pyridine solution of **10** at room temperature.

Integral intensities in ^{1}H NMR spectra were extracted using MNova[9] peak deconvolution tool. **^{1}H NMR** (400 MHz, pyridine-*d*$_5$) δ 36.7 (br. s., 1H), 27.7 (br. s., 1H), 25.7 (br. s., 3H), 8.9 (br. s., pyridine α-H), 8.1 (br. s., 1H), 7.61 – 7.50 (m, pyridine γ-H), 7.35 – 7.24 (m, pyridine β-H), 5.8 (br. s., 1H), -14.0 (br. s., 1H). **^{31}P NMR** (162 MHz, pyridine-*d*$_5$) δ -304.2. **Effective magnetic moment in solution** determined in pyridine-*d*$_5$ using Evans method: 5.19 μ_B. **UV-Vis** (acetonitrile): λ_{max} (ε)=471 ($1.2\cdot10^2$), 442 ($2.1\cdot10^2$), 417 ($2.5\cdot10^2$), 307 ($3.5\cdot10^4$), 231 ($6.3\cdot10^4$), 198 nm ($5.3\cdot10^4$ cm^{-1}M^{-1}). No satisfactory elemental analysis could be obtained due to the high reactivity of **8**.

Appended spectra: NMR in pyridine-*d*$_5$: ^{1}H (*Figure S67*, *Figure S68*), ^{31}P (*Figure S69*); UV-Vis in acetonitrile (*Figure S70*).

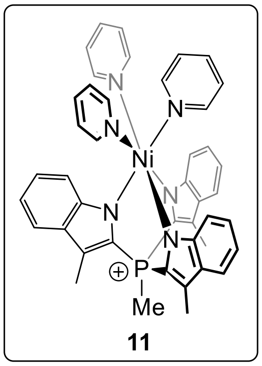

11

(TSMP)Ni(Py)$_3$ (11). Dry pyridine (30.0 ml) was added to a mixture of solid dipotassium salt **1** (contains 21.5 wt% of THF, 0.500 g, 0.768 mmol, 1.00 equiv.) and anhydrous NiCl$_2$·dme (0.169 g, 0.768 mmol, 1.00 equiv.). Deep-brown coloration ensued. After 12h of stirring, the reaction mixture turned clear and acquired emerald-green coloration. Subsequently, the solvent was removed *in vacuo* to give an olive-brown solid. The latter was suspended in THF (25.0 ml) with 8 drops of pyridine (improves solubility of the complex). The suspension was filtered, and the solid residue was washed with more THF until all color was extracted into the solution. Combined filtrate and washings were freed of solvent *in vacuo*. After this, the solid was redissolved in a minimal amount of pyridine, layered with an equal volume of hexane and left at room temperature for a week. Clear green blocky crystals were collected, washed with a small volume of pyridine/hexane (1:1 (v/v)) solvent mixture and dried on a vacuum line for 30 min (prolonged drying results into a color change from green to olive-brown and decreased solubility). Yield: 65.8% (0.369 g) of air-sensitive solid. Crystals suitable for X-ray diffraction analysis were grown by vapor diffusion of hexane into a pyridine solution of **11** at room temperature.

Integral intensities in ^{1}H NMR spectra were extracted using MNova[9] peak deconvolution tool. **^{1}H NMR** (400 MHz, pyridine-d_5) δ 29.7 (br. s., 1H), 15.2 (br. s., 1H), 9.1 (br. s., pyridine α-H), 7.67 – 7.52 (m, pyridine γ-H), 7.41 – 7.23 (m, pyridine β-H), 7.0 (br. s., 1H), 6.4 (br. s., 1H), 5.2 (br. s., 1H), 2.1 (br. s., 3H). **^{31}P NMR** (162 MHz, pyridine-d_5) δ -122.7 (br. s.). **Effective magnetic moment in solution** determined in pyridine-d_5 using Evans method: 2.82 μ_B. **UV-Vis** (acetonitrile): λ_{max} (ε)=198 ($5.8{\cdot}10^{4}$), 228 ($5.7{\cdot}10^{4}$), 242 ($6.1{\cdot}10^{4}$), 316 ($3.3{\cdot}10^{4}$), 588 nm (37 cm^{-1}M^{-1}). No satisfactory elemental analysis could be obtained due to the high reactivity of **9**.

Appended spectra: NMR in pyridine-d_5: ^{1}H (*Figure S71*, *Figure S72*), ^{31}P (*Figure S73*); UV-Vis in acetonitrile (*Figure S74*).

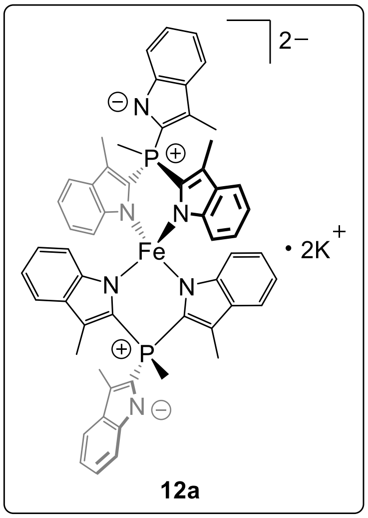

12a

Generation and characterization of crude [(TSMP)$_2$Fe]K$_2$ (12a). Dry THF (15.0 ml) was added to a mixture of solid dipotassium salt **1** (contains 21.5 wt% of THF, 0.150 g, 0.230 mmol, 2.00 equiv.) and anhydrous FeCl$_2$ (0.015 g, 0.12 mmol, 1.0 equiv.). The colorless mixture was stirred over 16h until all FeCl$_2$ dissolved forming a bright-yellow suspension. The latter was filtered, the solvent was removed *in vacuo*, yielding a dark-yellow oil. The complex could not be purified by means of crystallization and, hence, was analysed in a crude form using NMR spectroscopy. However, isolation of a crystalline tetrakis(benzo-15-crown-5) adduct **12b** was successful (see the synthesis below), which allowed to establish atomic connectivity using X-ray diffraction. Except for a number of peaks of impurities as well as benzo-15-crown-5 signals in **12b**, ^{1}H and ^{31}P NMR spectra of both **12a** and **12b** in acetonitrile-d_3 are identical.

Assuming that the X-ray diffraction-derived structure **12b** holds in solution, there should be three non-equivalent indolide units. This means that ^{1}H NMR spectra should display sixteen peaks: four of triple intensity with the rest of unit intensity. Instead, there are only four peaks with the ratio of integral intensities that does not match the overall composition of **12a**. This implies two possibilities: either not all peaks are visible due to fast relaxation and subsequent paramagnetic broadening, or the situation in solution is complicated with equilibriums involving oligomerization/intermolecular exchange. This point is further addressed below in the characterization section for tetrakis(benzo-15-crown-5) adduct **12b**.

^{1}H NMR (400 MHz, acetonitrile-*d*$_3$) δ 66.3 (br. s.), 21.6 (br. s.), 14.4 (br. s.), 6.0 (br. s.), -0.6 (br. s.), -6.1 (br. s.). **^{31}P NMR** (162 MHz, acetonitrile-*d*$_3$) δ 104.4 (br. s.). **ESI-TOF-MS** spectra in CH_3CN recorded in a negative mode show a product of one-electron oxidation of **12a**, which is in line with its high air-sensitivity: 922.3225 [*M*]$^-$ (calcd. 922.2767 [*M*]$^-$). No satisfactory elemental analysis could be obtained due to a number of impurities in crude **12a** combined with its high reactivity as well as solvation of potassium cations, due to which the compound retains an unknown amount of solvent.

Appended spectra: NMR in acetonitrile-*d*$_3$: ^{1}H (*Figure S75*), ^{31}P (*Figure S76*).

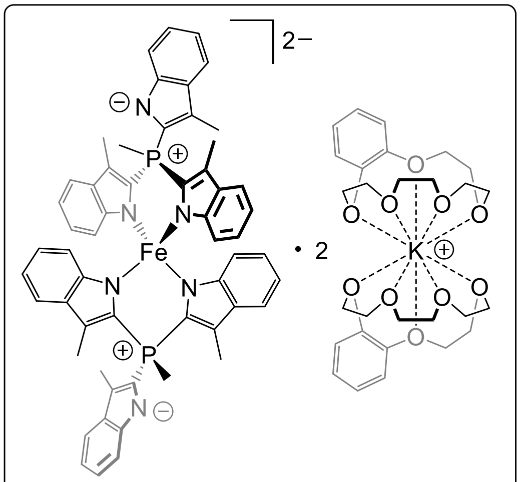

12b

[(TSMP)$_2$Fe][K(benzo-15-crown-5)$_2$]$_2$ (12b). Dry THF (150.0 ml) was added to a mixture of solid dipotassium salt **1** (contains 21.5 wt% of THF, 1.500 g, 2.302 mmol, 2.000 equiv.) and anhydrous $FeCl_2$ (0.146 g, 1.15 mmol, 1.00 equiv.). The mixture was stirred over 16h until all $FeCl_2$ dissolved forming a bright-yellow suspension. The latter was filtered, the volume of the liquor was reduced *in vacuo* to ca. 15 ml, and a solution of benzo-15-crown-5 (0.680 g, 2.53 mmol, 2.20 equiv.) in THF (5.0 ml) was added with stirring. After a few minutes, bright-yellow crystalline material started precipitating. The mixture was left standing at room temperature for 16h, at which point crystal formation stopped. It was then transferred into a freezer at -35 °C for additional 48h, where more crystalline material formed. The crystals were collected by vacuum filtration, washed with cold THF (4 x 20.0 ml) in small portions and dried *in vacuo*. This yielded a bright-yellow crystalline material in 40.7% (0.972 g) yield. Crystals suitable for X-ray diffraction analysis were grown by vapor diffusion of diethyl ether into a toluene/THF/acetonitrile (4:1:1 (v/v)) solution of **12b** at room temperature.

Assuming that the X-ray diffraction-derived structure **12b** holds in solution, there should be three non-equivalent indolide units. This means that ^{1}H NMR spectra should display sixteen peaks: four of triple intensity with the rest of unit intensity. Instead, there are only four paramagnetic peaks with the ratio of integral intensities that does not match the overall composition of **12b**. This implies two possibilities: either not all peaks are visible due to fast relaxation and subsequent paramagnetic broadening, or the situation in solution is complicated with equilibriums involving oligomerization/intermolecular exchange. Variable-temperature ^{1}H NMR measurements (see Section

S4.) indicate that there is indeed a temperature-dependent dynamic process that favors the hypothesis about oligomerization/intermolecular exchange, yet not excluding the paramagnetic broadening.

^{1}H NMR (400 MHz, acetonitrile-*d*$_3$) δ 66.3 (br. s.), 21.6 (br. s.), 14.4 (br. s.), 6.90 (br. s., Ar-H of benzo-15-crown-5), 6.76 (br. s., Ar-H of benzo-15-crown-5), 6.1 (br. s.), 4.20 – 3.17 (m, aliphatic C-H of benzo-15-crown-5), -0.6 (br. s.), -6.1 (br. s.). **^{31}P NMR** (162 MHz, acetonitrile-*d*$_3$) δ 104.2 (br. s.). **Effective magnetic moment in solution** determined in acetonitrile-*d*$_3$ using Evans method: 5.17 μ_B. **UV-Vis** (acetonitrile): λ_{max} (ε)= 308 ($3.5 \cdot 10^4$), 245 nm ($7.7 \cdot 10^4$ cm^{-1}M^{-1}). **ATR-FTIR** (neat) ṽ (cm^{-1}): 433 (M), 452 (M), 564 (W), 621 (M), 661 (W), 739 (VS), 808 (M), 853 (M), 884 (S), 937 (M), 1044 (S), 1076 (M), 1098 (S), 1123 (VS), 1217 (S), 1252 (VS), 1297 (M), 1337 (M), 1363 (M), 1455 (M), 1504 (S), 1597 (W), 1651 (VW), 2864 (M), 2904 (M), 3041 (W). **ESI-TOF-MS** spectra in CH_3CN recorded in a negative mode show a product of one-electron oxidation of **12b**, which is in line with its high air-sensitivity: 922.2360 [*M*]$^-$ (calcd. 922.2767 [*M*]$^-$). No satisfactory elemental analysis could be obtained due to high reactivity of **12b**.

Appended spectra: NMR in acetonitrile-*d*$_3$: ^{1}H (*Figure S77*), ^{31}P (*Figure S78*); UV-Vis in acetonitrile (Figure S79); ATR-FTIR (neat, *Figure S80*)., ^{1}H VT-NMR (*Figure S16*).

S3 X-ray crystal structure determinations

TSMPK$_2$ (1). $C_{56}H_{48}K_4N_6P_2 \cdot 0.5CH_3CN$, Fw = 1043.87, colourless block, 0.51 × 0.45 × 0.16 mm^3, monoclinic, Cc (no. 9), a = 20.0632(12), b = 12.0672(10), c = 42.305(4) Å, β = 95.794(2) °, V = 10190.0(14) Å^3, Z = 8, D_x = 1.361 g/cm^3, μ = 0.46 mm^{-1}. The diffraction experiment was performed on a Bruker Kappa ApexII diffractometer with sealed tube and Triumph monochromator (λ = 0.71073 Å) at a temperature of 150(2) K up to a resolution of $(\sin \theta/\lambda)_{max}$ = 0.65 Å^{-1}. The crystal appeared to be twinned, with a twofold rotation about *hkl*=(0,0,1) as twin operation. Consequently, two orientation matrices were used for the intensity integration with the Eval15 software.[10] A multi-scan absorption correction and scaling was performed with TWINABS[11] (correction range 0.68-0.75). A total of 102232 reflections was measured, 22187 reflections were unique (R_{int} = 0.032), 21465 reflections were observed [$I>2\sigma(I)$]. The structure was solved with Patterson superposition methods using SHELXT.[12] Structure refinement was performed with SHELXL-2016[13] on F^2 of all reflections based on an HKLF-5 file.[14] Non-hydrogen atoms were refined freely with anisotropic displacement parameters. All hydrogen atoms were introduced in calculated positions and refined with a riding model. 1270 Parameters were refined with two restraints (floating origin). R1/wR2 [$I > 2\sigma(I)$]: 0.0326 / 0.0827. R1/wR2 [all refl.]: 0.0342 / 0.0835. The twin fraction BASF refined to 0.1869(5); additional inversion twinning was not included in the refinement. S = 1.034. Residual electron density between -0.29 and 0.49 e/Å^3. Geometry calculations and checking for higher symmetry was performed with the PLATON program.[15]

<u>*Discussion:*</u> The asymmetric unit of the crystal is shown in *Figure S1*. The packing in the non-centrosymmetric space group Cc (no. 9) is characterized by the presence of a local inversion center at approximately (0, 0, ¼). This location prevents the transformation to the centrosymmetric space group C2/c (no. 15).

The metrics of the unit cell parameters allow a transformation to a *pseudo*-orthorhombic supercell with 5-fold volume. According to Mallard's law, such a situation can be the driving force for twin formation.[16] Twinning is actually found in the current crystal and can be described by a twofold rotation about *hkl*=(0,0,1), or equivalently about *uvw*=[1,0,0]. The a-axis of 20.06 Å indeed becomes a twofold axis in the 5-fold supercell. On a structural level, the twinning can be explained by stacking faults of the one-dimensional coordination polymers (*Figure S2*).

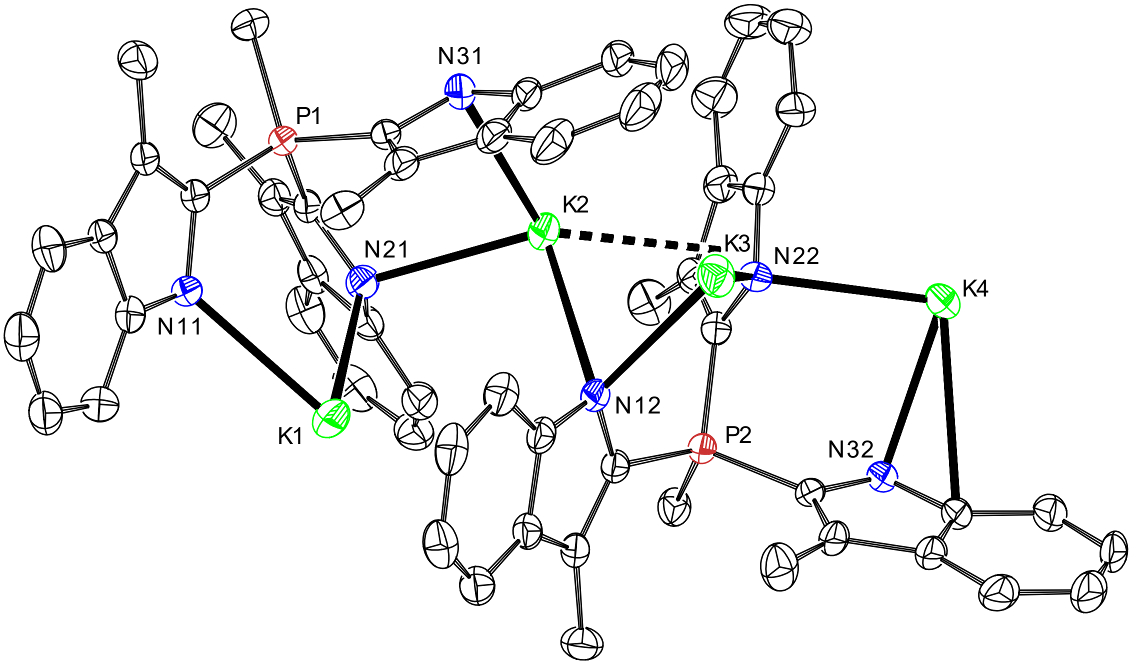

Figure S1. Asymmetric unit in the crystal structure of **1**. Only one of two independent residues is shown. Displacement ellipsoids are drawn at the 50% probability level. Hydrogen atoms and acetonitrile solvent molecules are omitted for clarity.

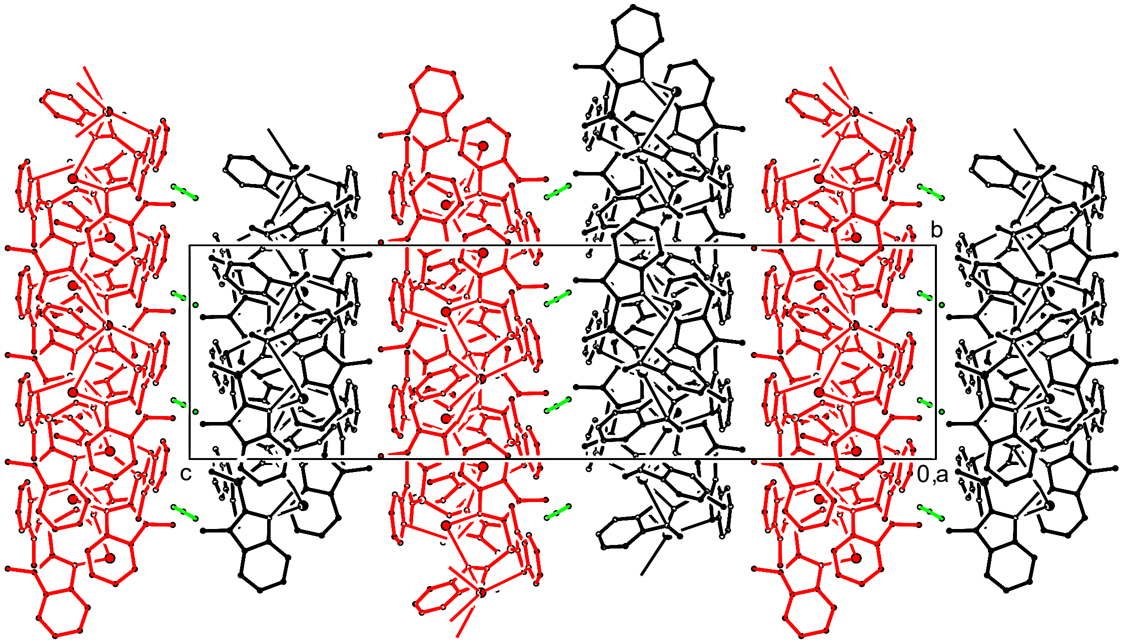

Figure S2. Packing of **1** in the crystal, projected along the a-axis. The two symmetry independent coordination chains are drawn in black and red, respectively. The acetonitrile solvent molecules are drawn in green. Hydrogen atoms are omitted for clarity. The crystal was twinned, and the twinning was described by a twofold rotation about the reciprocal c^*-axis. In the monoclinic crystal system this is equivalent to a rotation about the a-axis in direct space. It can be seen that the twinning does not cause much disturbance of the packing.

{[(TSMP)Cu]K}₄ (8). $[C_{182}H_{166}Cu_4K_4N_{26}P_4][C_{172}H_{156}Cu_4K_4N_{24}P_4] \cdot 6C_5H_5N$, Fw = 6820.07, yellow block, 0.29 × 0.19 × 0.17 mm^3, triclinic, P$\overline{1}$ (no. 2), a = 16.4610(6), b = 20.7224(6), c = 26.5518(7) Å, α = 78.716(1), β = 75.774(1), γ = 88.674(1) °, V = 8606.7(4) Å^3, Z = 1, D_x = 1.316 g/cm^3, μ = 0.68 mm^{-1}. The diffraction experiment was performed on a Bruker Kappa ApexII diffractometer with sealed tube and Triumph monochromator (λ = 0.71073 Å) at a temperature of 150(2) K up to a resolution of $(\sin \theta/\lambda)_{max}$ = 0.65 Å^{-1}. Intensity integration was performed with the Eval15 software.[10] A multi-scan absorption correction and scaling was performed with SADABS[17] (correction range 0.71-0.75). A total of 219470 reflections was measured, 39483 reflections were unique (R_{int} = 0.045), 26012 reflections were observed [I>2σ(I)]. The structure was solved with Patterson superposition methods using SHELXT.[12] Structure refinement was performed with SHELXL-2017[13] on F^2 of all reflections. Non-hydrogen atoms were refined freely with anisotropic displacement parameters. Six of the coordinated and non-coordinated pyridine molecules were refined with a disorder model. All hydrogen atoms were introduced in calculated positions and refined with a riding model. 2490 Parameters were refined with 4113 restraints (distances, angles, displacement parameters and molecular flatness of the pyridine molecules). R1/wR2 [I > 2σ(I)]: 0.0587 / 0.1538. R1/wR2 [all refl.]: 0.0964 / 0.1749. S = 1.019. Residual electron density between -0.64 and 0.86 e/Å^3. Geometry calculations and checking for higher symmetry was performed with the PLATON program.[15]

In addition to the discussion in the main text, molecular structure of {[(TSMP)Cu]K}₄ (**8**) is shown in *Figure S3* with selected distances and angles given in *Table S1* and *Table S2*.

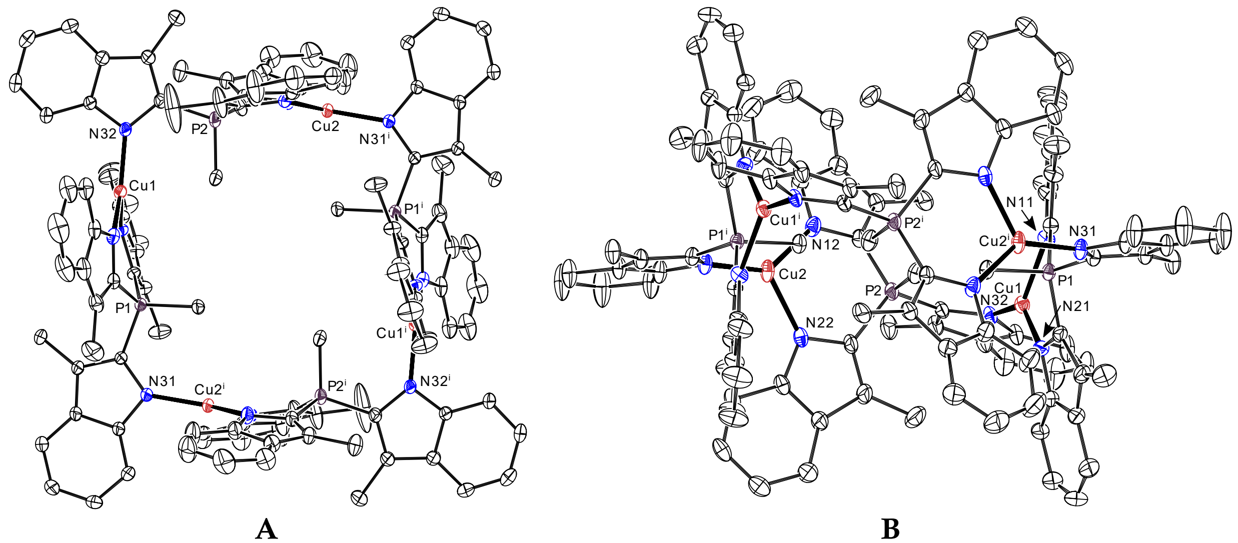

Figure S3. Molecular structure of **8** in the crystal (**A**: top view; **B**: side view). Displacement ellipsoids are drawn at the 30% probability level. Only one of two independent molecules is shown. Hydrogen atoms and indolide coordinated K$^+$ ions are omitted for clarity. K$^+$ coordinated and non-coordinated pyridine molecules are omitted as well. Symmetry code *i*: -x, -y, -z.

Table S1. Selected distances (Å) and angles (°) in the X-ray crystal structure of complex **8**. The unit cell of **8** contains two independent {[(TSMP)Cu]K}$_4$ molecules. Symmetry codes *i*: -x, -y, -z; *ii*: 1-x, 1-y, 1-z.

molecule 1		**molecule 2**	
Parameter	**Value**	**Parameter**	**Value**
Cu1-N11	2.000(3)	Cu3-N13	1.976(3)
Cu1-N21	1.960(3)	Cu3-N14^{ii}	1.940(2)
Cu1-N32	1.926(3)	Cu3-N23	1.991(3)
Cu2-N12	1.976(3)	Cu4-N24	1.967(3)
Cu2-N22	2.007(3)	Cu4-N33	1.920(2)
Cu2-N31^{i}	1.933(3)	Cu4-N34	2.004(3)
N11^Cu1^N21 (intracyclic)	99.68(10)	N13^Cu3^N23 (intracyclic)	100.62(10)
N11^Cu1^N32	125.74(11)	N13^Cu3^N14^{ii}	132.32(10)
N21^Cu1^N32	134.58(11)	N14^{ii}^Cu3^N23	126.60(11)
N12^Cu2^N22 (intracyclic)	99.26(11)	N24^Cu4^N34 (intracyclic)	99.02(11)
N12^Cu2^N31^{i}	136.95(12)	N24^Cu4^N33	133.92(11)
N22^Cu2^N31^{i}	123.61(11)	N33^Cu4^N34	126.85(11)
sum of angles around copper:		sum of angles around copper:	
Cu1	360.00(18)	Cu3	359.54(18)
Cu2	359.8(2)	Cu4	359.79(19)

Table S2. K…C distances indicating cation-π interactions in **8**.

molecule 1		**molecule 2**	
Parameter	**Value**	**Parameter**	**Value**
K1…C61	3.139(6)	K3…C83	2.906(3)
K1…C51	3.156(5)	K3…C33	3.104(3)
K1…C22	3.225(4)	K3…C13	3.369(3)
K1…C32	3.345(4)	K3…C73	3.370(4)
K2…C152	3.329(4)	K3…C23	3.423(3)
K2…C142	3.358(5)	K4…C214	3.002(4)
		K4…C264	3.018(4)
		K4…C224	3.121(5)
		K4…C254	3.182(4)
		K4…C234	3.242(5)
		K4…C244	3.271(5)

[(TSMP)CuP(OEt)$_3$][K(18-crown-6)·CH$_3$CN] (9b). [$C_{14}H_{27}KNO_6$][$C_{34}H_{39}CuN_3O_3P_2$] · ½ C_6H_6 · CH_3CN, Fw = 1087.73, colourless needle, 0.49 × 0.13 × 0.06 mm^3, monoclinic, I2/a (no. 15), a = 24.8978(5), b = 13.9828(3), c = 33.8978(7) Å, β = 110.867(1) °, V = 11027.2(4) Å^3, Z = 8, D$_x$ = 1.310 g/cm^3, μ = 0.59 mm^{-1}. The diffraction experiment was performed on a Bruker Kappa ApexII diffractometer with sealed tube and Triumph monochromator (λ = 0.71073 Å) at a temperature of

150(2) K up to a resolution of $(\sin \theta/\lambda)_{max}$ = 0.65 Å^{-1}. Intensity integration was performed with the Eval15 software.[10] A multi-scan absorption correction and scaling was performed with SADABS[17] (correction range 0.63-0.75). A total of 108621 reflections was measured, 12649 reflections were unique (R_{int} = 0.049), 9315 reflections were observed [$I>2\sigma(I)$]. The structure was solved with Patterson superposition methods using SHELXT.[12] Structure refinement was performed with SHELXL-2017[13] on F^2 of all reflections. Non-hydrogen atoms were refined freely with anisotropic displacement parameters. The non-coordinated acetonitrile molecule was refined with a disorder model. All hydrogen atoms were introduced in calculated positions and refined with a riding model. 679 Parameters were refined with 111 restraints (distances, angles, displacement parameters and molecular flatness of the solvent molecules). R1/wR2 [$I > 2\sigma(I)$]: 0.0440 / 0.1222. R1/wR2 [all refl.]: 0.0658 / 0.1358. S = 1.034. Residual electron density between -0.65 and 1.05 e/Å^3. Geometry calculations and checking for higher symmetry was performed with the PLATON program.[15]

Discussion: the crystal structure of **9b** is characterized by a [K(18-crown-6)(CH_3CN)] cation and a [(TSMP)CuP(OEt)$_3$] anion. Further, there are non-coordinated benzene and acetonitrile molecules in the unit cell. Molecular structure of **9b** is shown in *Figure S4.* Selected bond distances and angles are shown in *Table S3.*

The packing of the molecules in the crystal leads to a layer structure with the layers stacked in c-direction and intercalated with solvent molecules. As a consequence, there are strong *pseudo*-translational effects (*Figure S5*) which are also visible in the X-ray diffraction pattern. Within the layers, intermolecular bonding is dominated by C-H…π interactions between the crown ether in the cation and the indolide groups of the anion (*Figure S6*). The co-crystallized benzene is located on a twofold rotation axis in proximity of the K$^+$ center.

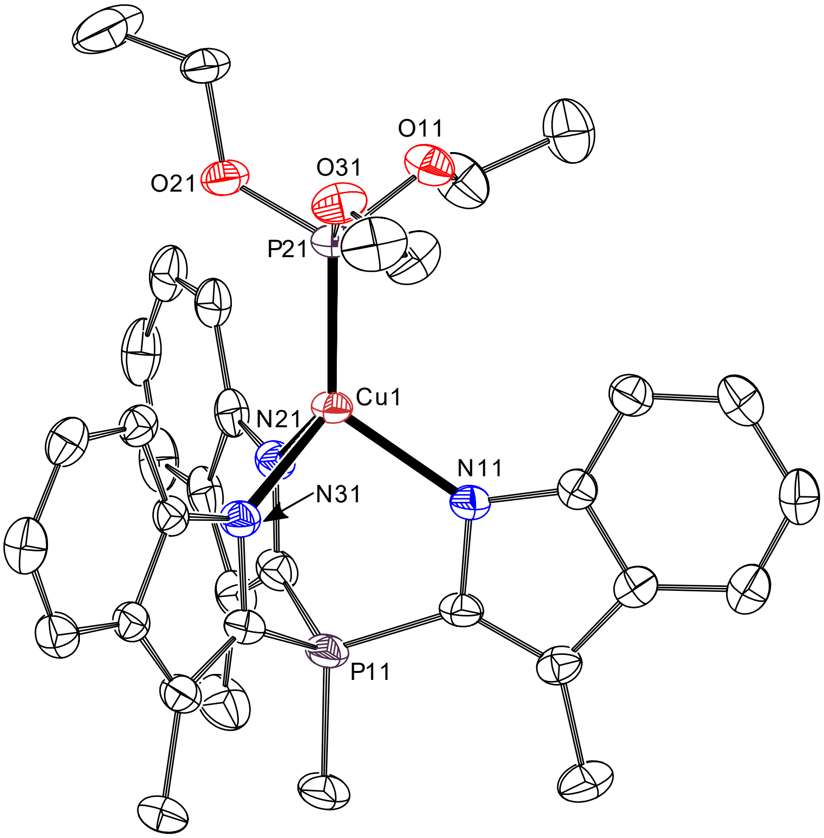

Figure S4. Molecular structure of the anion of **9b** in the crystal. Displacement ellipsoids are drawn at the 50% probability level. Hydrogen atoms, the [K(18-crown-6)(CH_3CN)] cation and non-coordinated benzene and acetonitrile molecules are omitted for clarity.

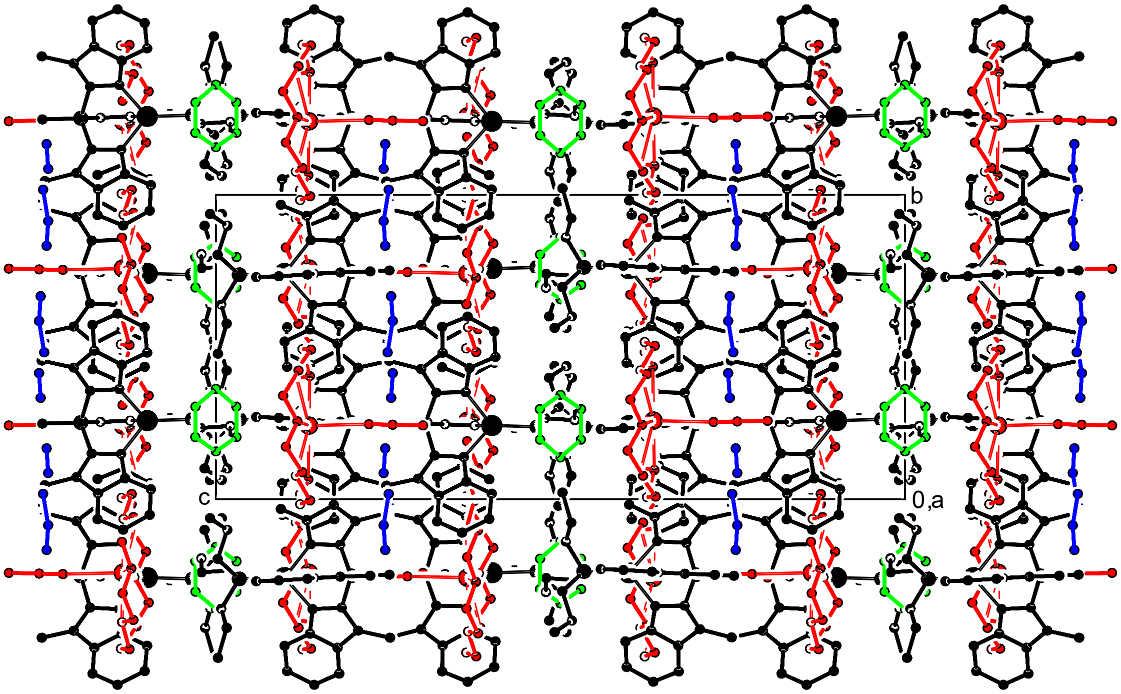

Figure S5. Packing of **9b** in the crystal. Projection along the a-axis. Cations are drawn in red, anions in black, benzene in green, and acetonitrile in blue. Only the major form of the disordered acetonitrile is shown. Hydrogen atoms are omitted for clarity. The structure has significant *pseudo*-translational symmetry in c-direction. Consequently, reflections with *h*=*odd* are weak.

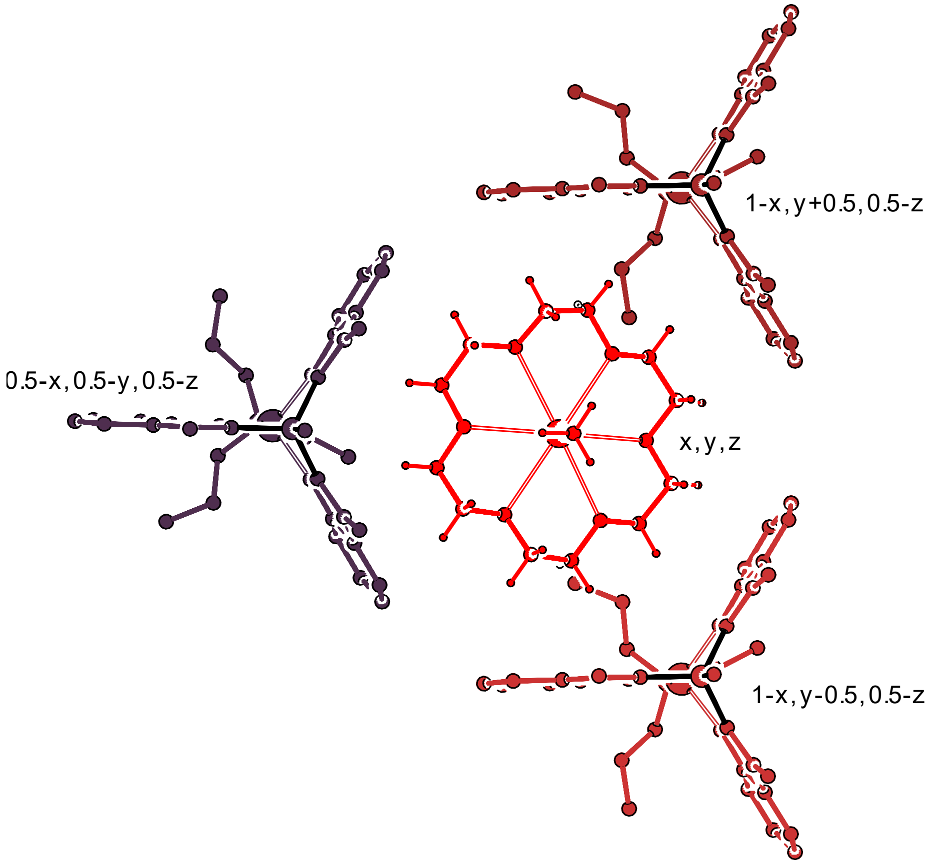

Figure S6. Intermolecular C-H…π interactions in **9b** viewed along the c-axis. The H-atoms of the crown ether act as donors, and the π-systems of the indolide groups as acceptors. C-H…π interactions between the methyl group of the coordinated acetonitrile and indolide are omitted for clarity.

Table S3. Selected distances (Å), angles and torsion angles (°) in the X-ray crystal structure of complex **9b**.

Parameter	**Value**
Cu1-N11	2.0759(19)
Cu1-N21	2.0654(19)
Cu2-N31	2.0622(19)
Cu1-P21	2.1201(6)
N11^Cu1^N21	95.06(7)
N21^Cu1^N31	92.38(8)
N11^Cu1^N31	94.54(7)
P21^Cu1^N11	123.28(6)
P21^Cu1^N21	121.85(6)
P21^Cu1^N31	121.97(5)
O11^P21^Cu1^N11	41.79(11)
angle sum O^P^O	300.37(16)

(TSMP)Fe(Py)$_3$ (10). $C_{43}H_{39}FeN_6P$ + disordered solvent, Fw = 726.62*, yellow needle, 0.38 × 0.07 × 0.03 mm^3, monoclinic, $P2_1/c$ (no. 14), a = 24.456(3), b = 18.0393(16), c = 19.450(3) Å, β = 113.125(7) °, V = 7891.4(17) Å^3, Z = 8, D_x = 1.223 g/cm^3*, μ = 0.46 mm^{-1}*. The diffraction experiment was performed on a Bruker Kappa ApexII diffractometer with sealed tube and Triumph monochromator (λ = 0.71073 Å) at a temperature of 150(2) K up to a resolution of $(\sin \theta/\lambda)_{max}$ = 0.61 Å^{-1}. The Eval15 software[10] was used for the intensity integration of this weakly diffracting crystal. A large anisotropic mosaicity[18] of 2.5 ° about *hkl*=(0,1,0) was used for the prediction of the reflection profiles. A numerical absorption correction and scaling was performed with SADABS[17] (correction range 0.65-1.00). A total of 55335 reflections was measured, 14669 reflections were unique (R_{int} = 0.159), 6802 reflections were observed [$I>2\sigma(I)$]. The structure was solved with Patterson superposition methods using SHELXT.[12] Structure refinement was performed with SHELXL-2018[13] on F^2 of all reflections. The crystal structure contains large voids (1106 Å^3 / unit cell) filled with disordered solvent molecules. Their contribution to the structure factors was secured by back-Fourier transformation with the SQUEEZE algorithm[19] resulting in 305 electrons / unit cell. Non-hydrogen atoms were refined freely with anisotropic displacement parameters. All hydrogen atoms were introduced in calculated positions and refined with a riding model. 927 Parameters were refined with no restraints. R1/wR2 [$I > 2\sigma(I)$]: 0.0891 / 0.1954. R1/wR2 [all refl.]: 0.1942 / 0.2417. S = 1.030. Residual electron density between -0.56 and 0.65 e/Å^3. Geometry calculations and checking for higher symmetry was performed with the PLATON program.[15]

Discussion: the molecular structure of (TSMP)Fe(Py)$_3$ (**10**) is shown in *Figure S7.* It has been found that **10** is isostructural to its Ni-containing analogue (TSMP)Fe(Py)$_3$ (**11**). Therefore, the crystallographic details for **10**, including the selected bond lengths and angles (*Table S4*), are discussed in the context of a comparison with **11** in the section below.

---

* Derived values do not contain the contribution of the disordered solvent molecules.

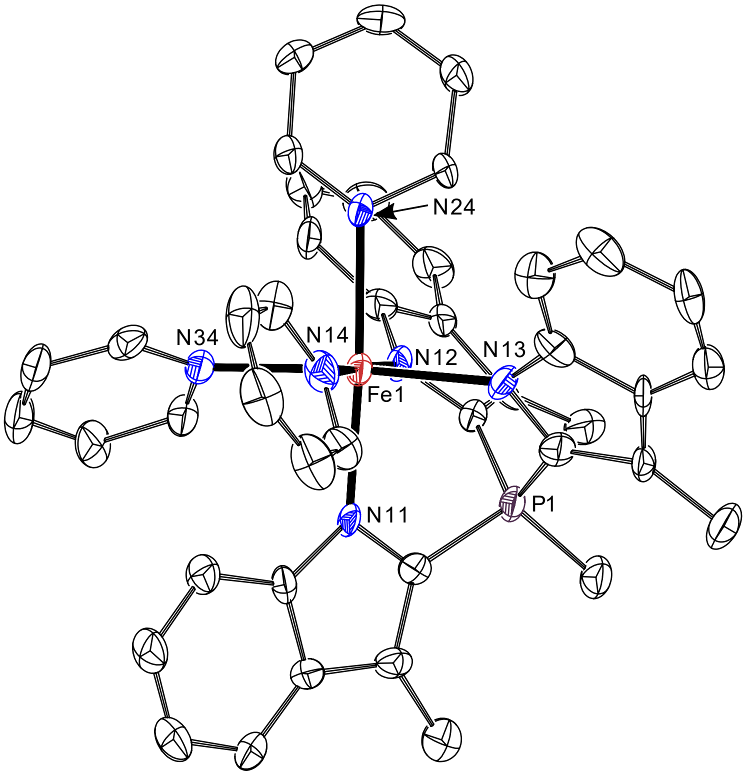

Figure S7. Displacement ellipsoid plot of **10** in the crystal (50% probability level). Only one of two independent molecules is shown. Hydrogen atoms and disordered solvent molecules are omitted for clarity.

(TSMP)Ni(Py)$_3$ (11). $C_{43}H_{39}N_6NiP \cdot 0.3\ C_6H_{14}$, Fw = 755.33, green needle, 0.32 × 0.08 × 0.05 mm^3, monoclinic, $P2_1/c$ (no. 14), a = 24.314(3), b = 17.888(2), c = 19.297(2) Å, β = 113.027(3) °, V = 7724.1(15) Å^3, Z = 8, D_x = 1.299 g/cm^3, μ = 0.58 mm^{-1}. The diffraction experiment was performed on a Bruker Kappa ApexII diffractometer with sealed tube and Triumph monochromator (λ = 0.71073 Å) at a temperature of 150(2) K up to a resolution of $(\sin \theta/\lambda)_{max}$ = 0.56 Å^{-1}. The Saint software[20] was used for the intensity integration. A numerical absorption correction and scaling was performed with SADABS[17] (correction range 0.82-1.00). A total of 66286 reflections was measured, 11139 reflections were unique (R_{int} = 0.221), 5916 reflections were observed [$I>2\sigma(I)$]. The structure was solved with Patterson superposition methods using SHELXT.[12] Structure refinement was performed with SHELXL-2018[13] on F^2 of all reflections. Non-hydrogen atoms were refined freely with anisotropic displacement parameters. The n-hexane solvent molecule was refined with partial occupancy. All hydrogen atoms were introduced in calculated positions and refined with a riding model. The crystal appeared to be twinned by *pseudo*-merohedry (*pseudo*-orthorhombic C-centered twin cell). The twin operation is a twofold rotation about *hkl*=(1,0,0) and the corresponding twin matrix (-1,0,-1 / 0,-1,0 / 0,0,1) was included in the refinement. 982 Parameters were refined with 1829 restraints (distances, angles and displacement parameters for all atoms except Ni and P). R1/wR2 [$I > 2\sigma(I)$]: 0.0877 / 0.1806. R1/wR2 [all refl.]: 0.1954 / 0.2320. S = 1.034. Twin fraction BASF = 0.2361(18). Residual electron density between -0.86 and 1.27 e/Å^3. Geometry calculations and checking for higher symmetry was performed with the PLATON program.[15]

Discussion: X-ray crystal structure determinations of **10** and **11** reveal that the two compounds are isostructural in the solid state. The asymmetric unit contains two independent metal complex molecules. They are related by a non-crystallographic twofold rotation approximately about *uvw*=[0,0,1]. This operation is not compatible with the monoclinic crystal system but might be the structural basis for twinning. Twinning was indeed found in the crystal of **11** (*vide supra*) and was described by a twofold rotation about *hkl*=(1,0,0). In the monoclinic case this equivalent to a rotation about *uvw*=[0,0,1].

The large standard uncertainties make a discussion of the geometric parameters difficult (*Table S4*). The longest M-N distances are found for M1-N34 (molecule 1) and M2-N38 (molecule 2). The Ni-N^{TSMP} distances are 0.05 Å shorter than Fe-N^{TSMP}, and Ni-N^{Py} are 0.11 Å shorter than Fe-N^{Py}.

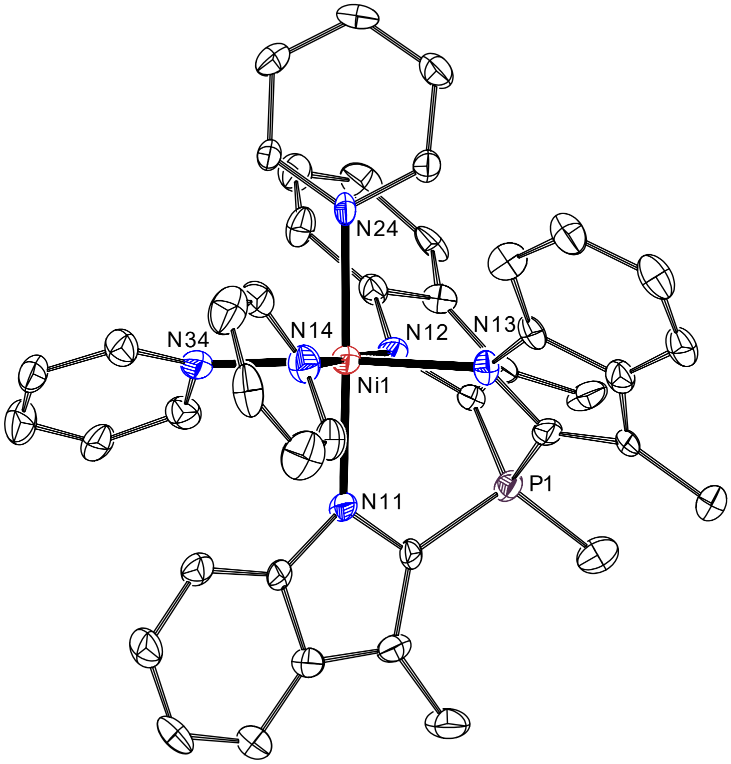

Figure S8. Displacement ellipsoid plot of **11** in the crystal (50% probability level). Only one of two independent molecules is shown. Hydrogen atoms and partially occupied *n*-hexane molecules are omitted for clarity.

Table S4. Selected XRD distances (Å) and angles (°) for (TSMP)M(Py)$_3$ complexes **10** and **11**.

molecule 1			**molecule 2**		
Parameter	**Value**		**Parameter**	**Value**	
	M=Fe (10)	**M=Ni (11)**		**M=Fe (10)**	**M=Ni (11)**
M1-N11^{L}	2.175(6)	2.127(7)	M2-N15^{L}	2.176(6)	2.123(7)
M1-N12^{L}	2.173(6)	2.115(7)	M2-N16^{L}	2.158(6)	2.102(7)
M1-N13^{L}	2.168(6)	2.138(7)	M2-N17^{L}	2.201(6)	2.148(7)
M1-N14^{Py}	2.272(7)	2.168(7)	M2-N18^{Py}	2.261(7)	2.163(8)
M1-N24^{Py}	2.294(6)	2.178(7)	M2-N28^{Py}	2.284(6)	2.164(7)
M1-N34^{Py}	2.351(6)	2.241(8)	M2-N38^{Py}	2.342(6)	2.234(7)
N11^{L}^M1^N12^{L}	89.5(2)	88.7(3)	N15^{L}^M2^N16^{L}	89.7(2)	89.3(3)
N12^{L}^M1^N13^{L}	91.3(2)	90.4(3)	N16^{L}^M2^N17^{L}	91.6(2)	89.9(3)
N11^{L}^M1^N13^{L}	89.9(2)	89.8(3)	N15^{L}^M2^N17^{L}	89.8(2)	89.2(3)
N14^{Py}^M1^N24^{Py}	90.5(3)	91.2(3)	N18^{Py}^M2^N28^{Py}	89.4(2)	90.1(3)
N24^{Py}^M1^N34^{Py}	89.7(2)	91.4(3)	N28^{Py}^M2^N38^{Py}	91.1(2)	92.5(3)
N14^{Py}^M1^N34^{Py}	88.9(2)	89.8(3)	N18^{Py}^M2^N38^{Py}	90.7(2)	91.9(3)
N11^{L}^M1^N24^{Py} (trans)	175.1(2)	174.8(3)	N15^{L}^M2^N28^{Py} (trans)	175.2(2)	176.3(3)
N12^{L}^M1^N14^{Py} (trans)	177.7(2)	177.0(4)	N16^{L}^M2^N18^{Py} (trans)	176.1(2)	176.0(3)
N13^{L}^M1^N34^{Py} (trans)	174.4(2)	174.6(3)	N17^{L}^M2^N38^{Py} (trans)	173.5(2)	174.1(3)

[(TSMP)$_2$Fe][K(benzo-15-crown-5)$_2$]$_2$ (12b). [$C_{28}H_{40}KO_{10}$]$_2$[$C_{56}H_{48}FeN_6P_2$] · ½ C_7H_8 · ½ $C_4H_{10}O$ · CH_3CN, Fw = 2198.37, yellow block, 0.37 × 0.10 × 0.03 mm^3, triclinic, $P\overline{1}$ (no. 2), a = 17.8742(12), b = 18.1808(12), c = 19.8655(13) Å, α = 109.771(3), β = 108.424(2), γ = 95.566(1) °, V = 5611.4(7) Å^3, Z = 2, D_x = 1.301 g/cm^3, μ = 0.31 mm^{-1}. The diffraction experiment was performed on a Bruker Kappa ApexII diffractometer with sealed tube and Triumph monochromator (λ = 0.71073 Å) at a temperature of 150(2) K up to a resolution of $(\sin \theta/\lambda)_{max}$ = 0.61 Å^{-1}. Intensity integration was performed with the Eval15 software.[10] A multi-scan absorption correction and scaling was performed with SADABS[17] (correction range 0.65-0.75). A total of 83986 reflections was measured, 20904 reflections were unique (R_{int} = 0.088), 11765 reflections were observed [$I>2\sigma(I)$]. The structure was solved with Patterson superposition methods using SHELXT.[12] Structure refinement was performed with SHELXL-2016[13] on F^2 of all reflections. Non-hydrogen atoms were refined freely with anisotropic displacement parameters. The toluene and diethyl ether molecules were disordered on inversion centers, respectively. All hydrogen atoms were introduced in calculated positions and refined with a riding model. 1426 Parameters were refined with 168 restraints (concerning the disordered solvent molecules). R1/wR2 [$I > 2\sigma(I)$]: 0.0641 / 0.1423. R1/wR2 [all refl.]: 0.1356 / 0.1715. S = 1.017. Residual electron density between -0.44 and 1.26 e/Å^3. Geometry calculations and checking for higher symmetry was performed with the PLATON program.[15]

In addition to the discussion in the main text, molecular structure of [(TSMP)$_2$Fe][K(benzo-15-crown-5)$_2$]$_2$ (**12b**) is shown in *Figure S9* with selected distances and angles given in *Table S5*.

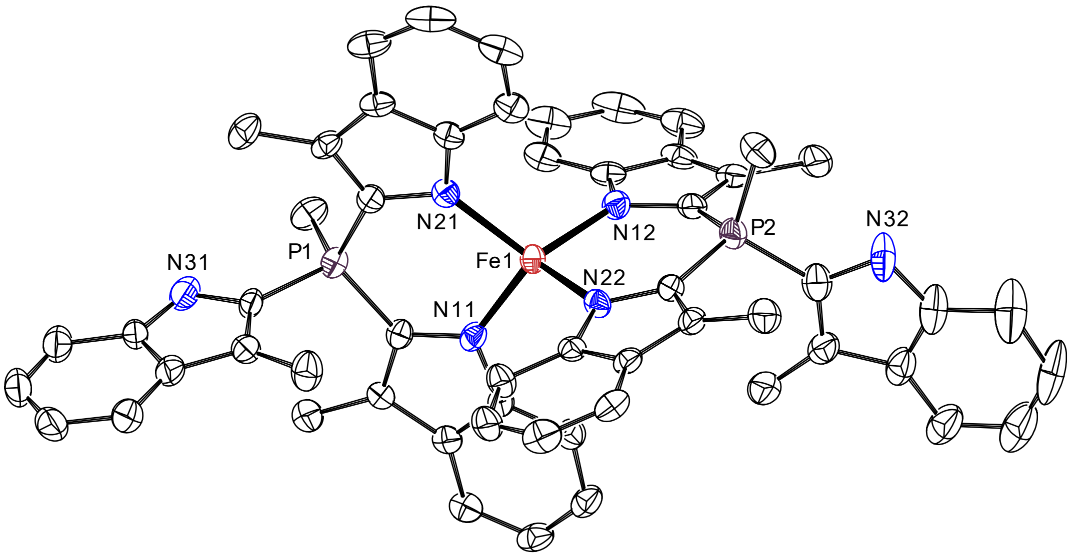

Figure S9. Molecular structure of the anion of **12b** in the crystal. Displacement ellipsoids are drawn at the 50% probability level. Hydrogen atoms, the [K(benzo-15-crown-5)$_2$] cations and non-coordinated toluene, diethyl ether and acetonitrile molecules are omitted for clarity.

Table S5. Selected distances (Å) and angles (°) in the X-ray crystal structure of complex **12b**.

Parameter	**Value**
Fe1-N11	2.017(3)
Fe1-N12	2.028(3)
Fe1-N21	2.019(3)
Fe1-N22	2.028(3)
N11^Fe1^N21 (endocyclic)	96.78(13)
N12^Fe1^N22 (endocyclic)	96.35(13)
N11^Fe1^N12 (exocyclic)	118.90(13)
N21^Fe1^N22 (exocyclic)	119.68(13)

S4 Peripheral discussions

S4.1 NMR of tris-(*N*-Boc-3-methylindol-2-yl)methylphosphonium iodide (5)

It is worth pointing out that tris-2-(*N*-Boc-skatyl)methylphosphonium iodide (**5**) exists in DCM-d_2 solution as a *ca.* 1.00:0.15 mixture of interexchanging tris-*exo* (**5a**) and bis-*exo*-mono-*endo* (**5b**) rotamers (top left corner in *Figure S10*).[*] To elaborate, the ^{31}P NMR spectrum of **5** (*Figure S10*, right panel) shows two peaks in a ratio of 1.00 to 0.15: the former being a sharp quartet (**A**), as expected for *J*-coupling with a methyl group, while the latter is a broad singlet (**B**). ^{1}H-^{31}P ASAPHMQC spectra (*Figure S11*) show a correlation between these two peaks and two ^{1}H doublets between 2.7 and 2.9 ppm ($CH_3{}^{P}{}_{A}$ and $CH_3{}^{P}{}_{B}$ in *Figure S10*, left panel), which have a similar ratio of integral intensities (1.04:0.15). We assign these doublets to methyl phosphonium groups of the individual rotamers, $CH_3{}^{P}{}_{A}$ and $CH_3{}^{P}{}_{B}$. Aside from that, the ^{1}H NMR spectrum shows an intense set of four aromatic signals ($H^{Ar}{}_{A}$) and two singlets ($CH_3{}^{Ar}{}_{A}$ and $CH_3{}^{Boc}{}_{A}$) which are consistent with a C_3-symmetric topology of **5a**. NOESY spectrum (*Figure S12*, left panel) indicates spatial proximity of $CH_3{}^{P}{}_{A}$ and $CH_3{}^{Boc}{}_{A}$ protons, therefore signifying a tris-*exo* rotamer **5a**. Another set of ^{1}H peaks in *Figure S12* – $H^{Ar}{}_{B}$, $CH_3{}^{Ar}{}_{B}$ and $CH_3{}^{Boc}{}_{B}$ – indicates an asymmetric rotamer **5b**, which is in chemical exchange with **5a** as shown by NOESY spectra (*Figure S12*, right panel). As for its configuration, the NOESY cross-peaks do not have sufficient intensity for us to extract geometric information. However, variable-temperature NMR studies show that population of **5b** decreases at lower temperature, *viz.*: the ratio of **5a**:**5b** at 25 °C is *ca.* 1.00:0.15 whereas at -40 °C it is 1.00:0.07. This means that rotamer **5b** is more energetic, likely due to steric repulsion. Therefore, from general considerations, we assign **5b** to have a bis-*exo*-mono-*endo* configuration since this is the next least strained one. The presence of two interconverting rotamers for phosphonium salts is not unprecedented and was previously observed by NMR.[21]

---

[*] Due to a lot of steric hindrance and, thus, rather high rotational barriers around C^{Ar}-P bonds in **5**, there are two possible configurations for each derivatized indole ring: with a Boc group pointing towards and away from a phosphonium methyl. Accordingly, we choose to call the first configuration "*exo*-", whereas the second one is "*endo*-".

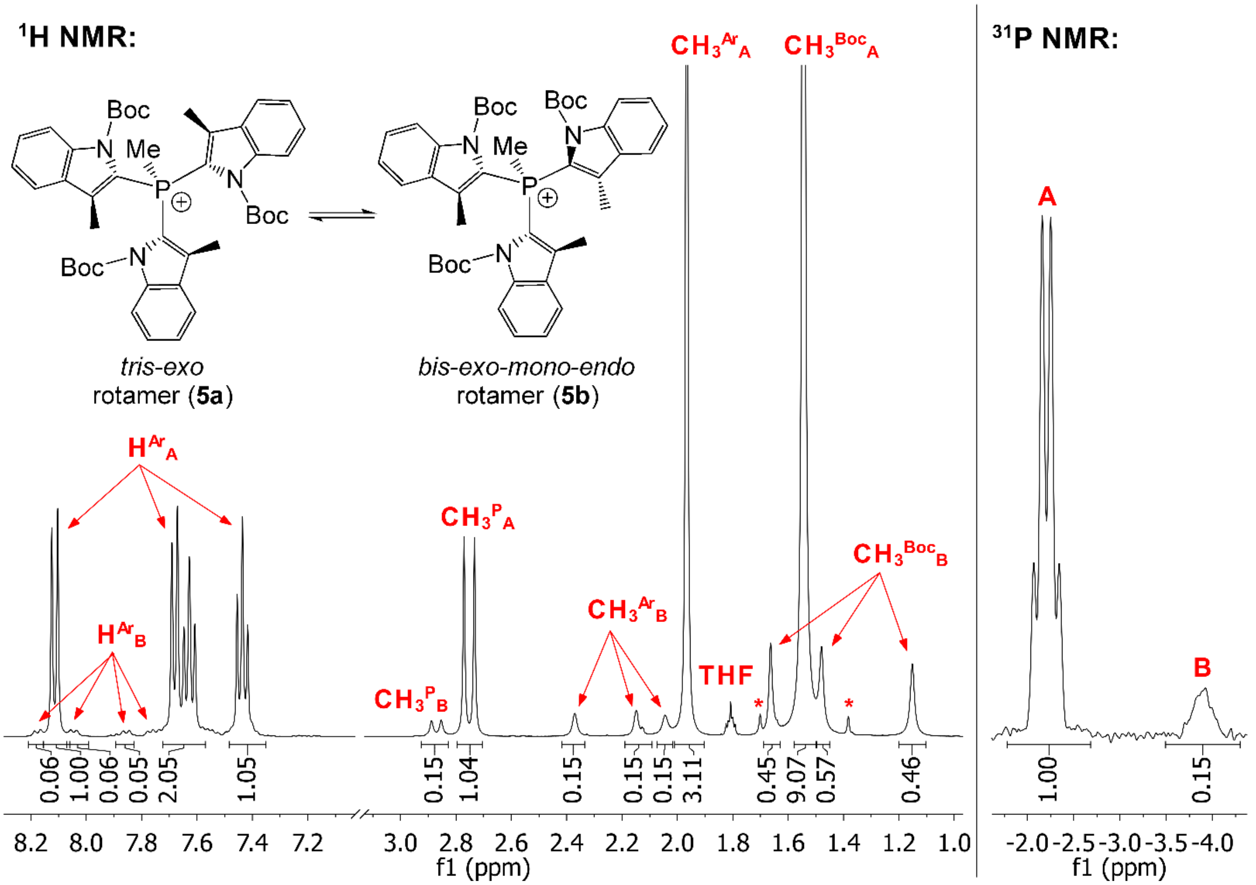

Figure S10. ¹H (400 MHz) and ³¹P NMR (162 MHz) spectra of **5** measured in DCM-d_2. Integral intensities are extracted using MestReNova[9] peak deconvolution tools. Asterisks indicate $CH_3^{Boc}{}_A$ peak satellites. Full spectra in *Figure S25* and *Figure S29*.

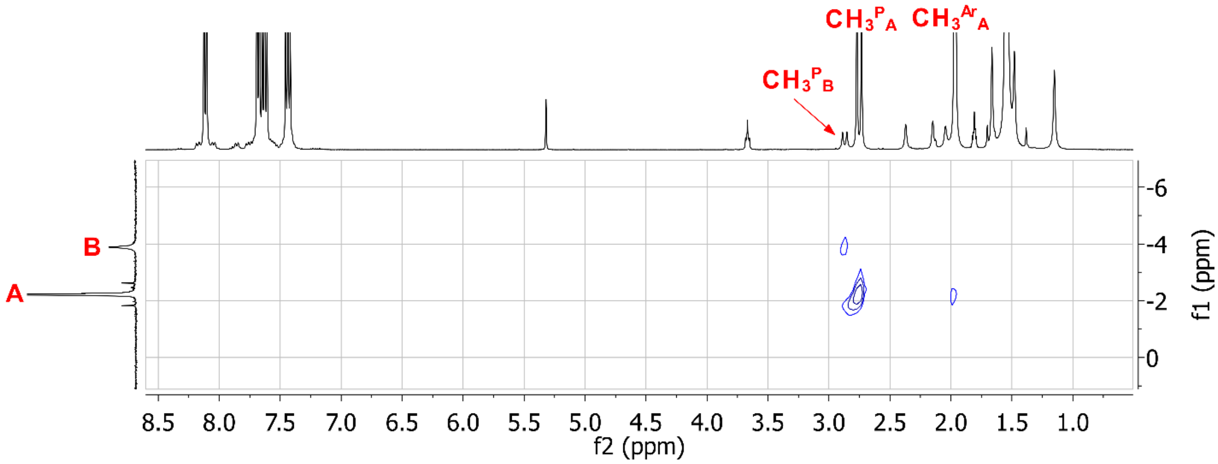

Figure S11. ¹H-³¹P ASAPHMQC spectrum of **5** in DCM-d_2. Full spectrum in *Figure S30*.

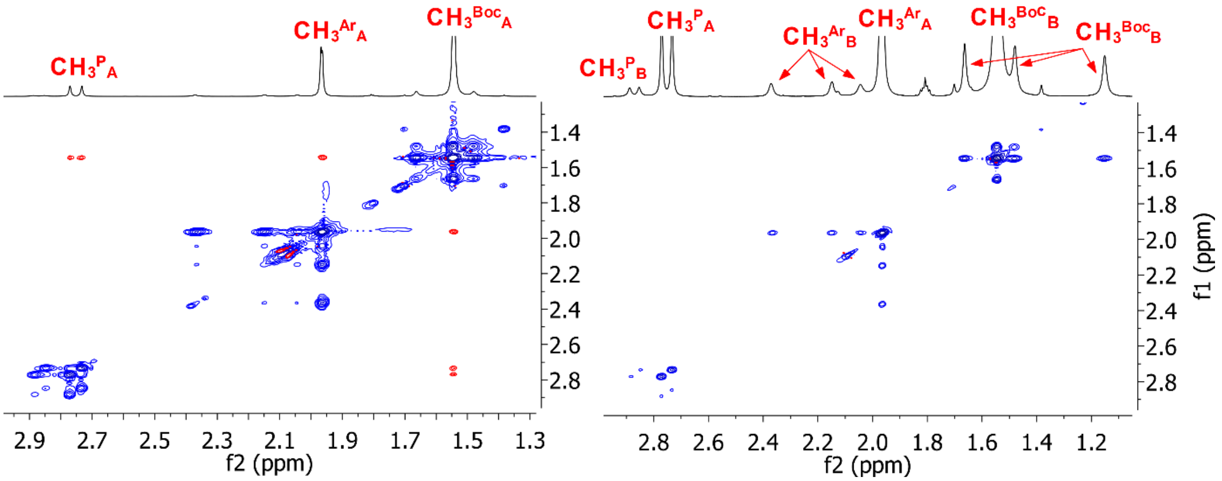

Figure S12. NOESY spectrum of **5** in DCM-d_2 shown at two different levels of intensity. Blue cross-peaks indicate chemical exchange, red cross-peaks show NOE. Full spectrum in *Figure S26.*

S4.2 gCOSY and NOESY NMR of {[(TSMP)Cu]K}$_4$ (8)

gCOSY and NOESY NMR (400 MHz) spectra of complex **8** with assignments provided (*Figure S13*).

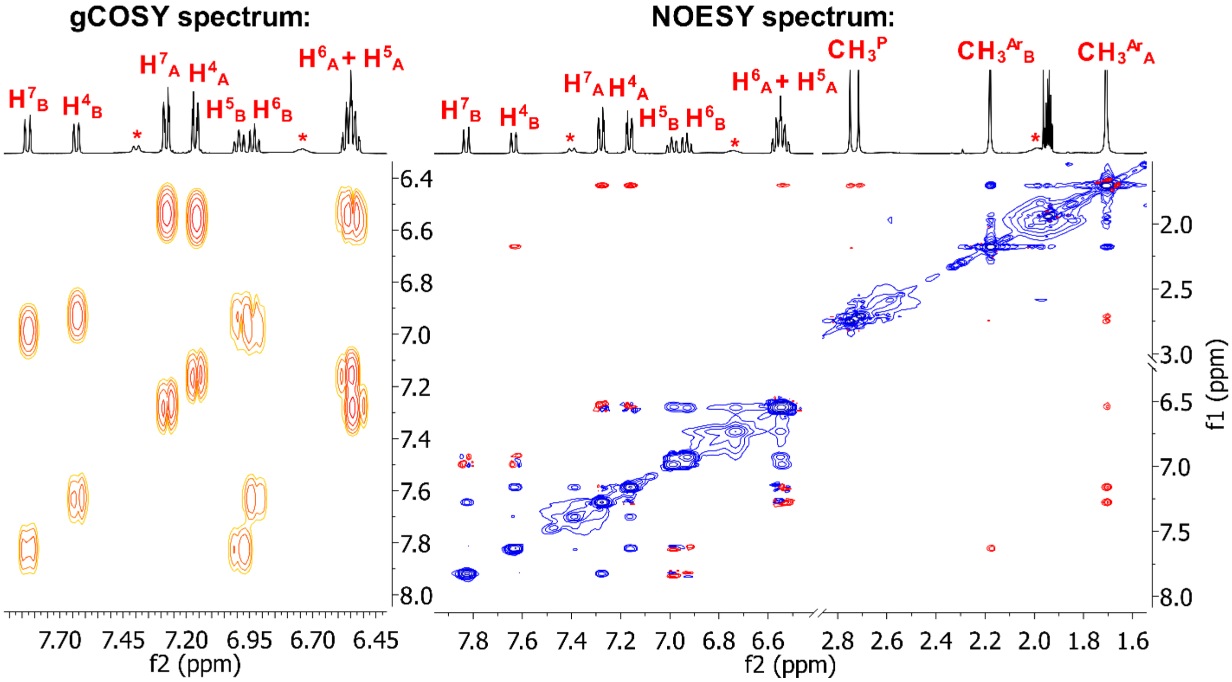

Figure S13. Magnitude gCOSY and NOESY NMR spectra of **8** in acetonitrile-d_3. Blue-phase cross-peaks indicate chemical exchange, red-phase cross-peaks show NOE, mixed-phase cross-peaks are due to unsuppressed COSY correlations. Full spectra in *Figure S41*, *Figure S42* and *Figure S43.*

S4.3 ^{1}H NMR of {[(TSMP)Cu]K}$_4$ (8) before and after addition of P(OEt)$_3$

^{1}H NMR spectra (400 MHz) of complex **8** in acetonitrile-d_3 (*Figure S14*) before and after addition of 4 equiv. of P(OEt)$_3$. Note that the addition provides a spectrum with higher symmetry.

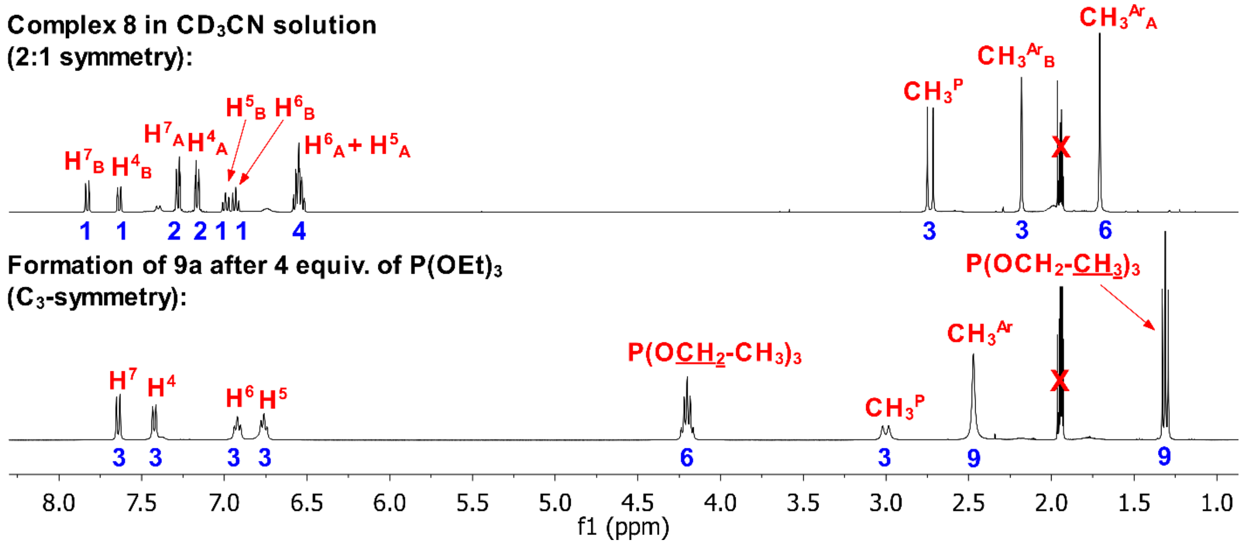

Figure S14. ^{1}H NMR spectra of **8** in acetonitrile-d_3 before and after addition of P(OEt)$_3$. Integral intensities shown in blue were rounded to the nearest integer. Full spectra in *Figure S40* and *Figure S49*.

S4.4 NOE spectra of [(TSMP)CuP(OEt)$_3$]K (9a)

^{1}H (400 MHz) 1D NOE spectra of [(TSMP)CuP(OEt)$_3$]K complex (**9a**) in acetonitrile-d_3 (*Figure S15*).

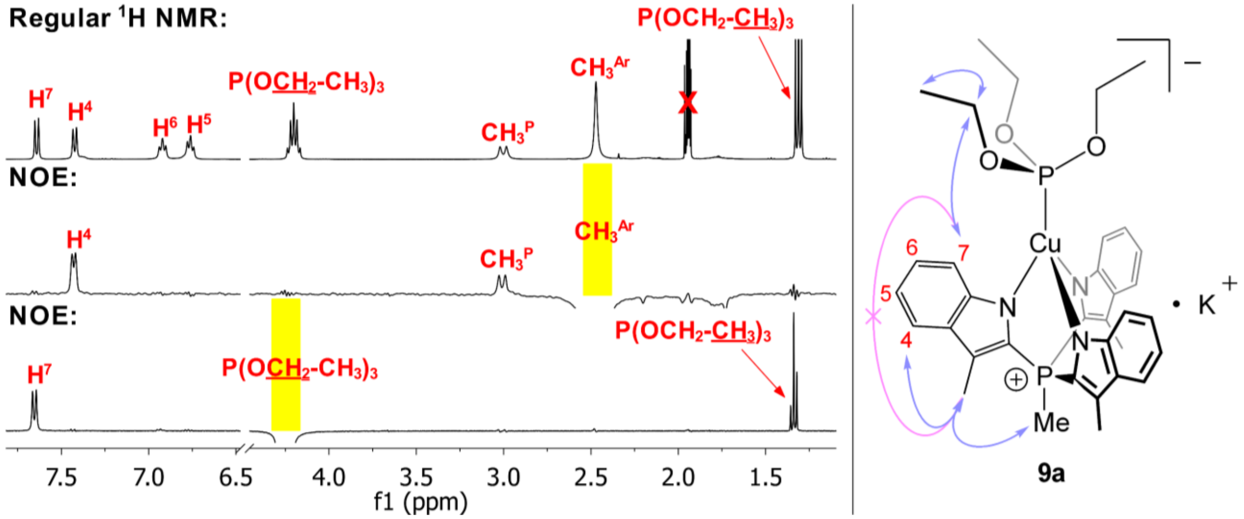

Figure S15. Left panel: ^{1}H NMR (400 MHz) and 1D NOE spectra of [(TSMP)CuP(OEt)$_3$]K complex (**9a**) in acetonitrile-d_3. Yellow rectangles show saturation windows. *Right panel*: NOE correlations mapped on the structural formula of **9a**. Due to C$_3$-symmetry of the molecule, only the unique ones are shown. Lilac arrows indicate detected NOE correlations; the pink arrow shows a correlation that cannot be observed due to large distance between resonating protons. Nevertheless, this correlation is present in the spectra of {[(TSMP)Cu]K}$_4$ (**8**) due to its oligomeric nature. Full spectra in *Figure S49*, *Figure S52* and *Figure S53*.

S4.5 Variable-temperature NMR studies of [(TSMP)$_2$Fe][K(benzo-15-crown-5)$_2$]$_2$ (12b)

Variable-temperature ^{1}H NMR spectra in acetonitrile-d_3 are shown in *Figure S16*. They feature a number of paramagnetic peaks, four of which (**A**-**D**) are well-defined throughout most of the covered temperature range. They obey Curie's law (*Figure S17*), which excludes the possibility of spin-crossover. Note that, while paramagnetic signals generally tend to broaden at lower temperature, peaks **A** and **B** show an opposite trend. Such behaviour implies an additional source of line-broadening, which may be complex dynamic behaviour in solution.

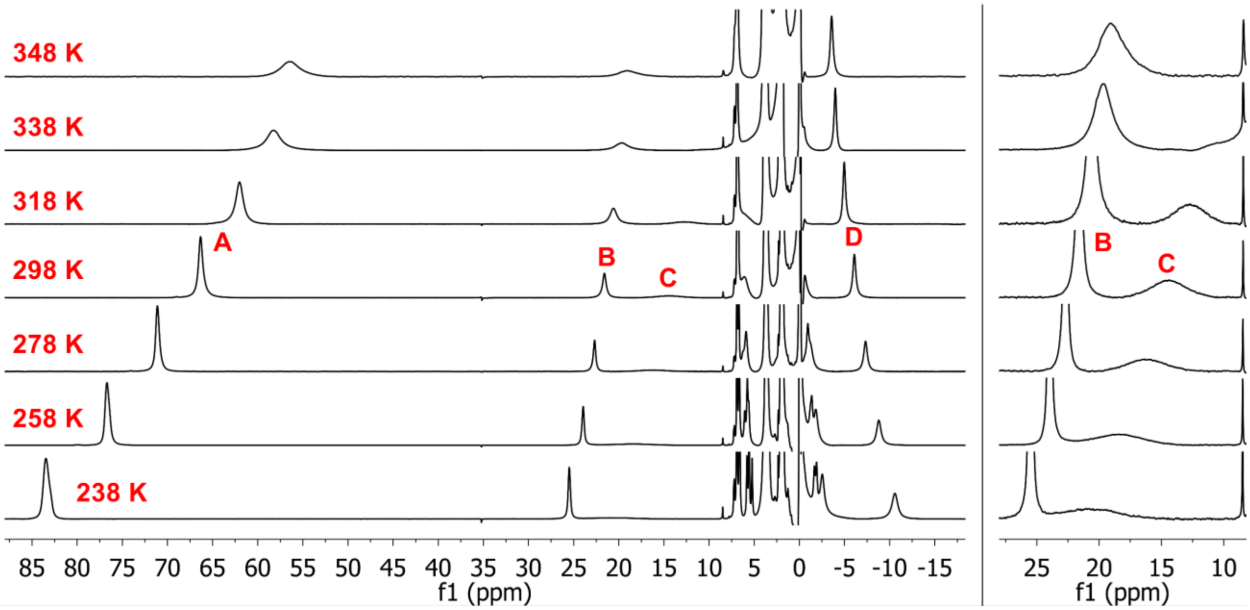

Figure S16. Variable-temperature ^{1}H NMR (400 MHz) spectra of **12b** in acetonitrile-d_3.

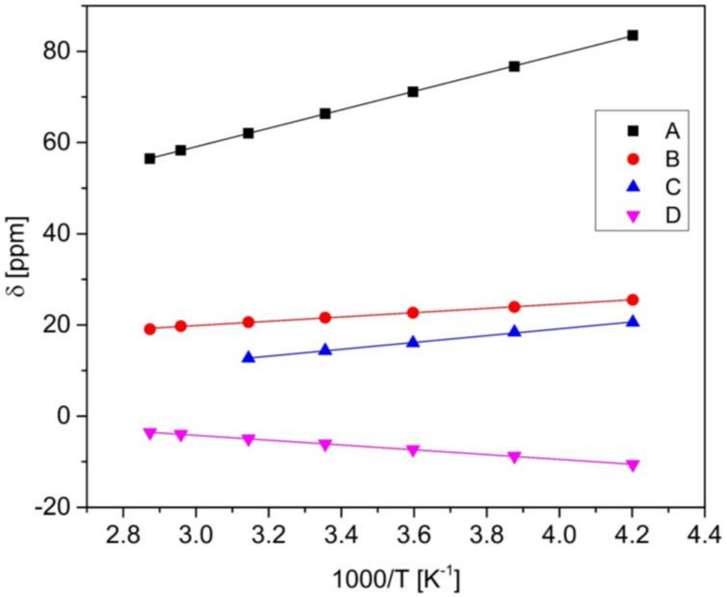

Figure S17. Linear dependence of chemical shifts *vs.* inverse temperature demonstrating Curie behavior. Linear fitting parameters for: **A**: Intercept: -1.63±0.21, Slope: 20.23±0.06; Adj. R^2: 0.99993; **B**: Intercept: 5.70±0.27; Slope: 4.72±0.08; Adj. R^2: 0.99779; **C**: Intercept: -10.84±0.43; Slope: 7.5±0.12; Adj. R^2: 0.99845; **D**: Intercept: 11.61±0.08; Slope: -5.27±0.02; Adj. R^2: 0.99985.

S5 Literature references

(1) Gokel, G. W.; Cram, D. J.; Liotta, C. L.; Harris, H. P.; Cook, F. L. Preparation and Purification of 18-Crown-6[1,4,7,10,13,16-Hexaoxacyclooctadecane]. *J. Org. Chem.* **1974**, *39* (16), 2445–2446. https://doi.org/10.1021/jo00930a037.

(2) Fulmer, G. R.; Miller, A. J. M.; Sherden, N. H.; Gottlieb, H. E.; Nudelman, A.; Stoltz, B. M.; Bercaw, J. E.; Goldberg, K. I. NMR Chemical Shifts of Trace Impurities: Common Laboratory Solvents, Organics, and Gases in Deuterated Solvents Relevant to the Organometallic Chemist. *Organometallics* **2010**, *29* (9), 2176–2179. https://doi.org/10.1021/om100106e.

(3) Kupče, E.; Freeman, R. Fast Multidimensional NMR by Polarization Sharing. *Magn. Reson. Chem.* **2007**, *45* (1), 2–4. https://doi.org/10.1002/mrc.1931.

(4) VnmrJ 4.2, Revision A. Agilent Technologies: Santa Clara, USA 2014.

(5) Evans, D. F. 400. The Determination of the Paramagnetic Susceptibility of Substances in Solution by Nuclear Magnetic Resonance. *J. Chem. Soc.* **1959**, 2003–2005. https://doi.org/10.1039/jr9590002003.

(6) Piguet, C. Paramagnetic Susceptibility by NMR: The “Solvent Correction” Removed for Large Paramagnetic Molecules. *J. Chem. Educ.* **1997**, *74* (7), 815. https://doi.org/10.1021/ed074p815.

(7) Bain, G. A.; Berry, J. F. Diamagnetic Corrections and Pascal’s Constants. *J. Chem. Educ.* **2008**, *85* (4), 532. https://doi.org/10.1021/ed085p532.

(8) Grehn, L.; Ragnarsson, U. A Convenient Method for the Preparation of 1-(Tert-Butyloxycarbonyl) Pyrroles. *Angew. Chemie Int. Ed. English* **1984**, *23* (4), 296–301. https://doi.org/10.1002/anie.198402961.

(9) MestReNova v.9.0.1-13254. Mestrelab Research S.L. 2014.

(10) Schreurs, A. M. M.; Xian, X.; Kroon-Batenburg, L. M. J. EVAL15 : A Diffraction Data Integration Method Based on Ab Initio Predicted Profiles. *J. Appl. Crystallogr.* **2010**, *43* (1), 70–82. https://doi.org/10.1107/S0021889809043234.

(11) Sheldrick, G. M. TWINABS. Universität Göttingen, Germany 2014.

(12) Sheldrick, G. M. SHELXT – Integrated Space-Group and Crystal-Structure Determination. *Acta Crystallogr. Sect. A Found. Adv.* **2015**, *71* (1), 3–8. https://doi.org/10.1107/S2053273314026370.

(13) Sheldrick, G. M. Crystal Structure Refinement with SHELXL. *Acta Crystallogr. Sect. C Struct. Chem.* **2015**, *71* (1), 3–8. https://doi.org/10.1107/S2053229614024218.

(14) Herbst-Irmer, R.; Sheldrick, G. M. Refinement of Twinned Structures with SHELXL97. *Acta Crystallogr. Sect. B Struct. Sci.* **1998**, *54* (4), 443–449. https://doi.org/10.1107/S0108768197018454.

(15) Spek, A. L. Structure Validation in Chemical Crystallography. *Acta Crystallogr. Sect. D Biol. Crystallogr.* **2009**, *65* (2), 148–155. https://doi.org/10.1107/S090744490804362X.

(16) Le Page, Y. Mallard’s Law Recast as a Diophantine System: Fast and Complete Enumeration of Possible Twin Laws by [Reticular] [Pseudo] Merohedry. *J. Appl. Crystallogr.* **2002**, *35* (2),

175–181. https://doi.org/10.1107/S0021889801021574.

(17) Sheldrick, G. M. SADABS. Universität Göttingen, Germany 2014.

(18) Duisenberg, A. J. M. Diffractometry and Reflection Profiles of Anisotropic Mosaic and Split Crystals. *Acta Crystallogr. Sect. A Found. Crystallogr.* **1983**, *39* (2), 211–216. https://doi.org/10.1107/S0108767383000483.

(19) Spek, A. L. PLATON SQUEEZE: A Tool for the Calculation of the Disordered Solvent Contribution to the Calculated Structure Factors. *Acta Crystallogr. Sect. C Struct. Chem.* **2015**, *71* (1), 9–18. https://doi.org/10.1107/S2053229614024929.

(20) Bruker. SAINT-Plus. Bruker AXS Inc., Madison, Wisconsin, USA 2001.

(21) Martin-Mothes, E.; Puig, E.; Vendier, L.; Bijani, C.; Grellier, M.; Bontemps, S.; Martin-Mothes, E., Puig, E., Vendier, L., Bijani, C., Grellier, M., & Bontemps, S. Ortho-Phenyl Dialkylphosphonium Sulfonate Compounds: Two Rotamers in Equilibrium. *Dalt. Trans.* **2018**, *47* (30), 10139–10146. https://doi.org/10.1039/C8DT02400F.

S6 Spectra

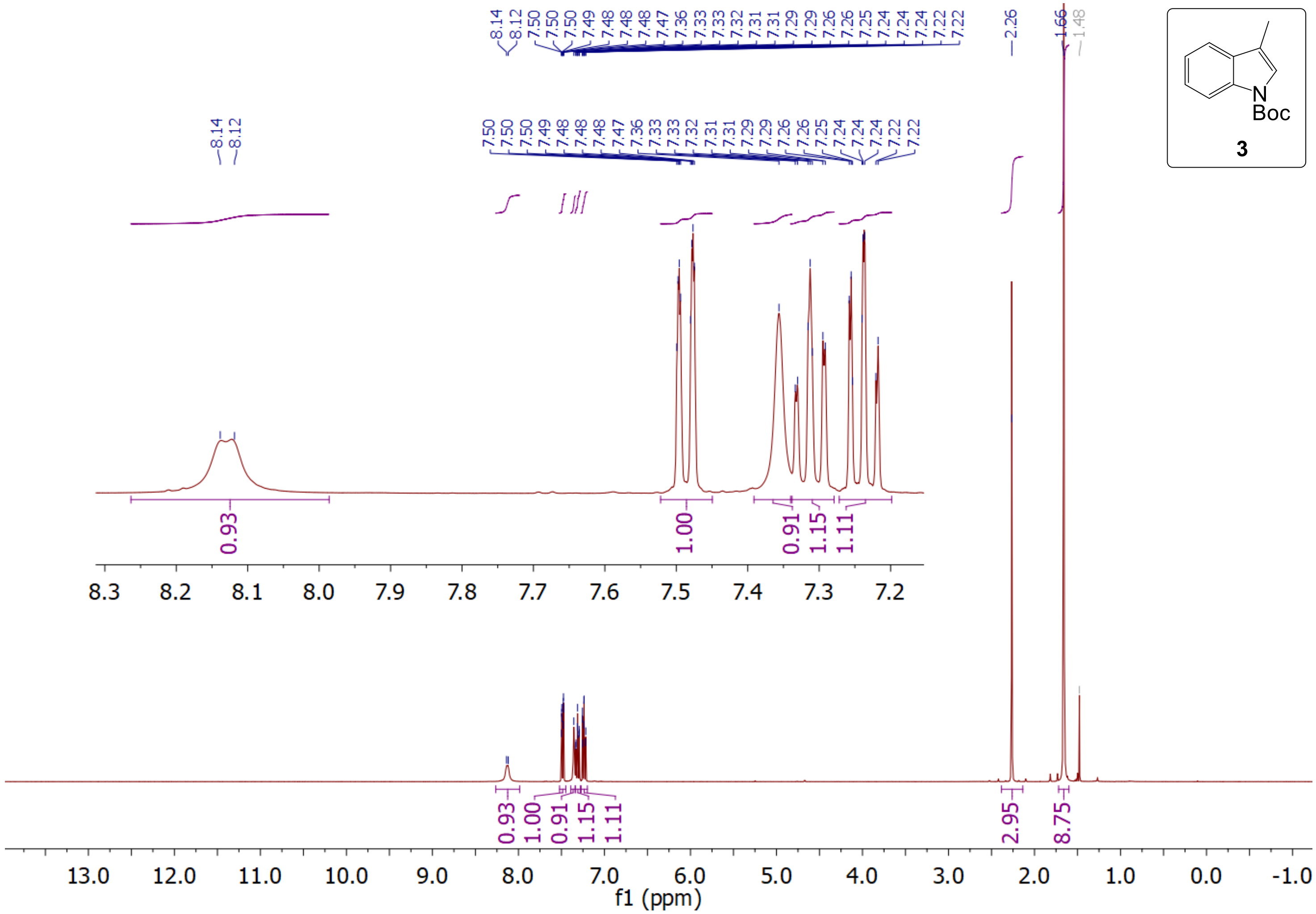

Figure S18. ^{1}H NMR spectrum of compound **3** in chloroform-*d*. Impurities: 1.48 ppm – unidentified, presumably leftover Boc$_2$O.

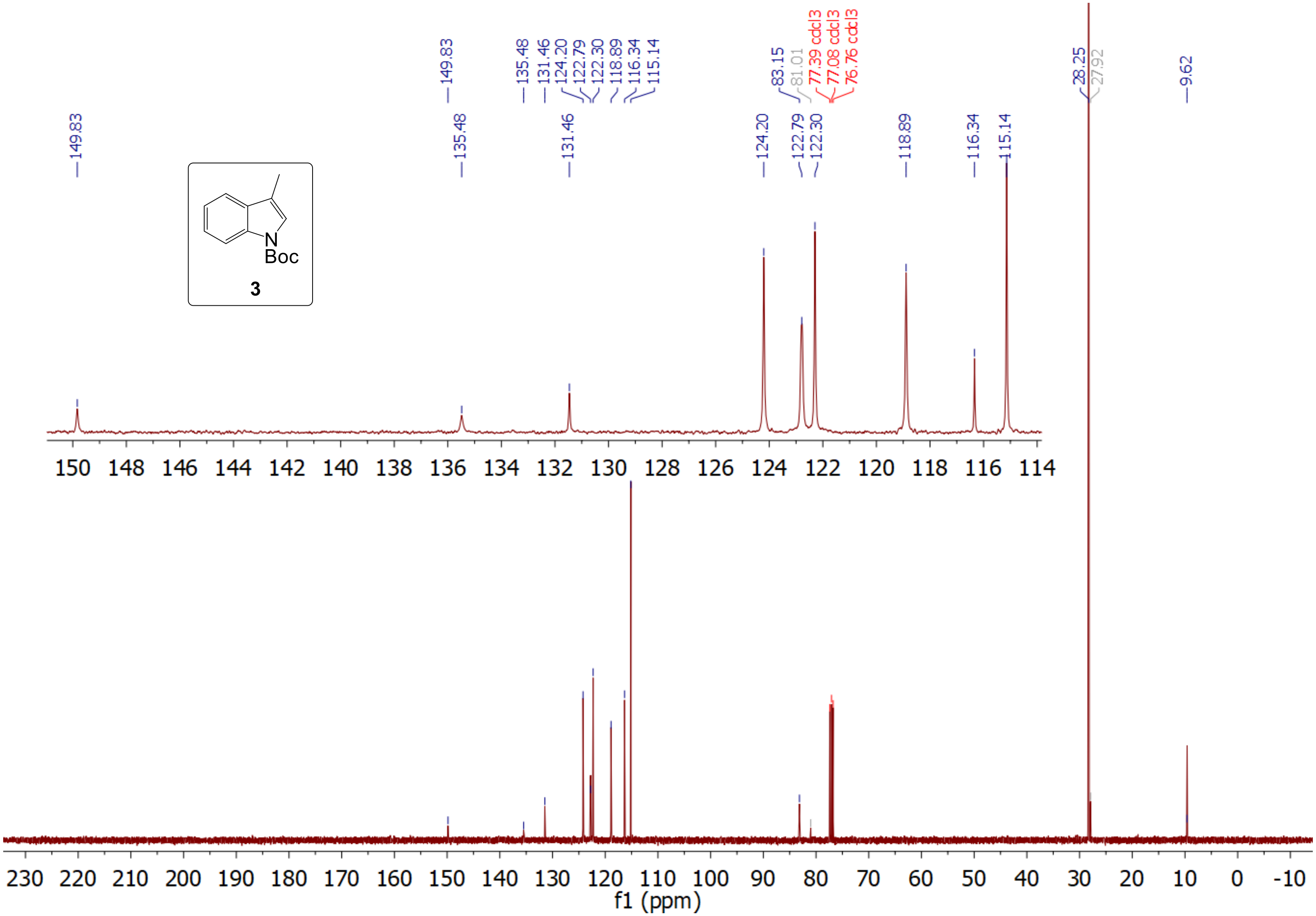

Figure S19. $^{13}C\{^1H\}$ NMR spectrum of compound **3** in chloroform-*d*. Impurities: 27.92 and 81.01 ppm – unidentified, presumably leftover Boc_2O.

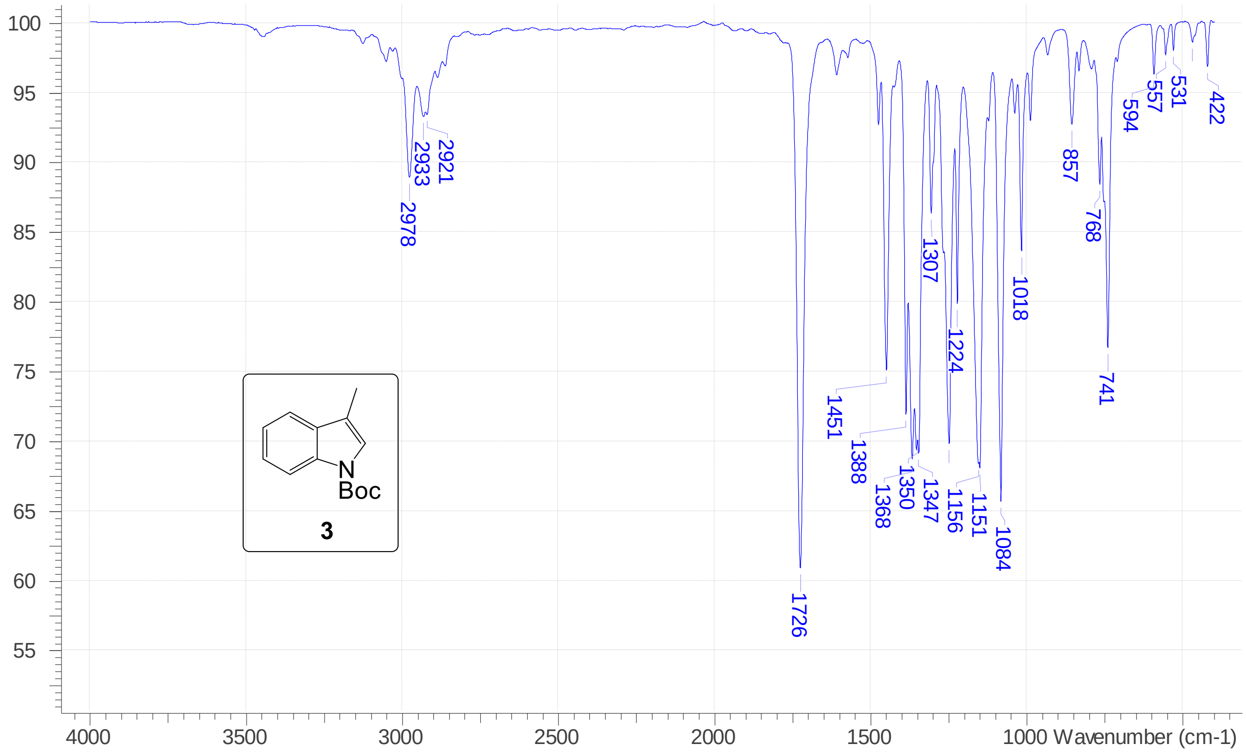

Figure S20. ATR-FTIR (neat) spectrum of compound **3**.

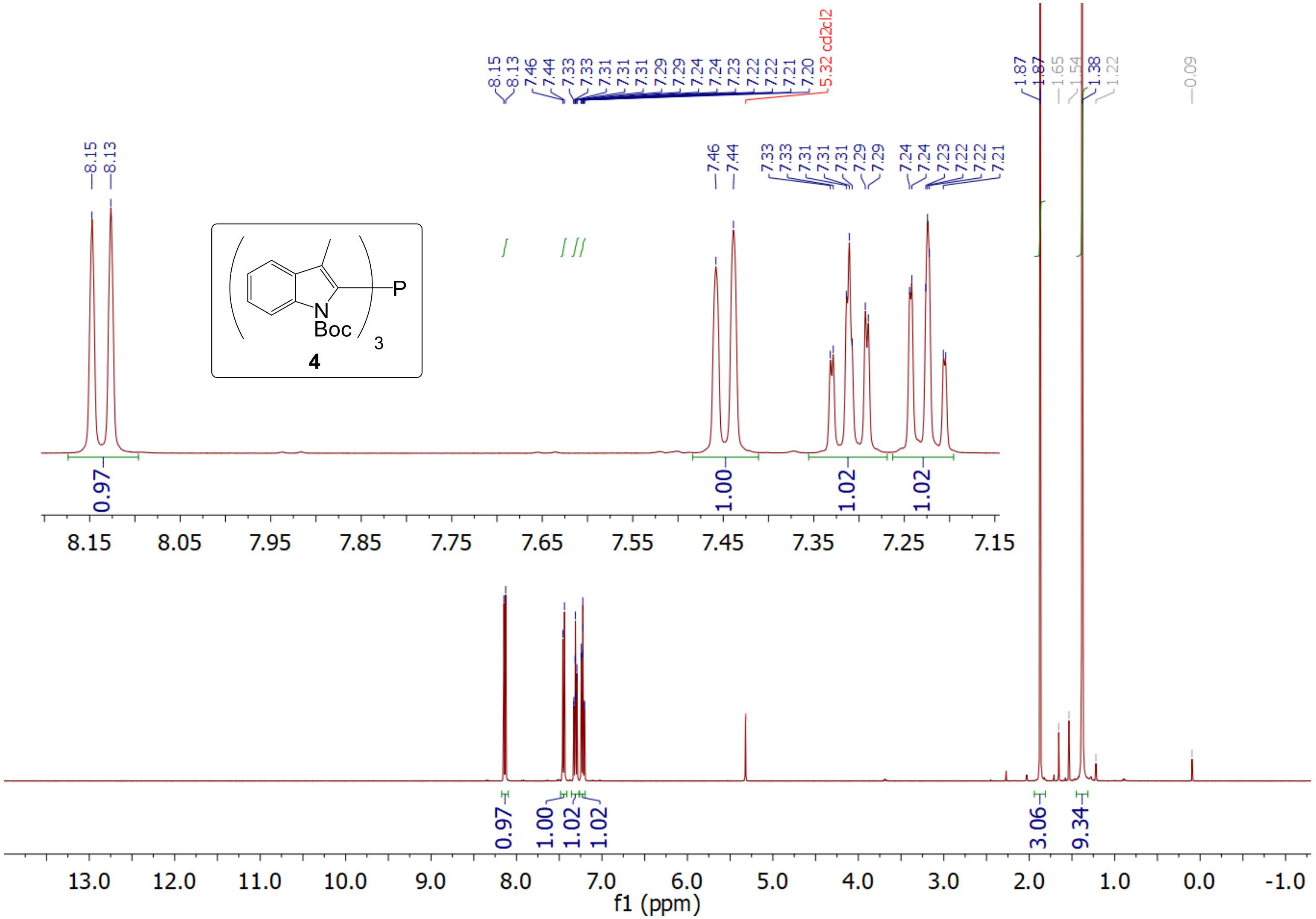

Figure S21. ^{1}H NMR spectrum of compound **4** in dichloromethane-d_2. Impurities: 0.09 ppm – traces of grease, 1.54 ppm – traces of water in deuterated solvent.

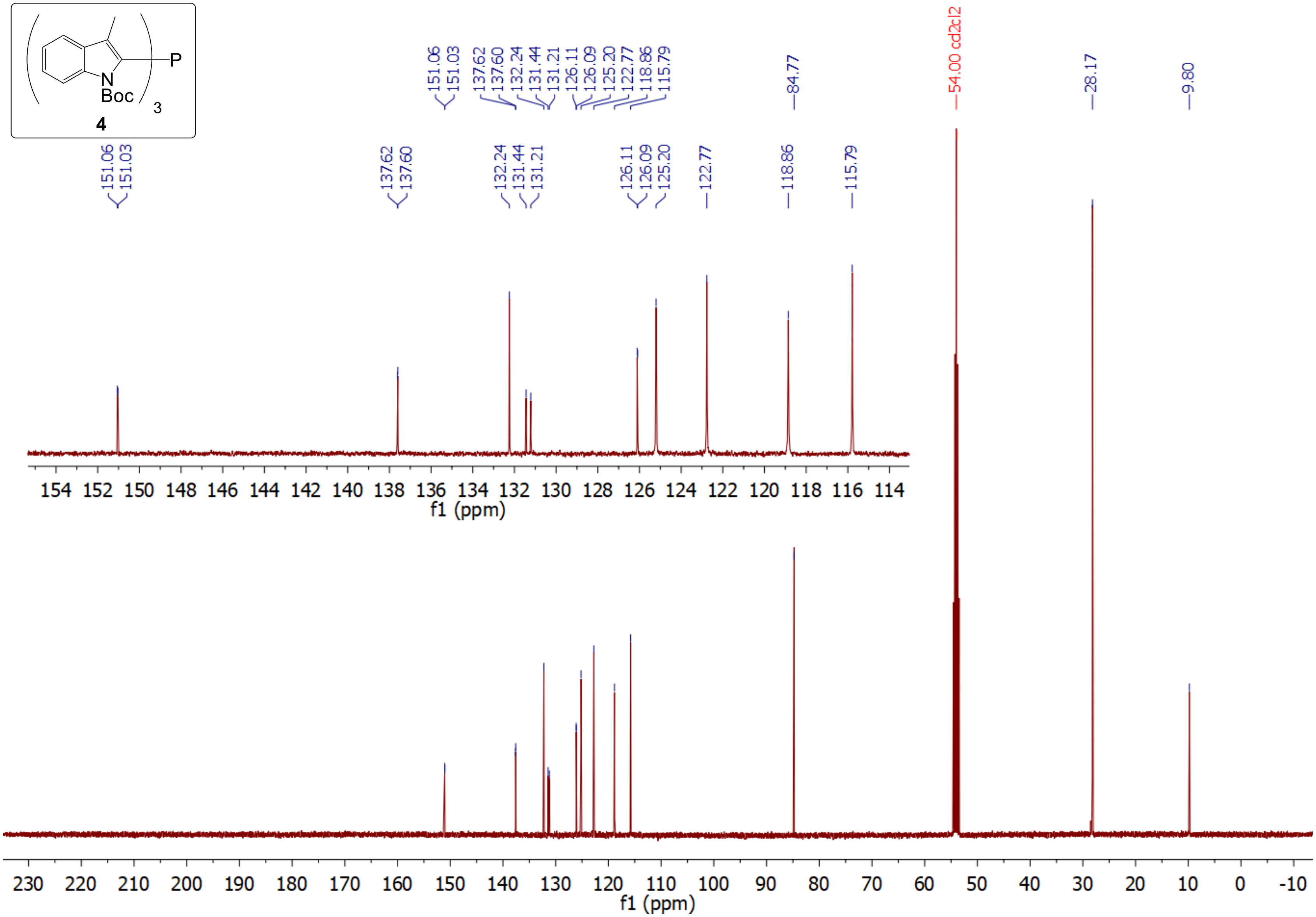

Figure S22. $^{13}C\{^{1}H\}$ NMR spectrum of compound **4** in dichloromethane-d_2.

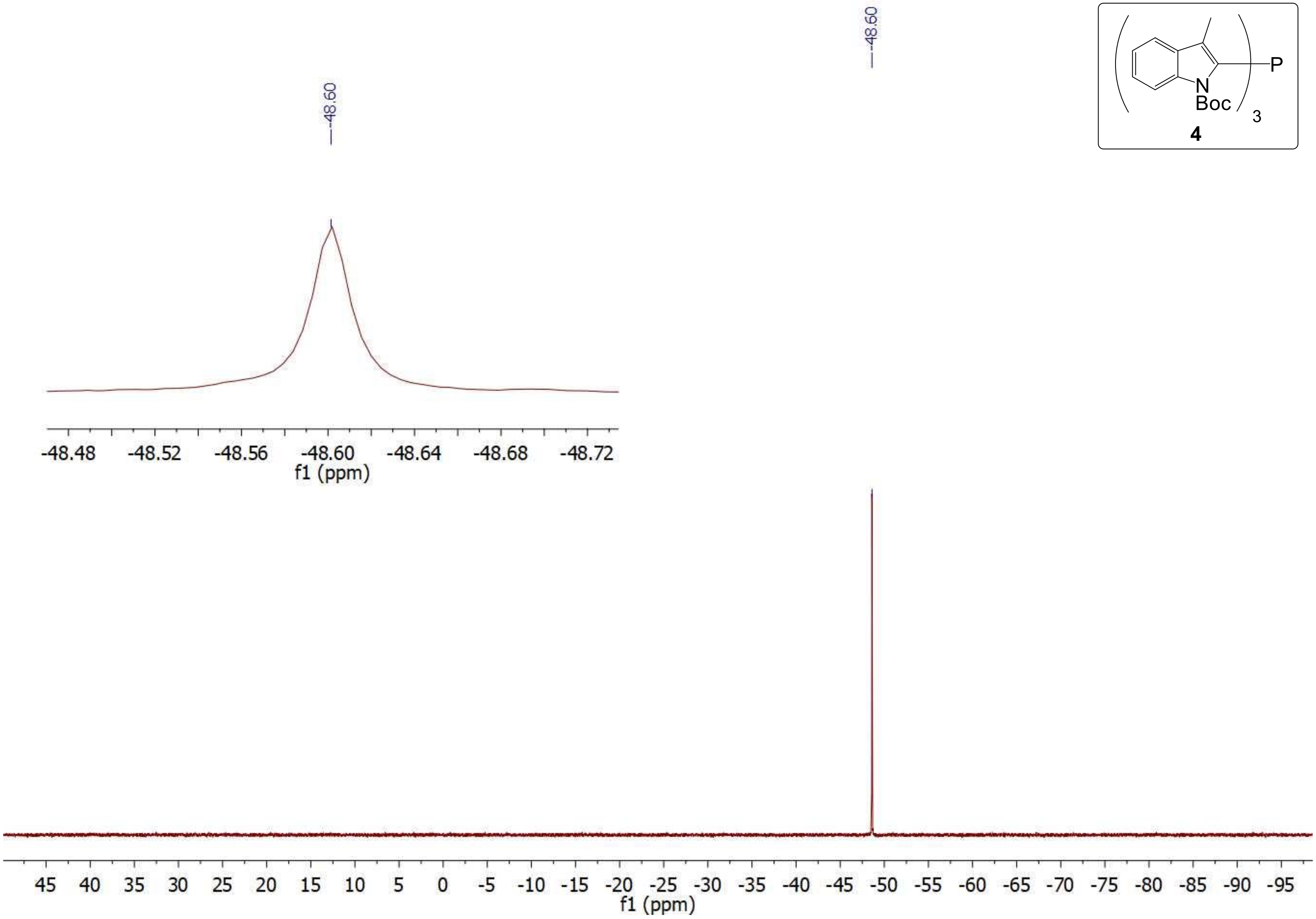

Figure S23. ^{31}P NMR spectrum of compound **4** in dichloromethane-d_2.

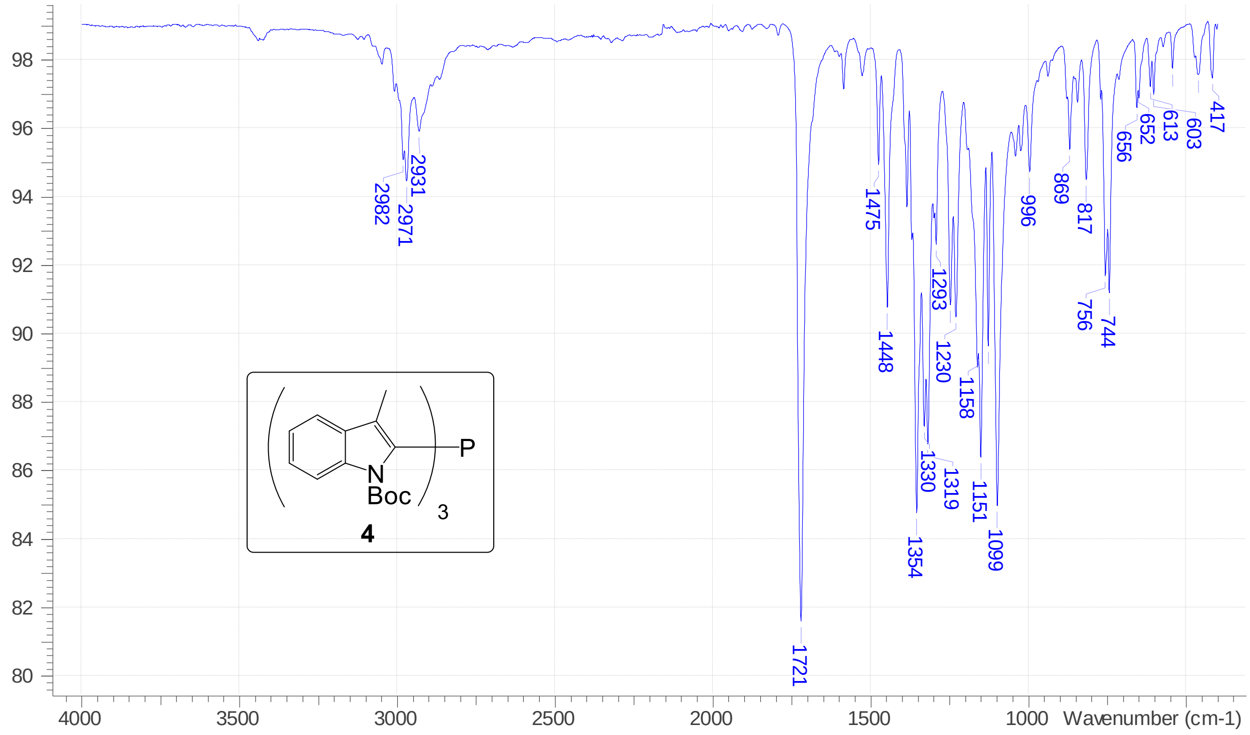

Figure S24. ATR-FTIR (neat) spectrum of compound **4**.

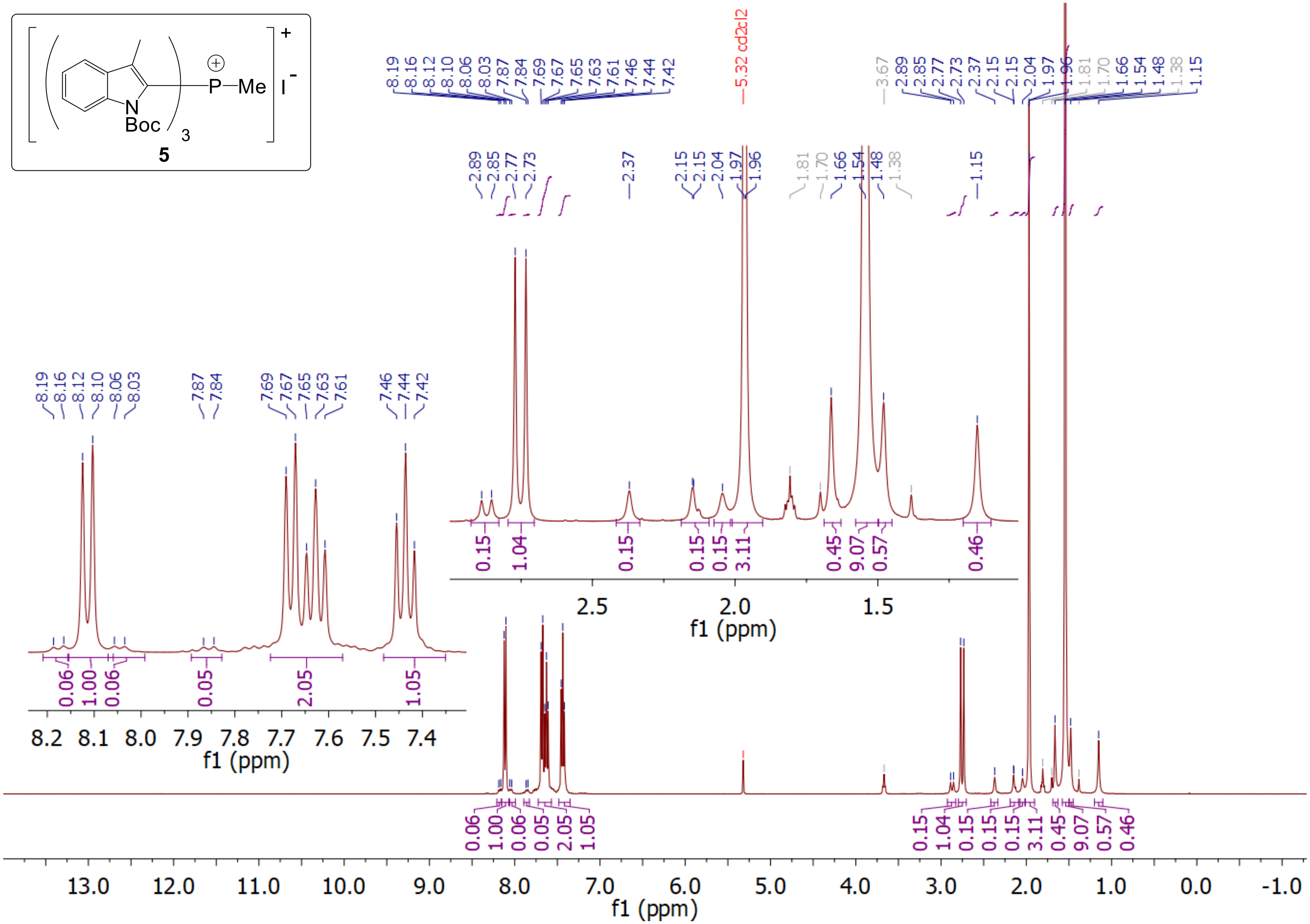

Figure S25. ^{1}H NMR spectrum of compound **5** in dichloromethane-d_2. Impurities: 1.81 and 3.67 ppm – traces of THF. The peaks at 1.38 and 1.70 ppm are ^{13}C satellites ($J_{H,C}$ = 127.4 Hz) of the peak at 1.54 ppm.

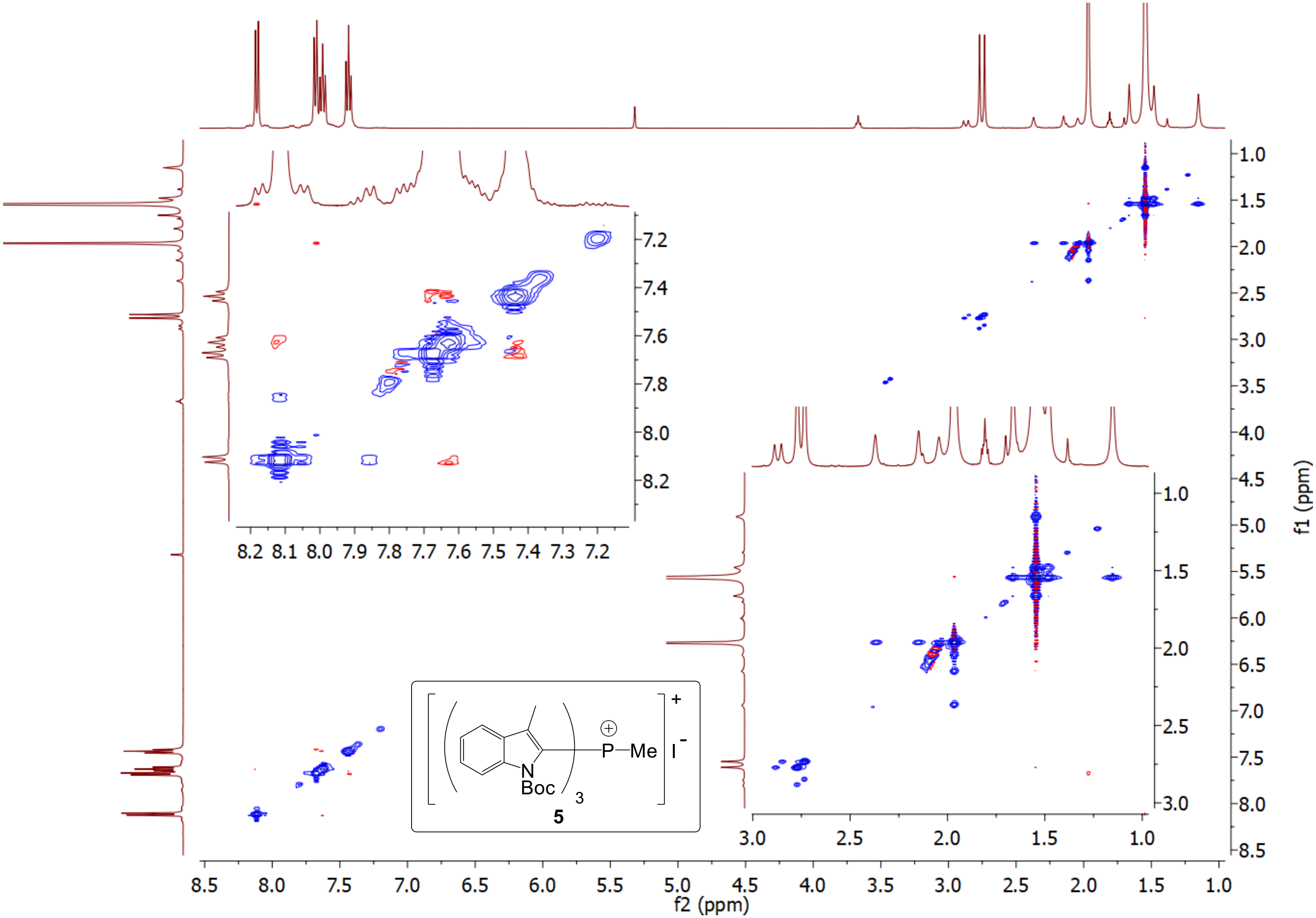

Figure S26. ^{1}H NOESY NMR spectrum of compound **5** in dichloromethane-d_2.

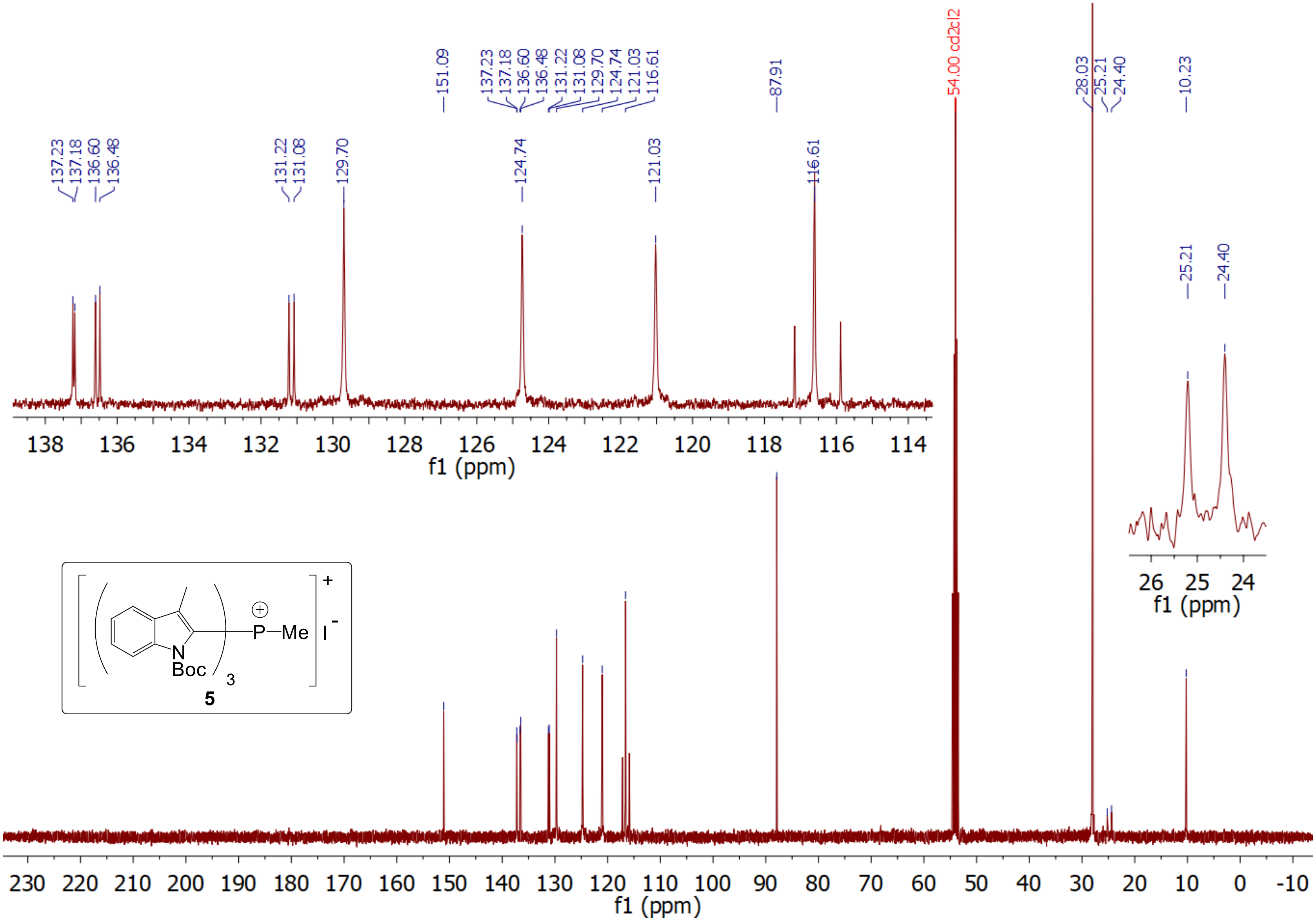

Figure S27. $^{13}C\{^{1}H\}$ NMR spectrum of compound **5** in dichloromethane-d_2.

5

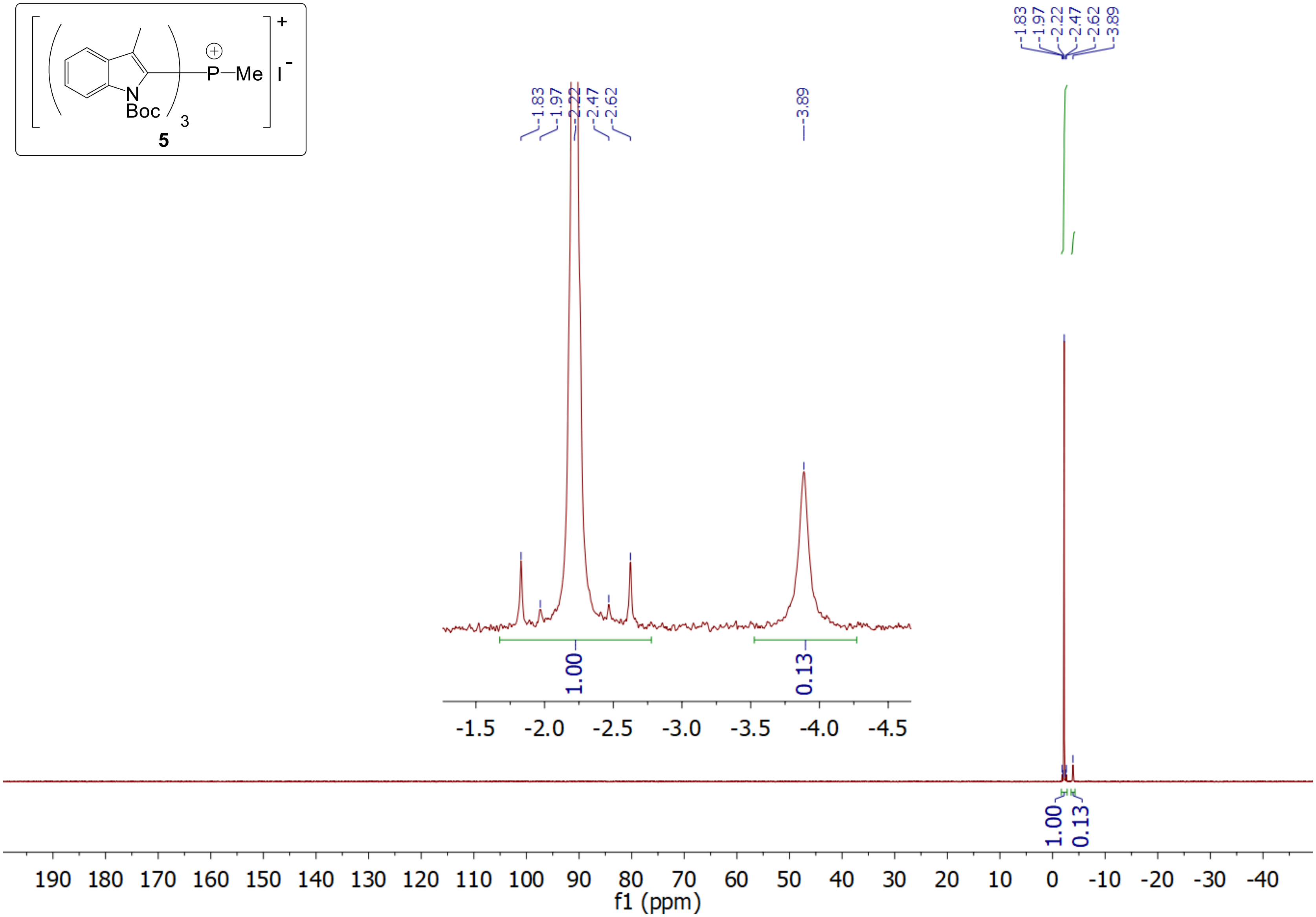

Figure S28. $^{31}P\{^{1}H\}$ NMR spectrum of compound **5** in dichloromethane-*d_2*.

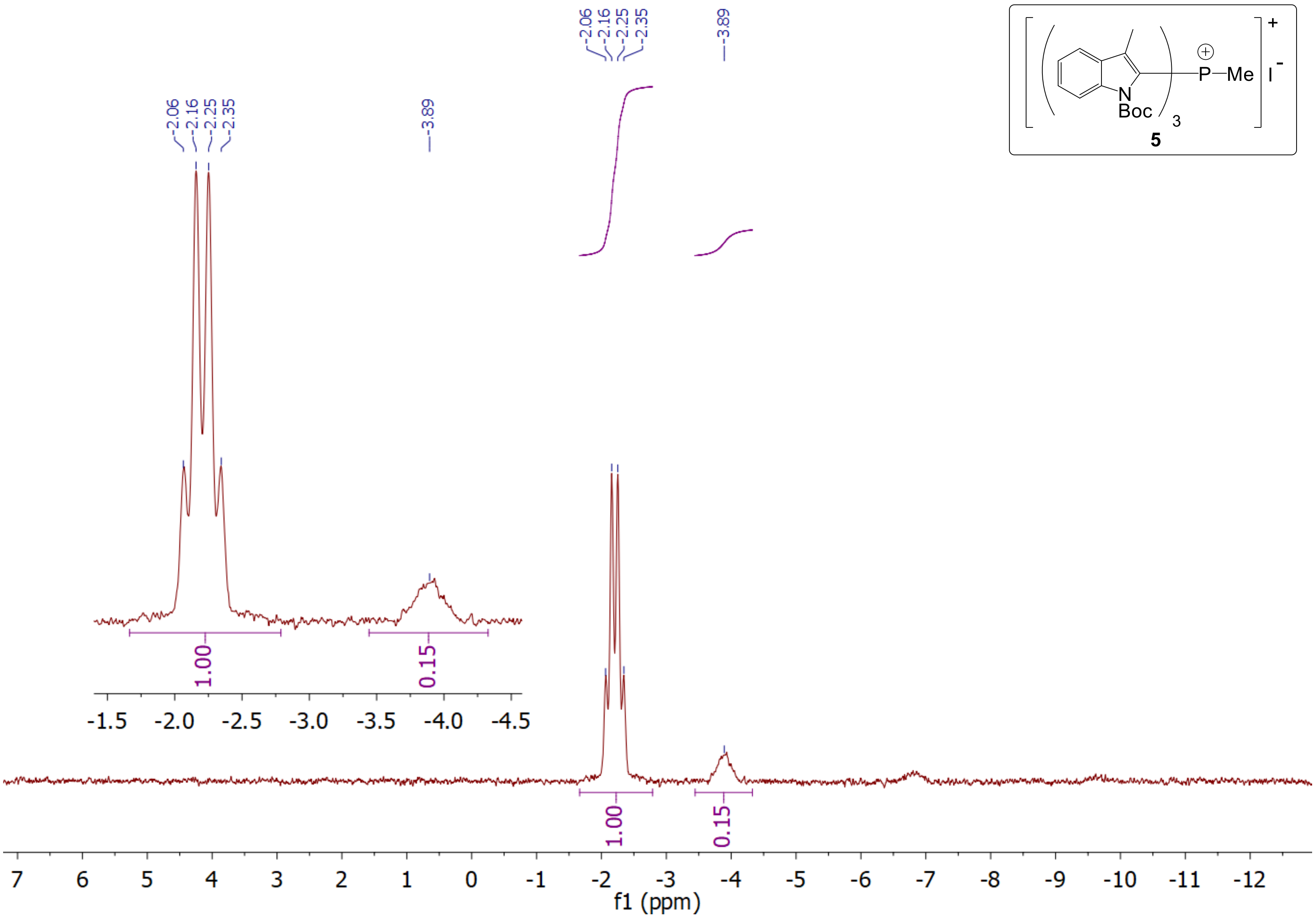

Figure S29. ^{31}P NMR spectrum of compound **5** in dichloromethane-d_2.

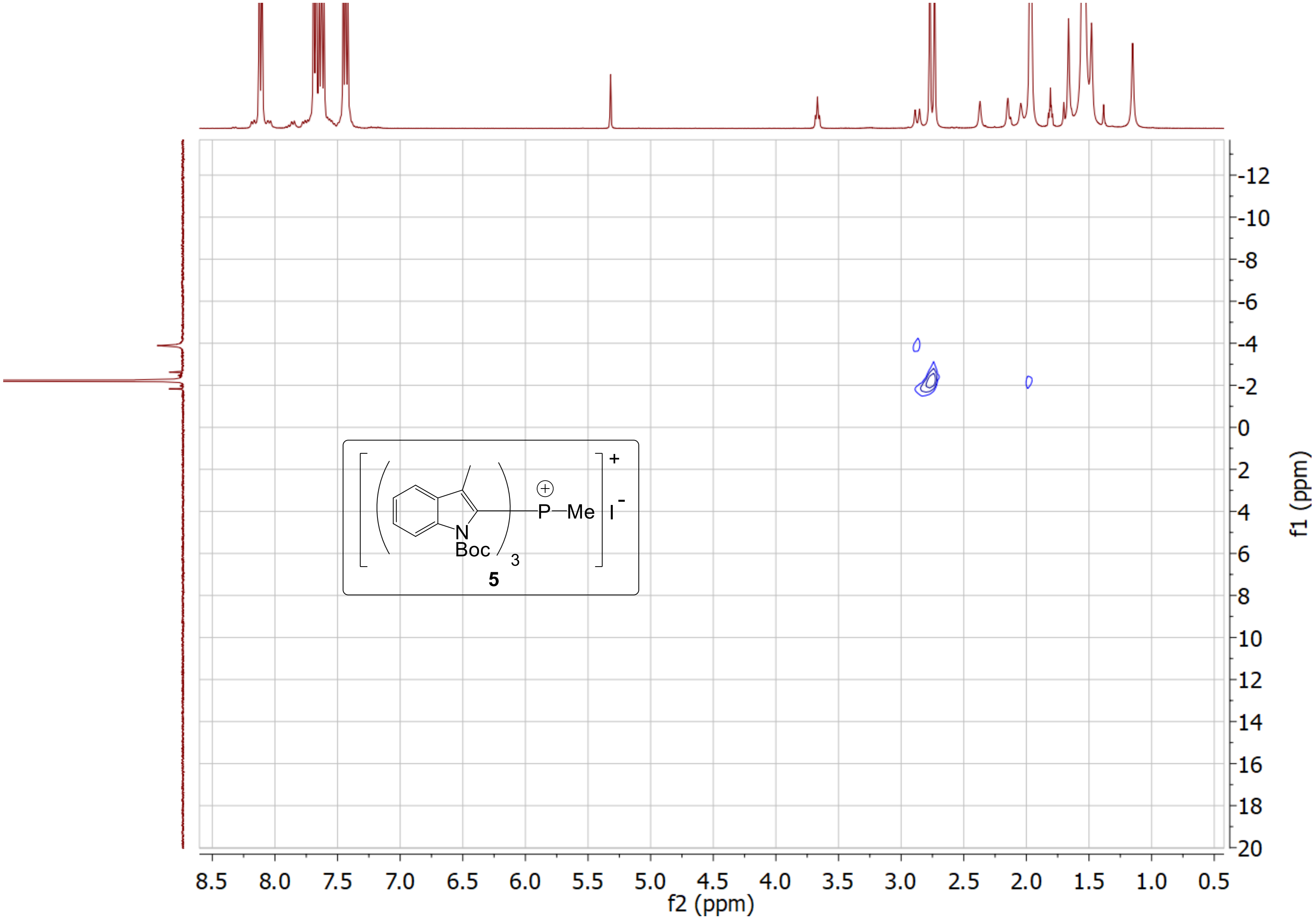

Figure S30. ^{1}H-^{31}P ASAPHMQC NMR spectrum of compound **5** in dichloromethane-d_2.

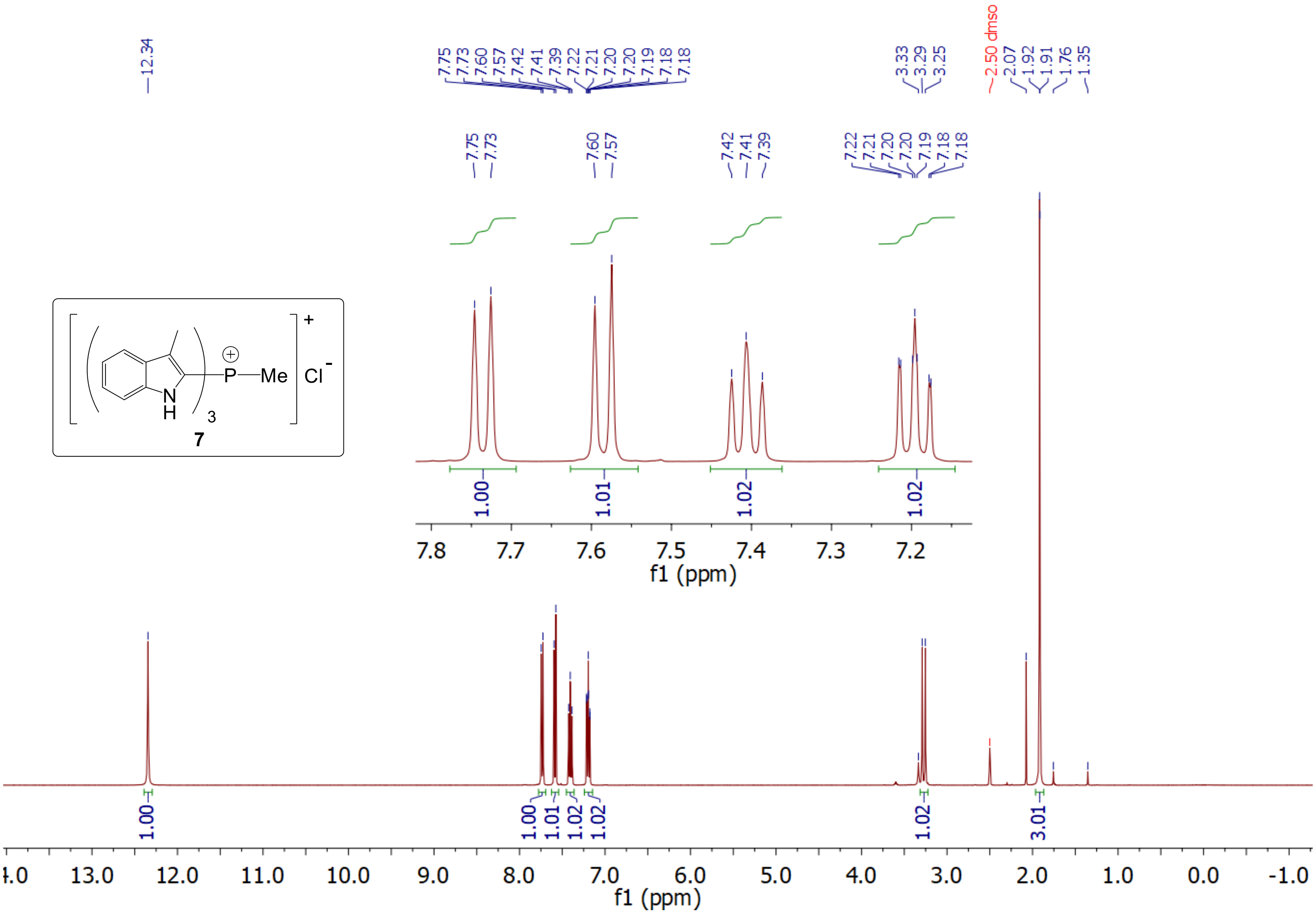

Figure S31. ^{1}H NMR spectrum of compound **7** in DMSO-d_6. Impurities: 2.07 ppm – acetonitrile, 3.33 ppm – traces of water, other minor peaks are unidentified impurities.

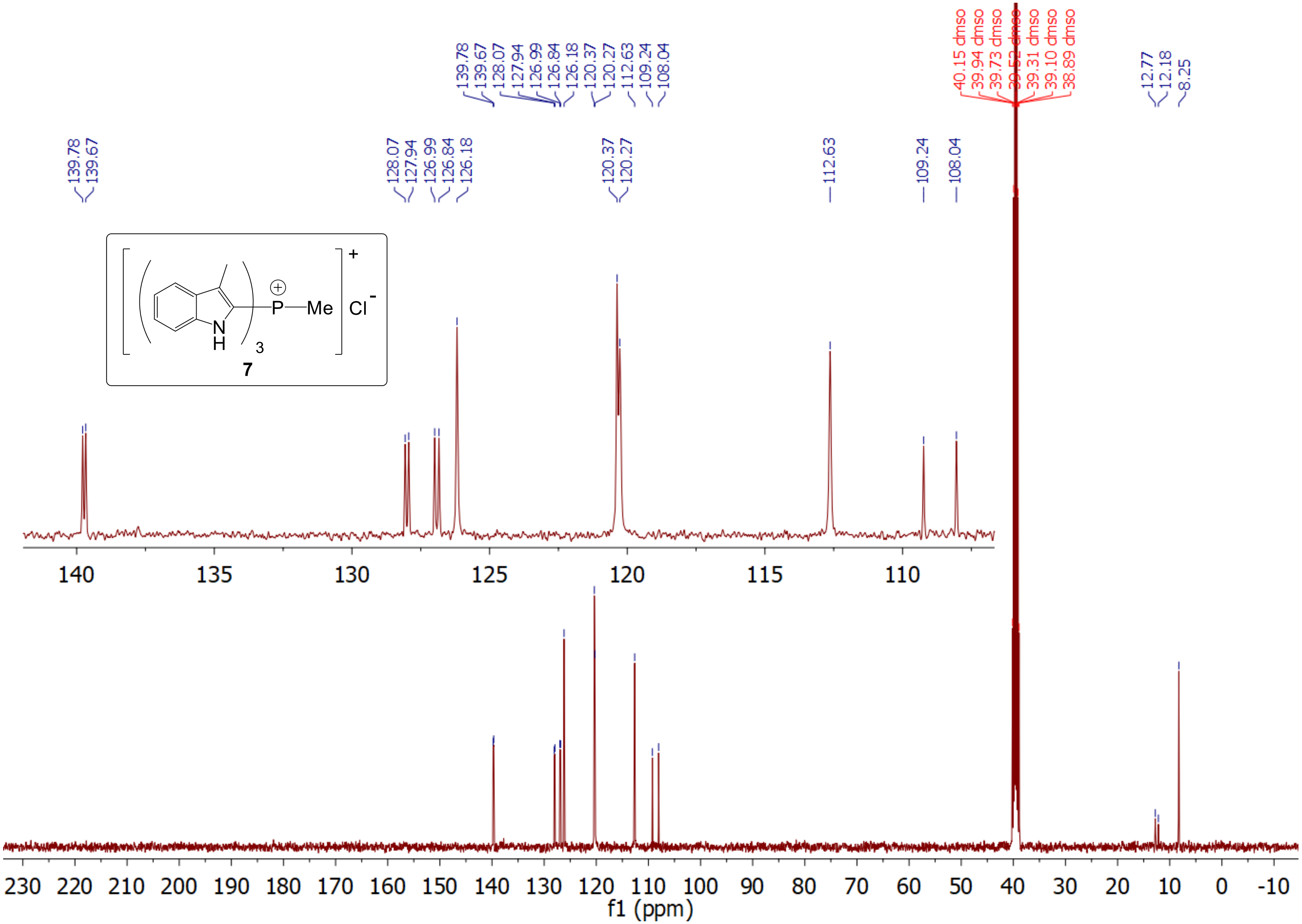

Figure S32. $^{13}C\{^{1}H\}$ NMR spectrum of compound **7** in DMSO-d_6.

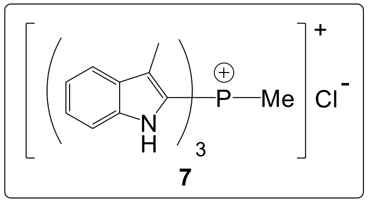

7

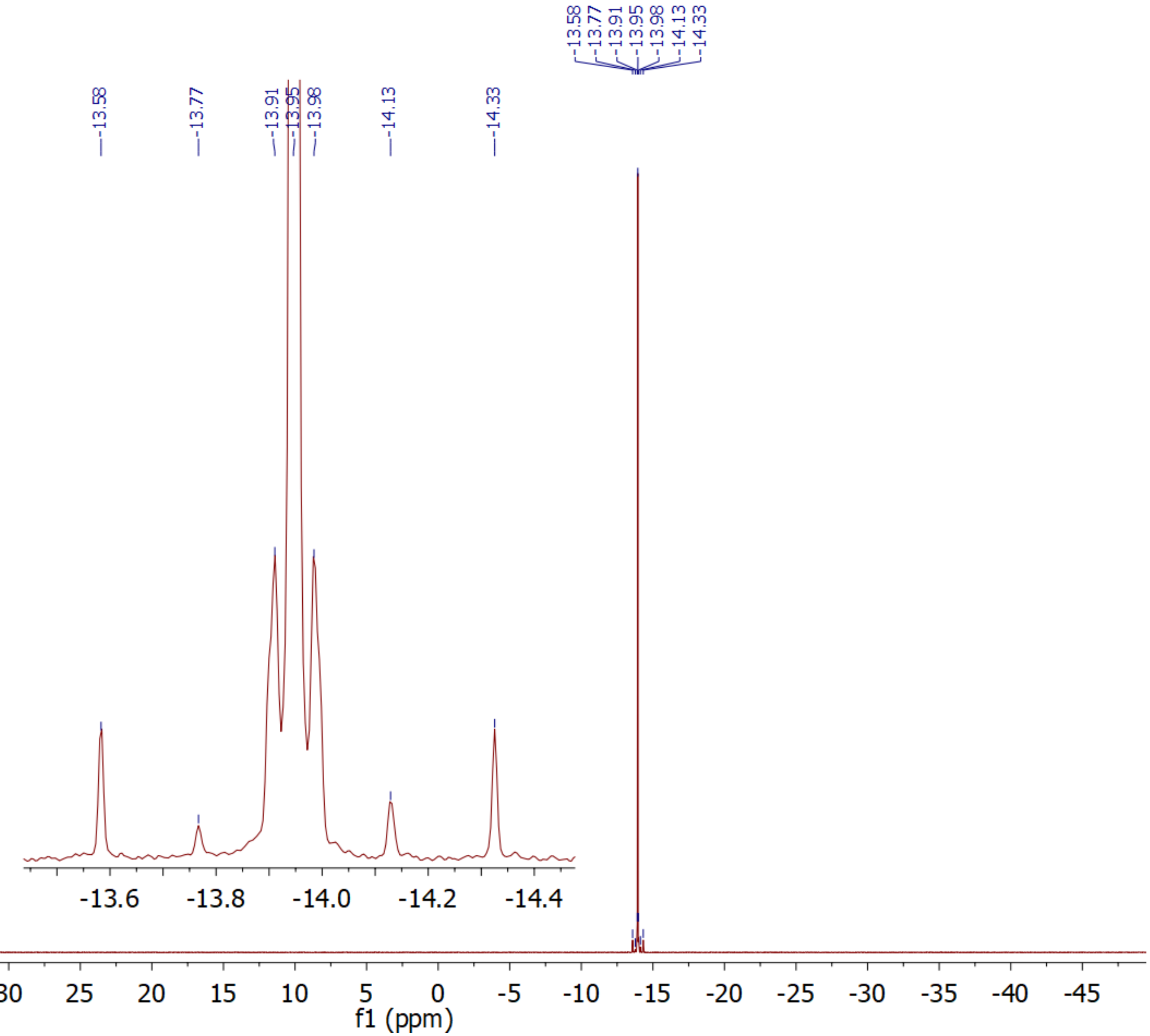

Figure S33. $^{31}P\{^{1}H\}$ NMR spectrum of compound **7** in DMSO-*d*$_6$.

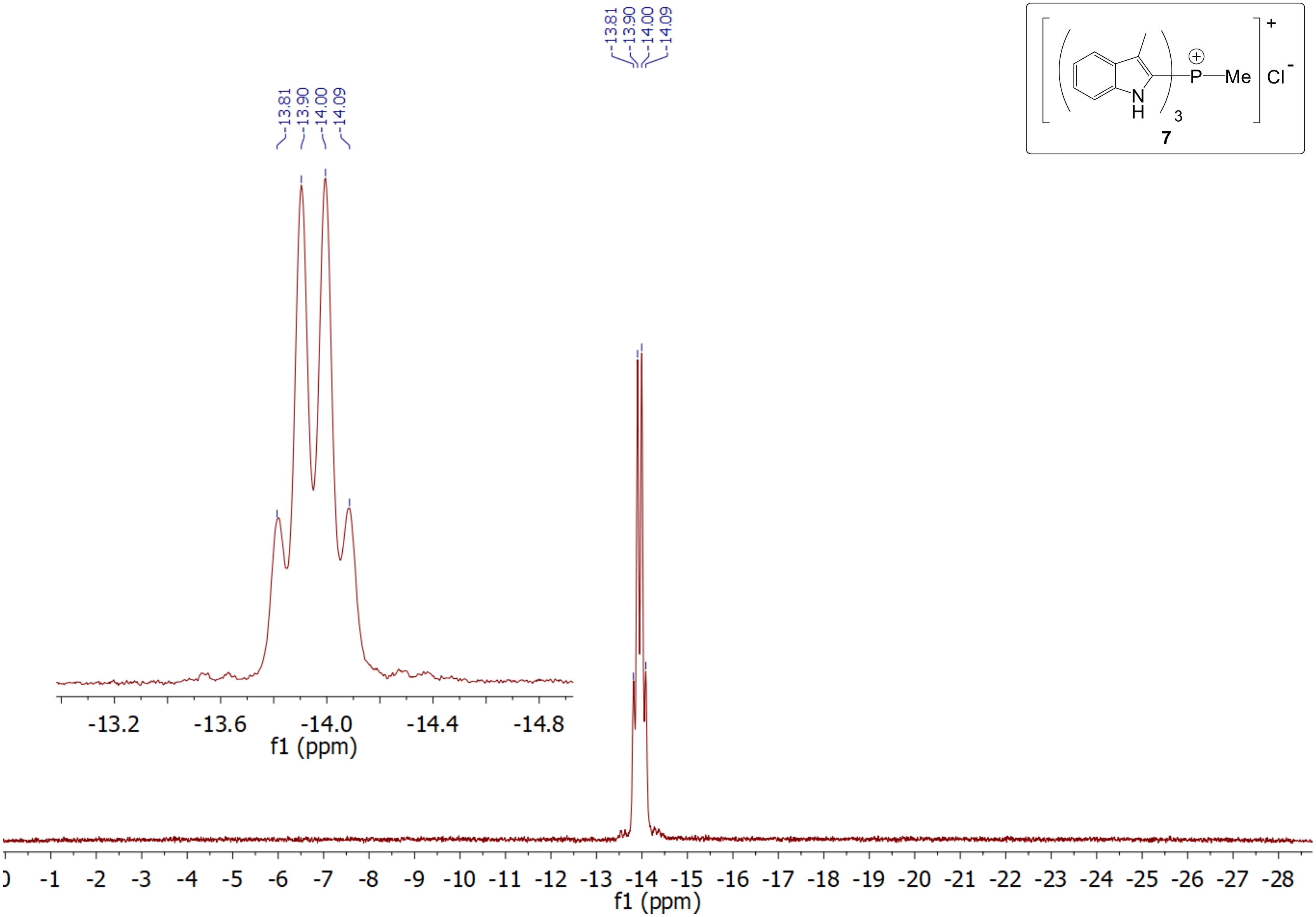

7

Figure S34. ^{31}P NMR spectrum of compound **7** in DMSO-d_6.

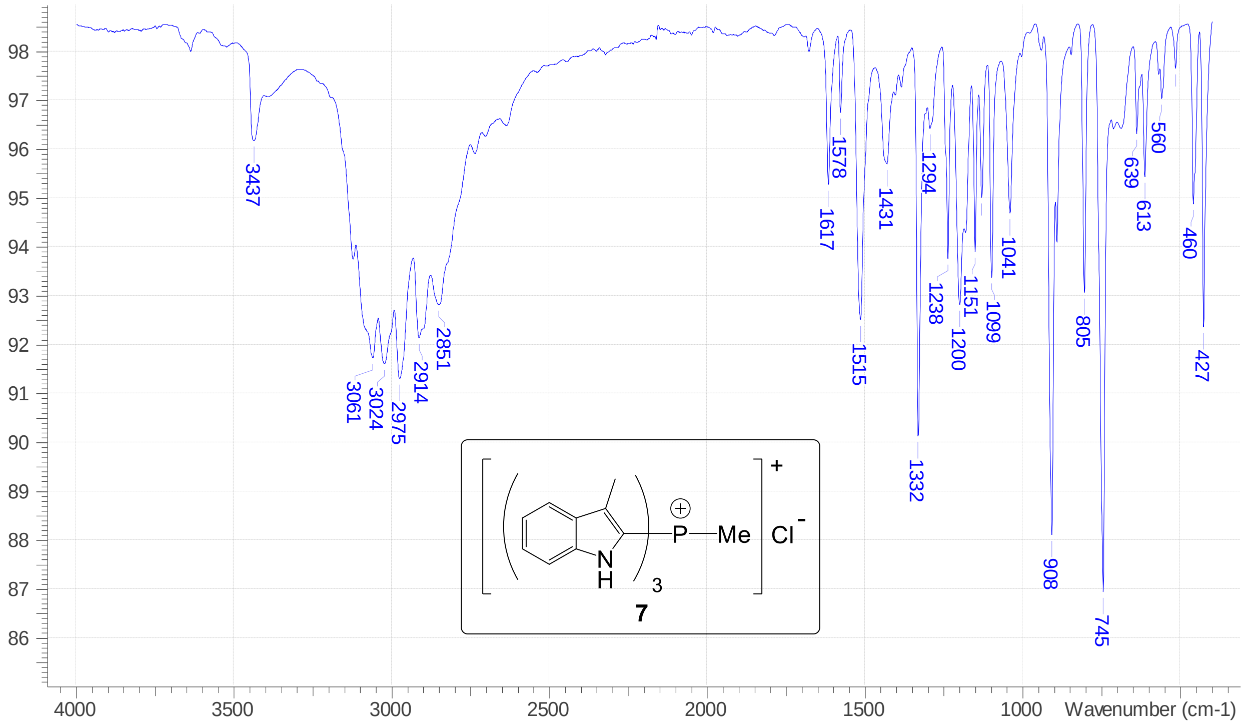

Figure S35. ATR-FTIR (neat) spectrum of compound **7**.

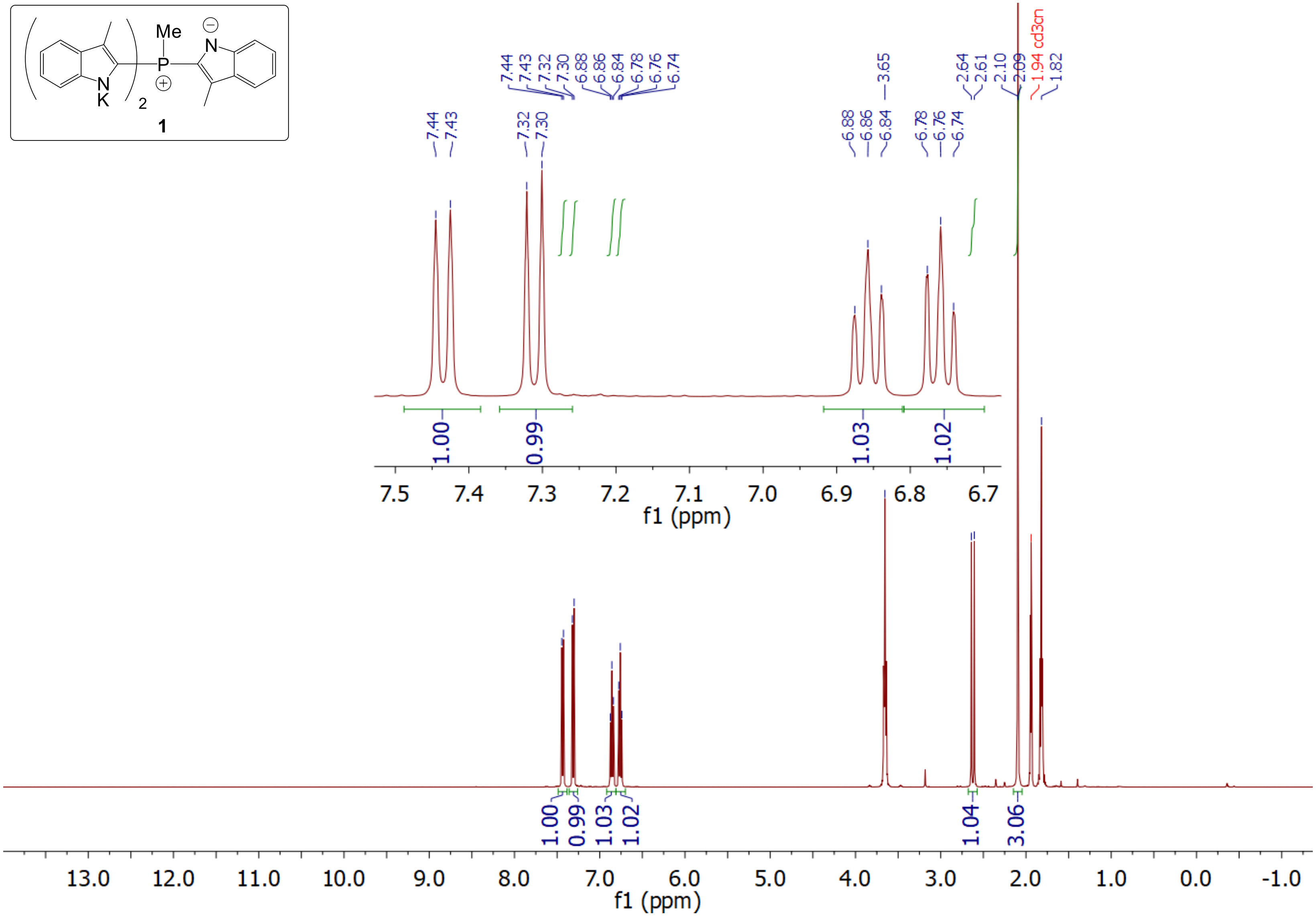

Figure S36. ^{1}H NMR spectrum of compound **1** in acetonitrile-d_3. Impurities: 1.82 and 3.65 ppm – traces of THF, other minor peaks – unidentified impurities.

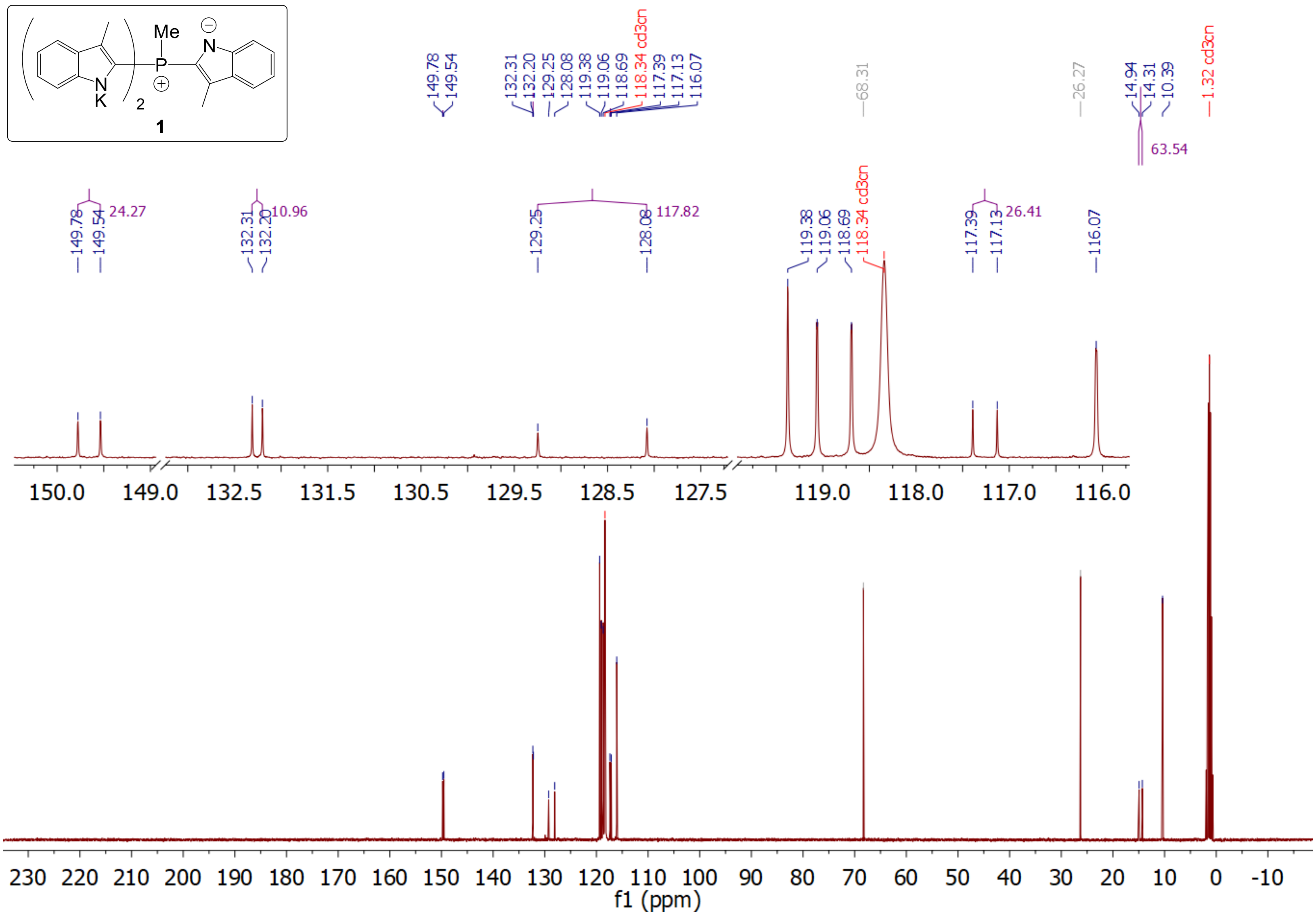

Figure S37. $^{13}C\{^{1}H\}$ NMR spectrum of compound **1** in acetonitrile-d_3.

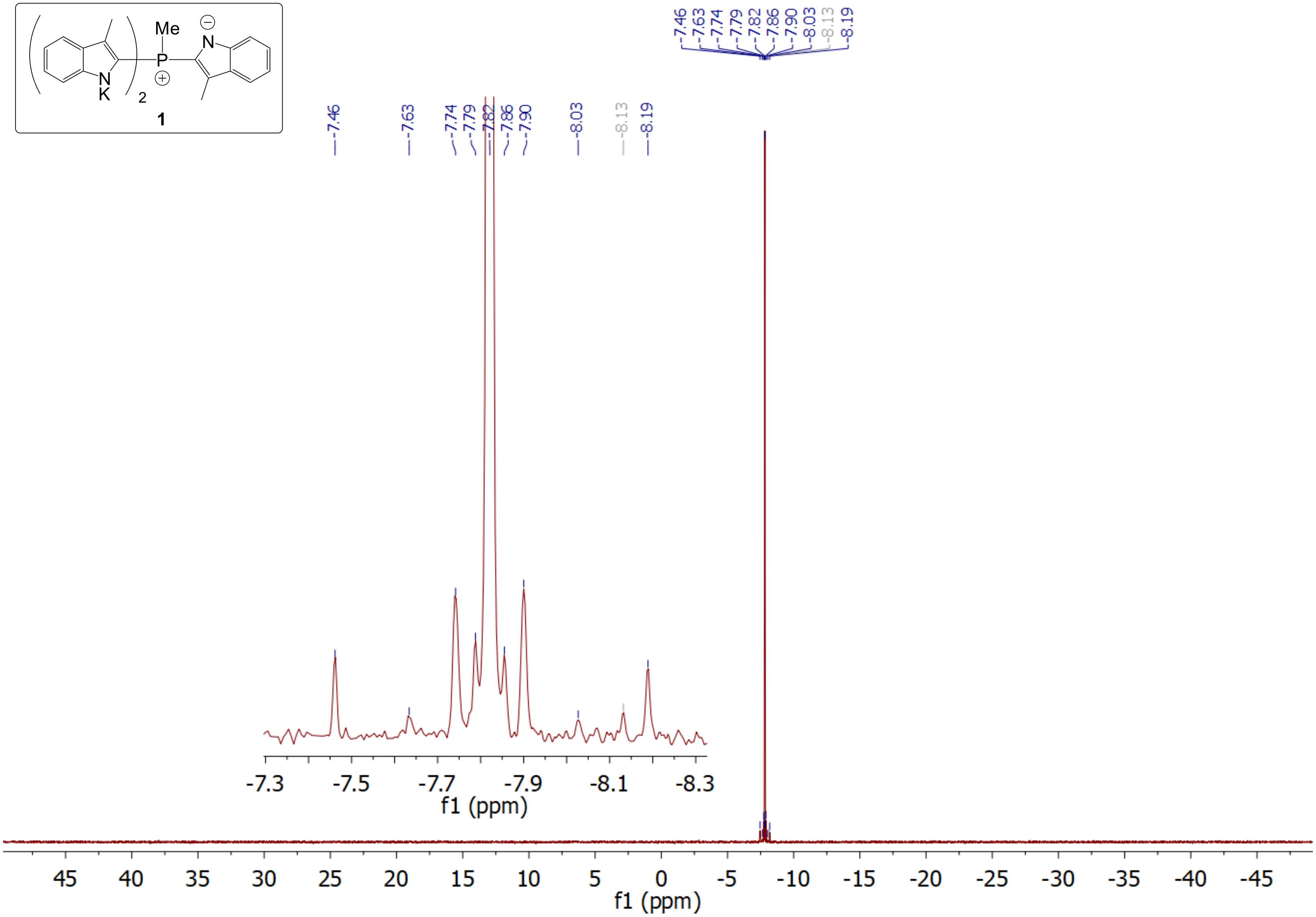

Figure S38. $^{31}P\{^{1}H\}$ NMR spectrum of compound **1** in acetonitrile-*d_3*. Impurities: -8.13 ppm – unidentified.

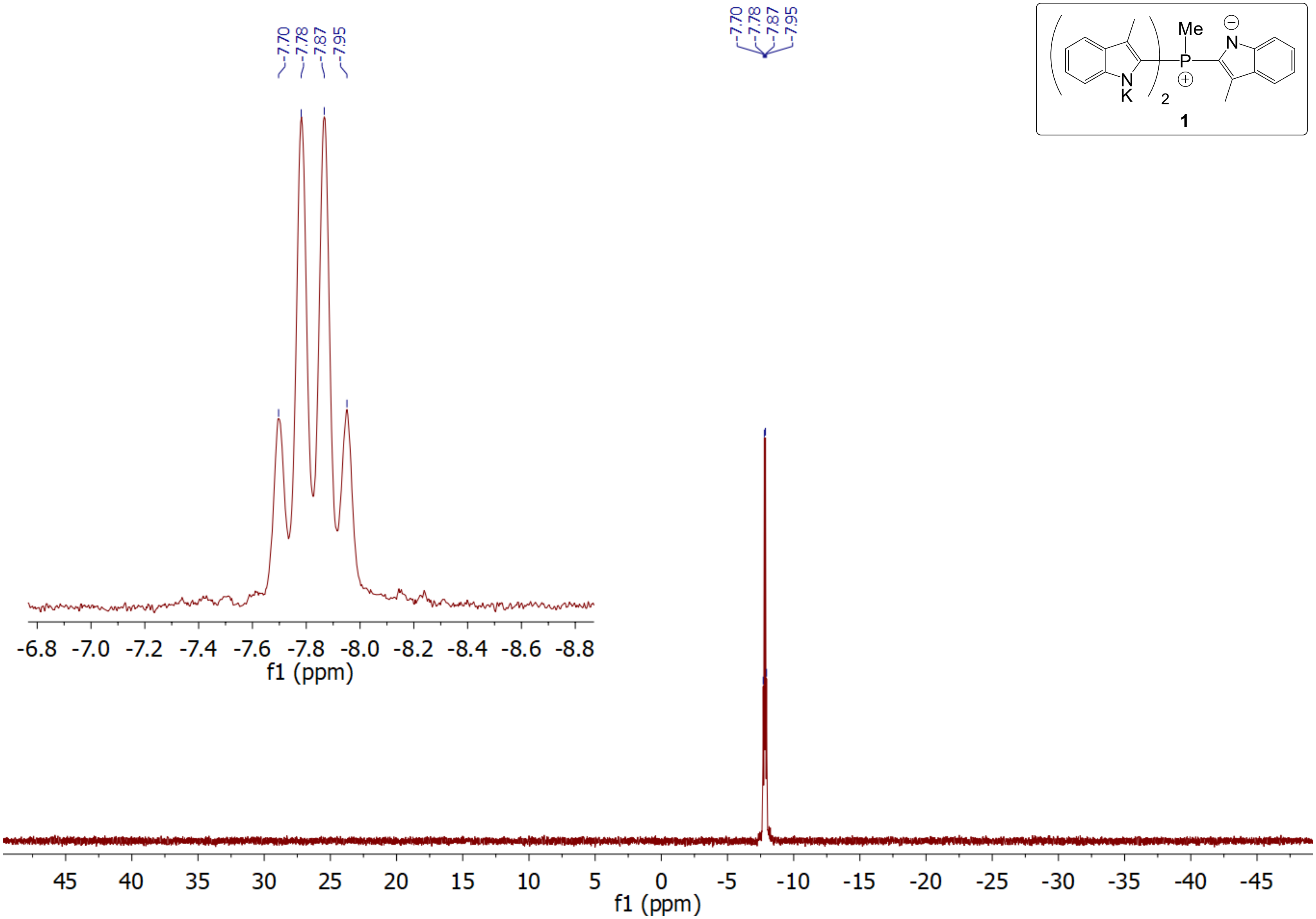

Figure S39. ^{31}P NMR spectrum of compound **1** in acetonitrile-d_3.

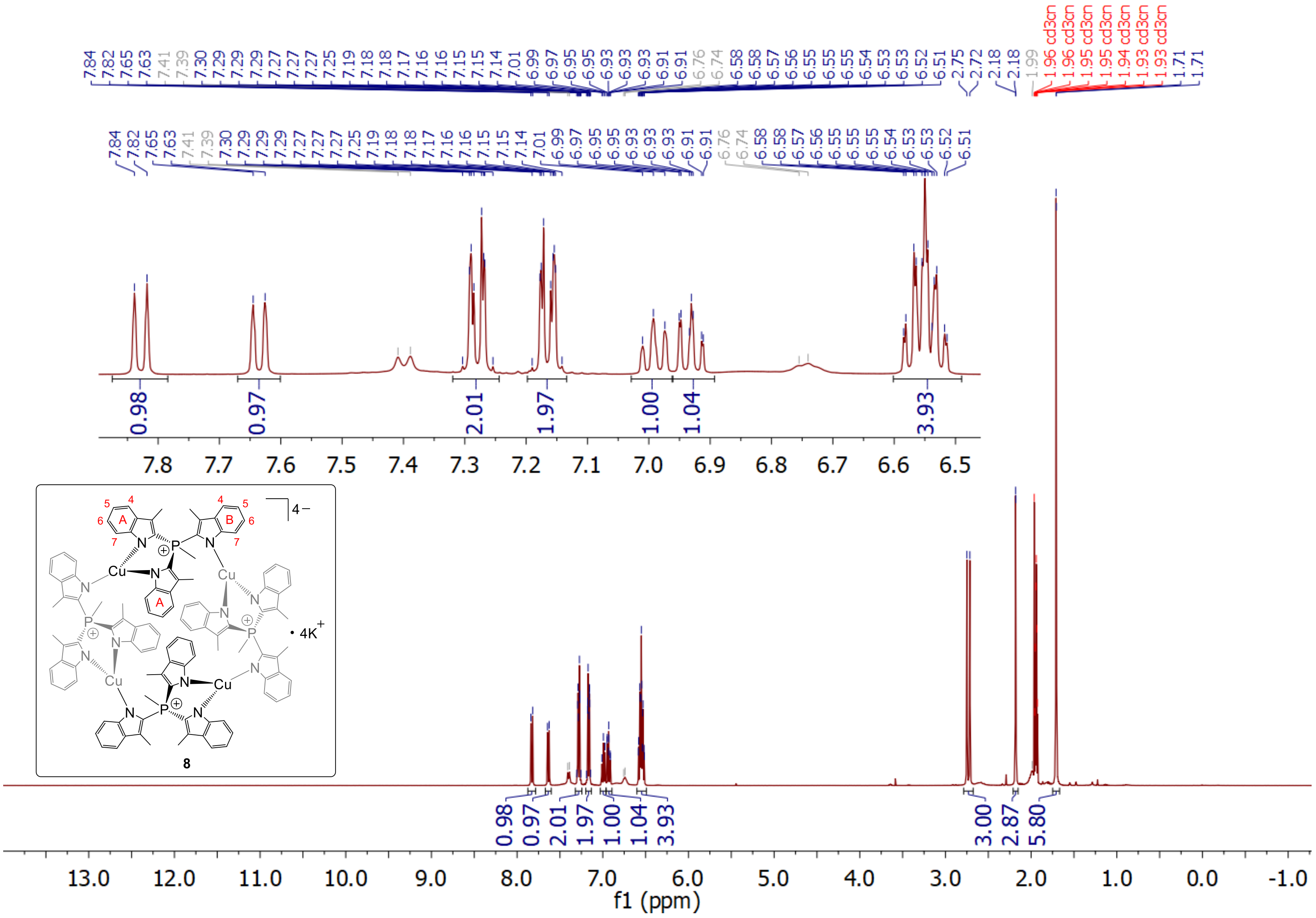

Figure S40. ^{1}H NMR spectrum of complex **8** in acetonitrile-d_3. Peaks at 6.7-6.8 ppm and ca. 7.4 ppm belong to a minor unassigned form of **8** in solution.

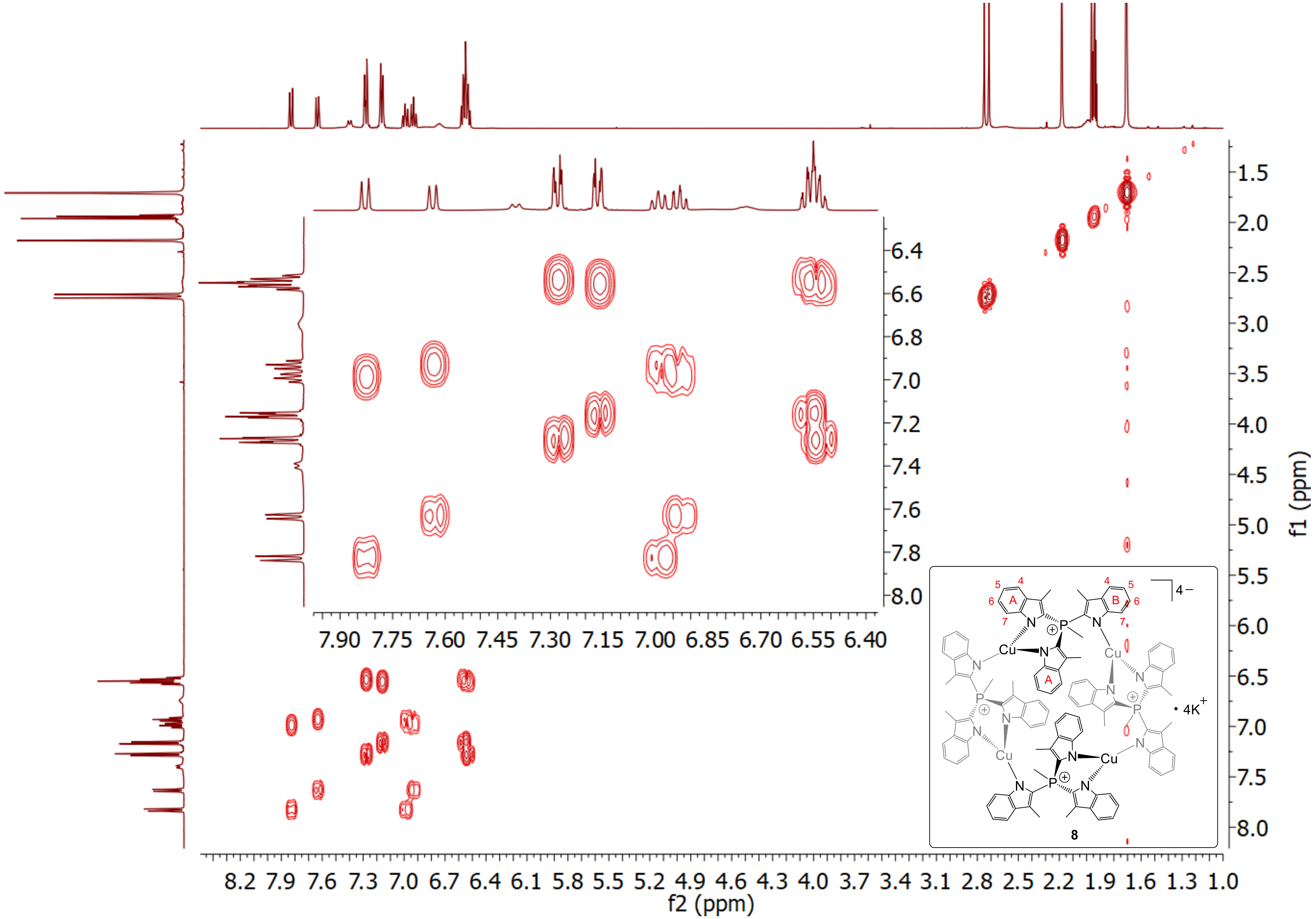

Figure S41. ^{1}H gCOSY spectrum of complex **8** in acetonitrile-d_3.

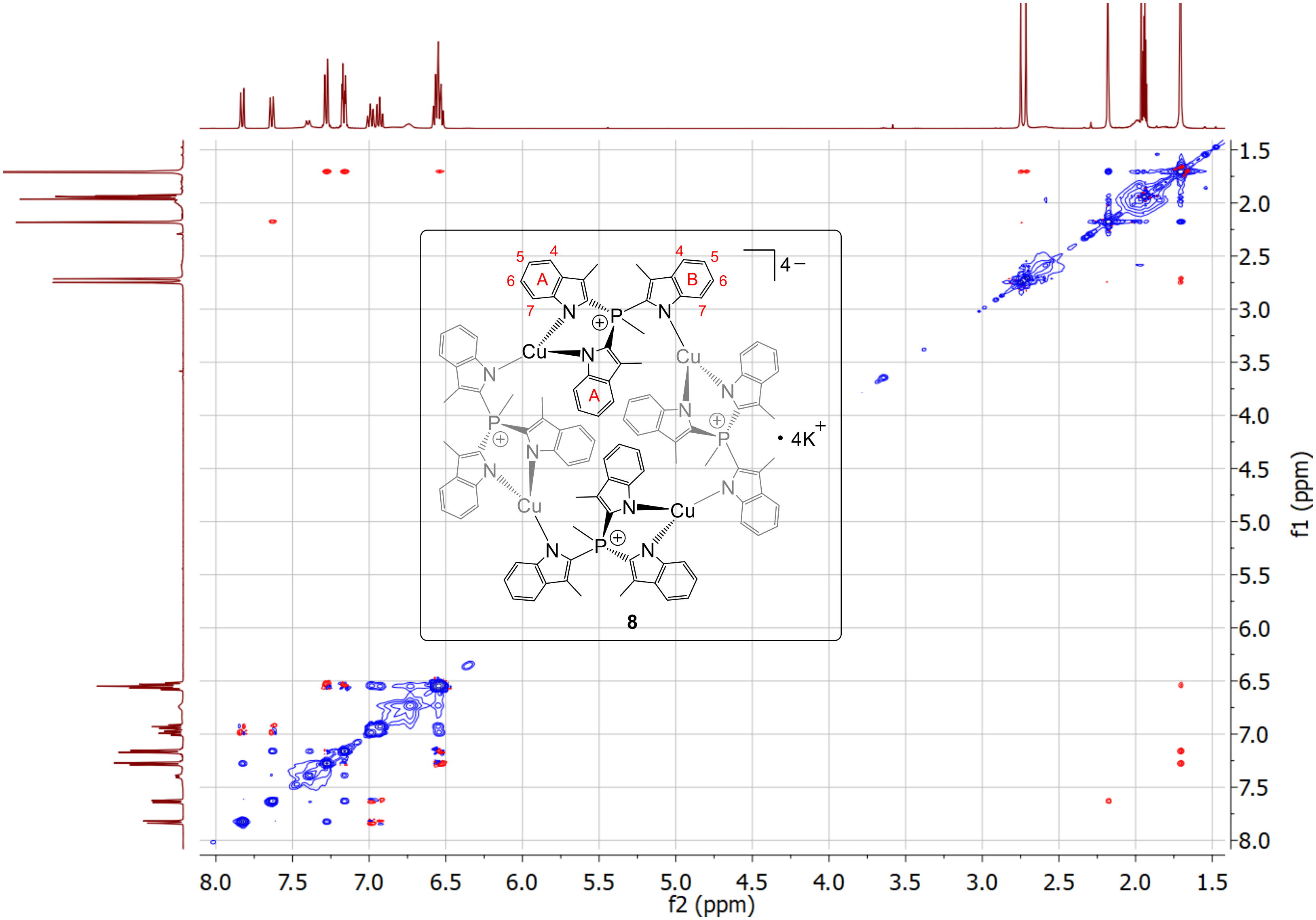

Figure S42. ^{1}H NOESY spectrum of complex **8** in acetonitrile-*d*$_3$.

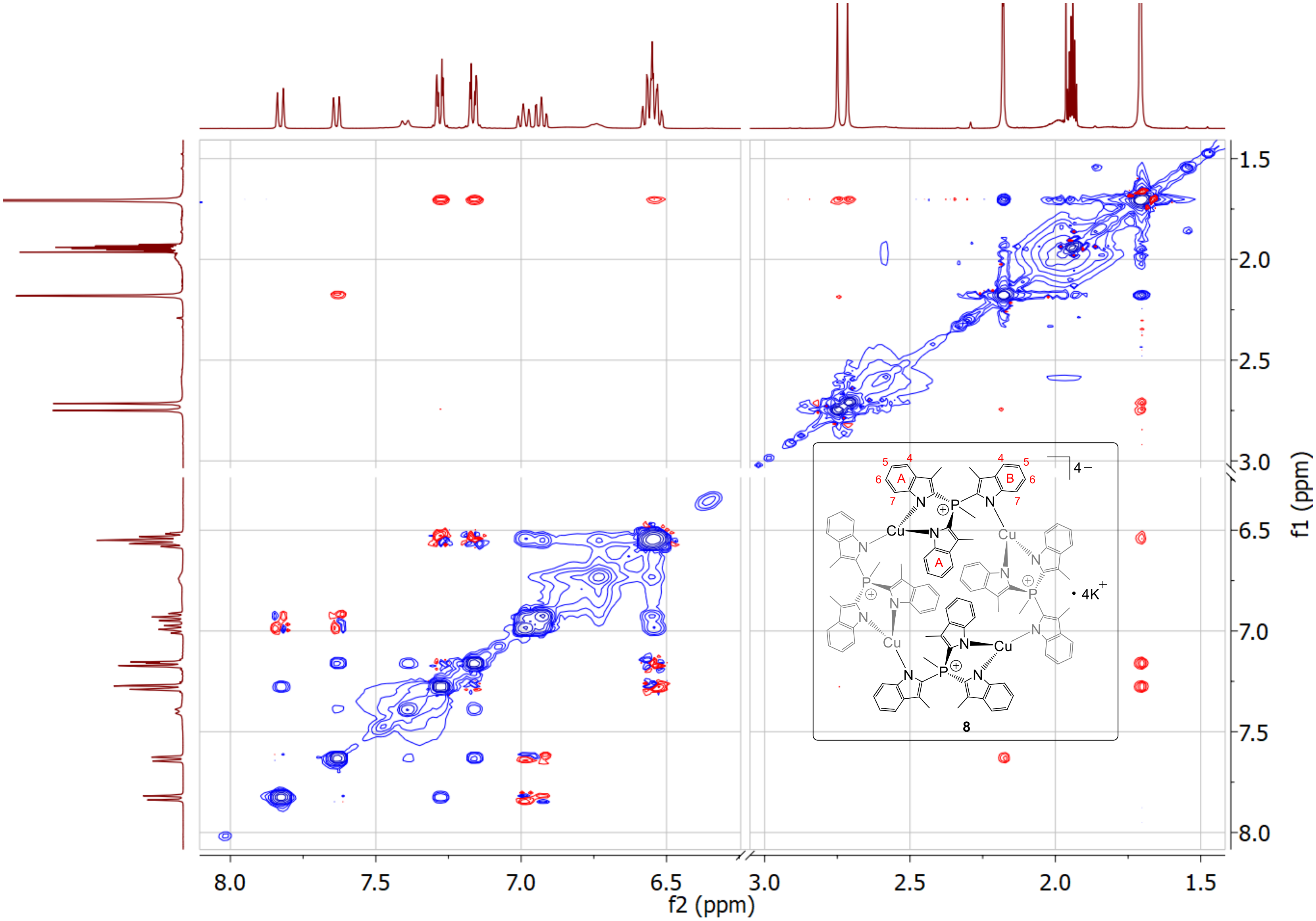

Figure S43. ^{1}H NOESY spectrum of complex **8** in acetonitrile-d_3 (expanded).

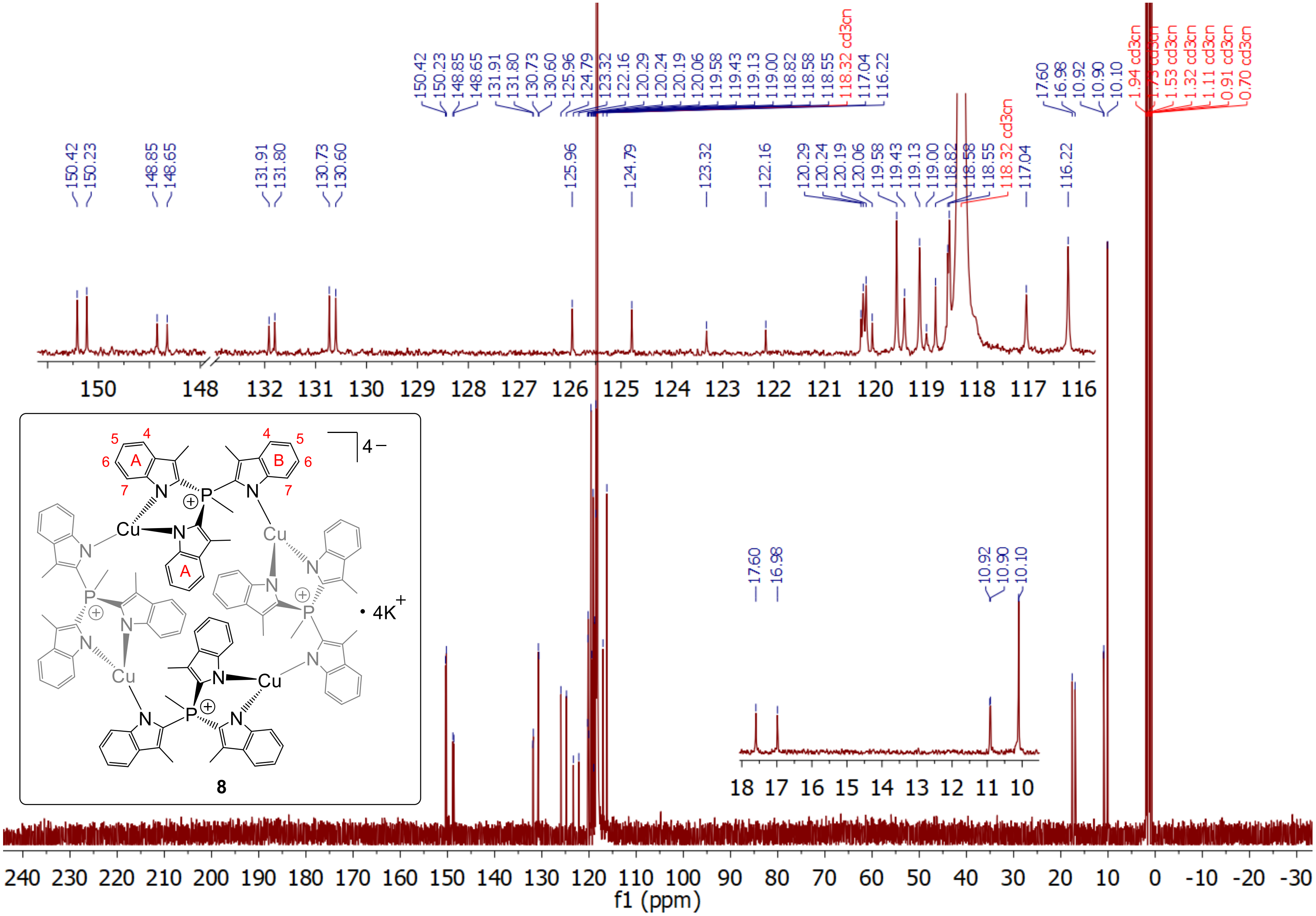

Figure S44. $^{13}C\{^1H\}$ NMR spectrum of complex **8** in acetonitrile-d_3.

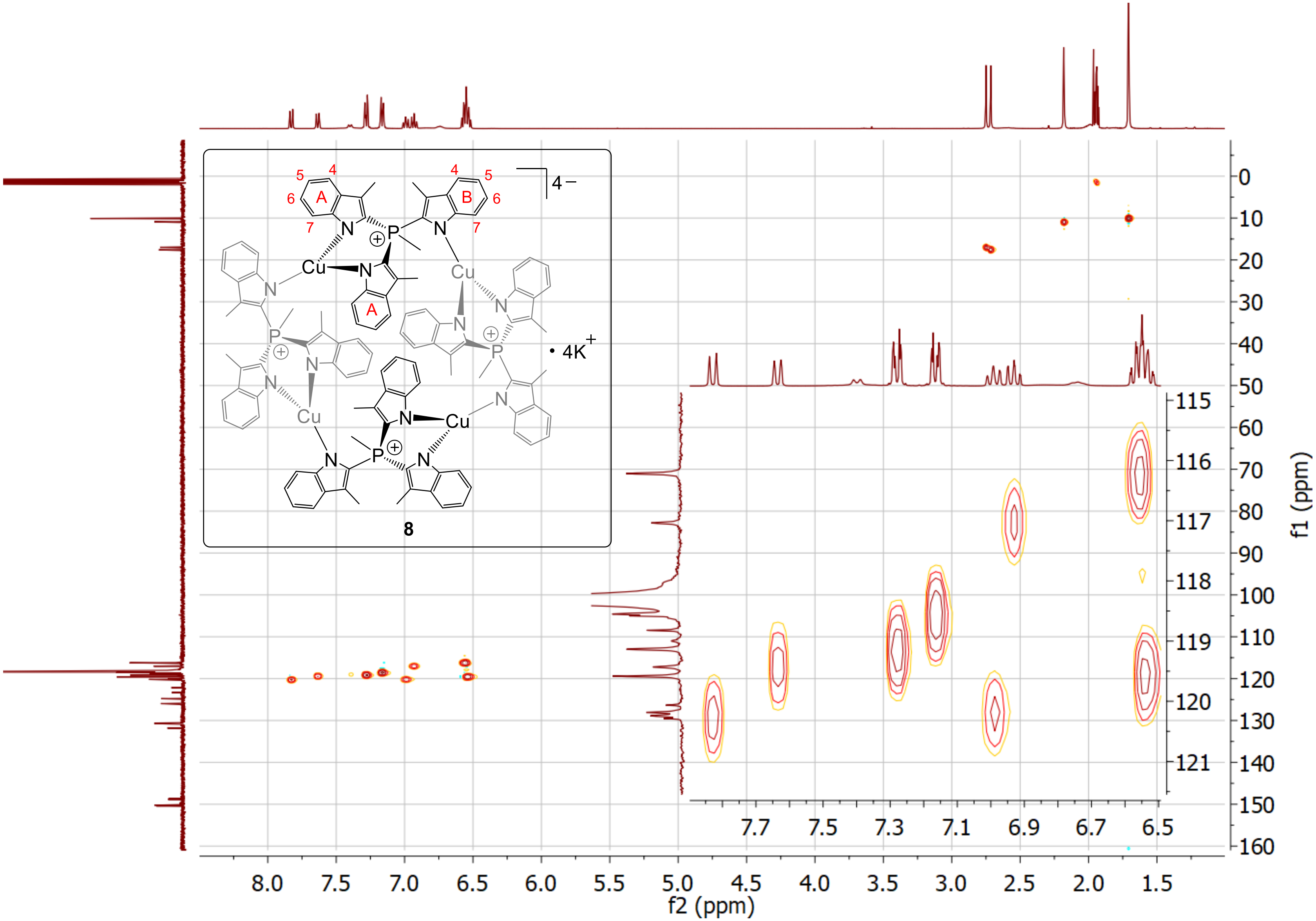

Figure S45. ^{1}H-^{13}C HSQC spectrum of complex **8** in acetonitrile-d_3.

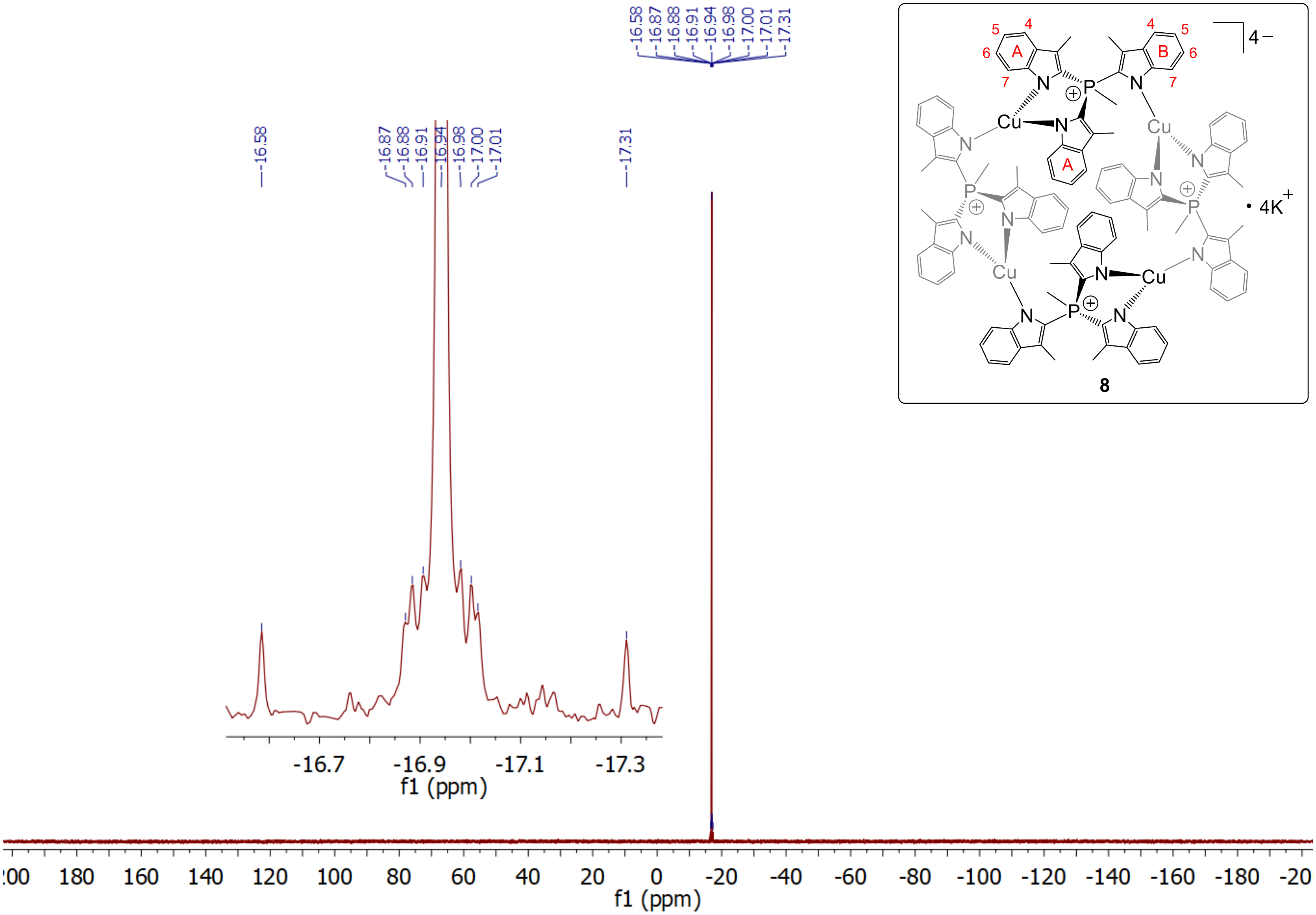

Figure S46. ^{31}P{^{1}H} NMR spectrum of complex **8** in acetonitrile-*d*$_3$.

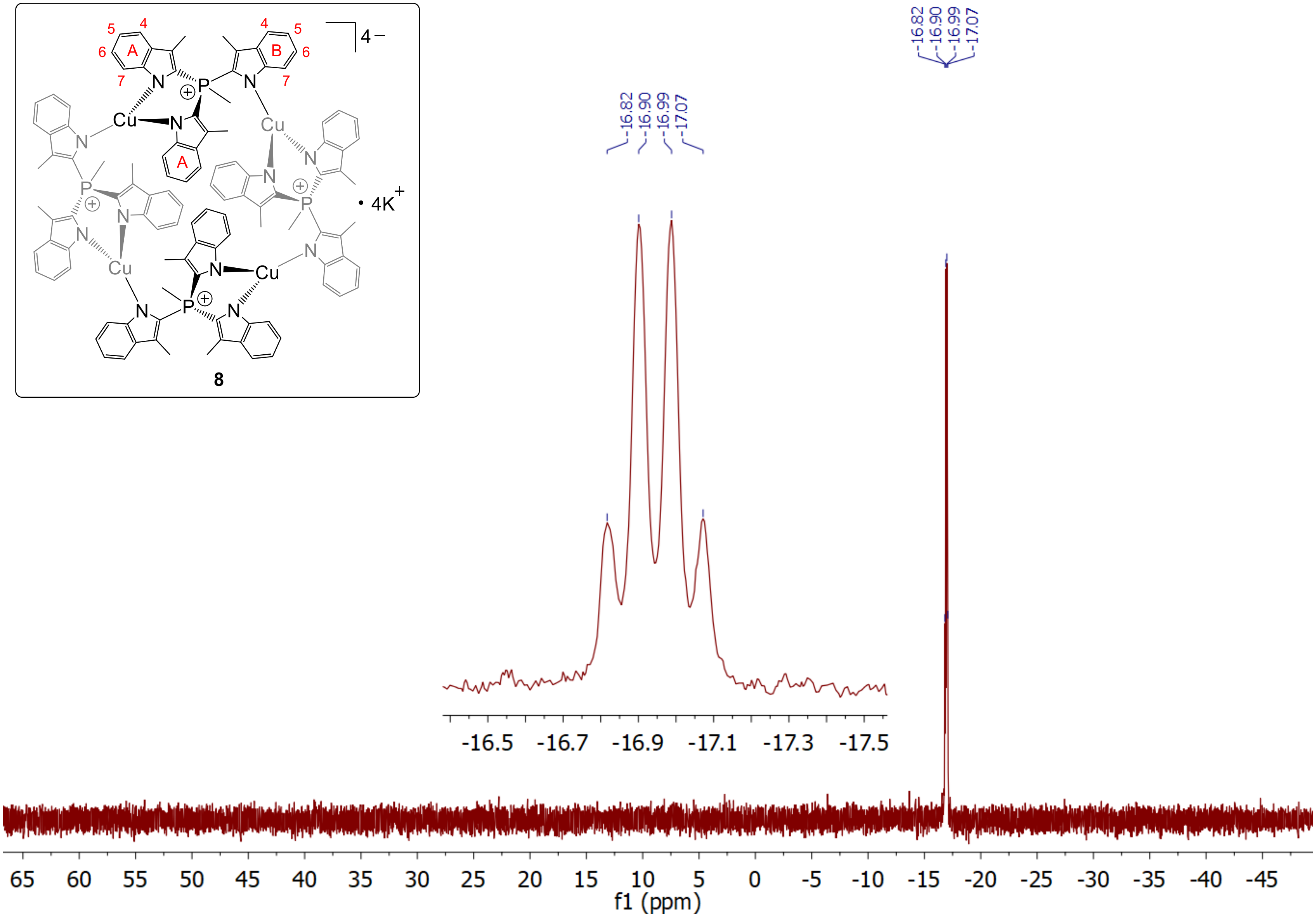

Figure S47. ^{31}P NMR spectrum of complex **8** in acetonitrile-*d*$_3$.

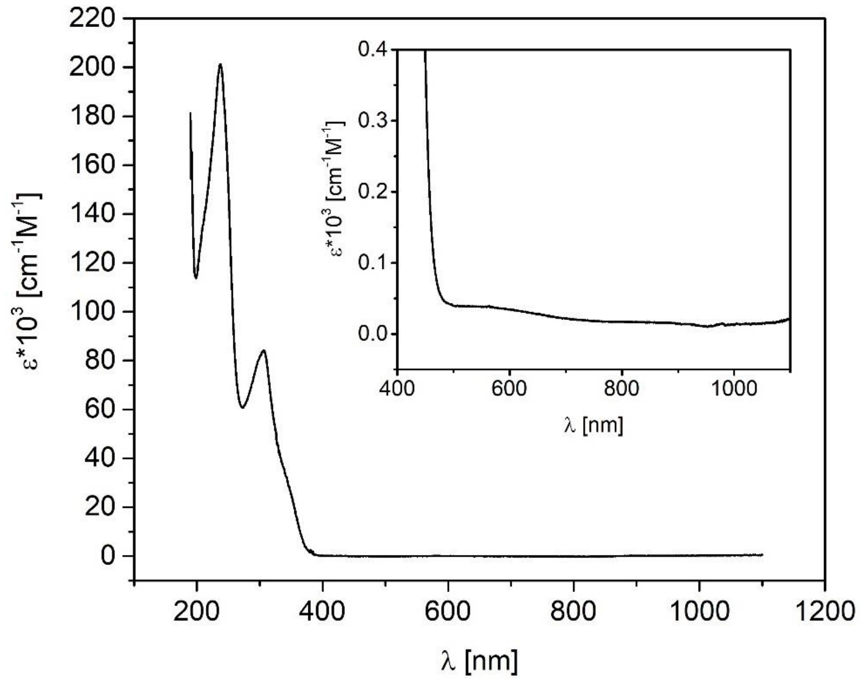

Figure S48. UV-Vis spectrum of compound **8** in acetonitrile.

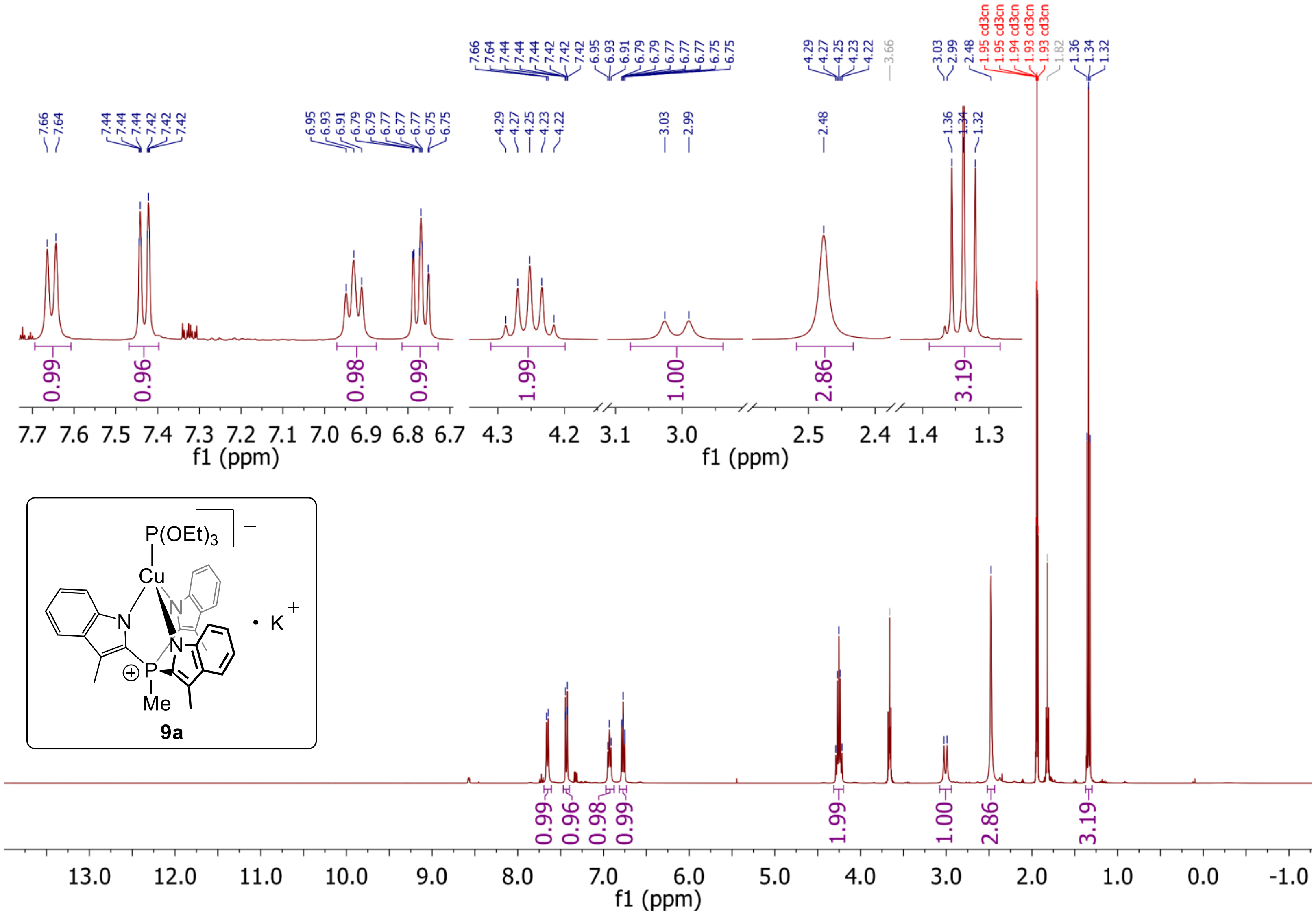

Figure S49. ^{1}H NMR spectrum of complex **9a** in acetonitrile-d_3. Impurities:1.82, 3.66 ppm – THF, other minor peaks are unidentified impurities.

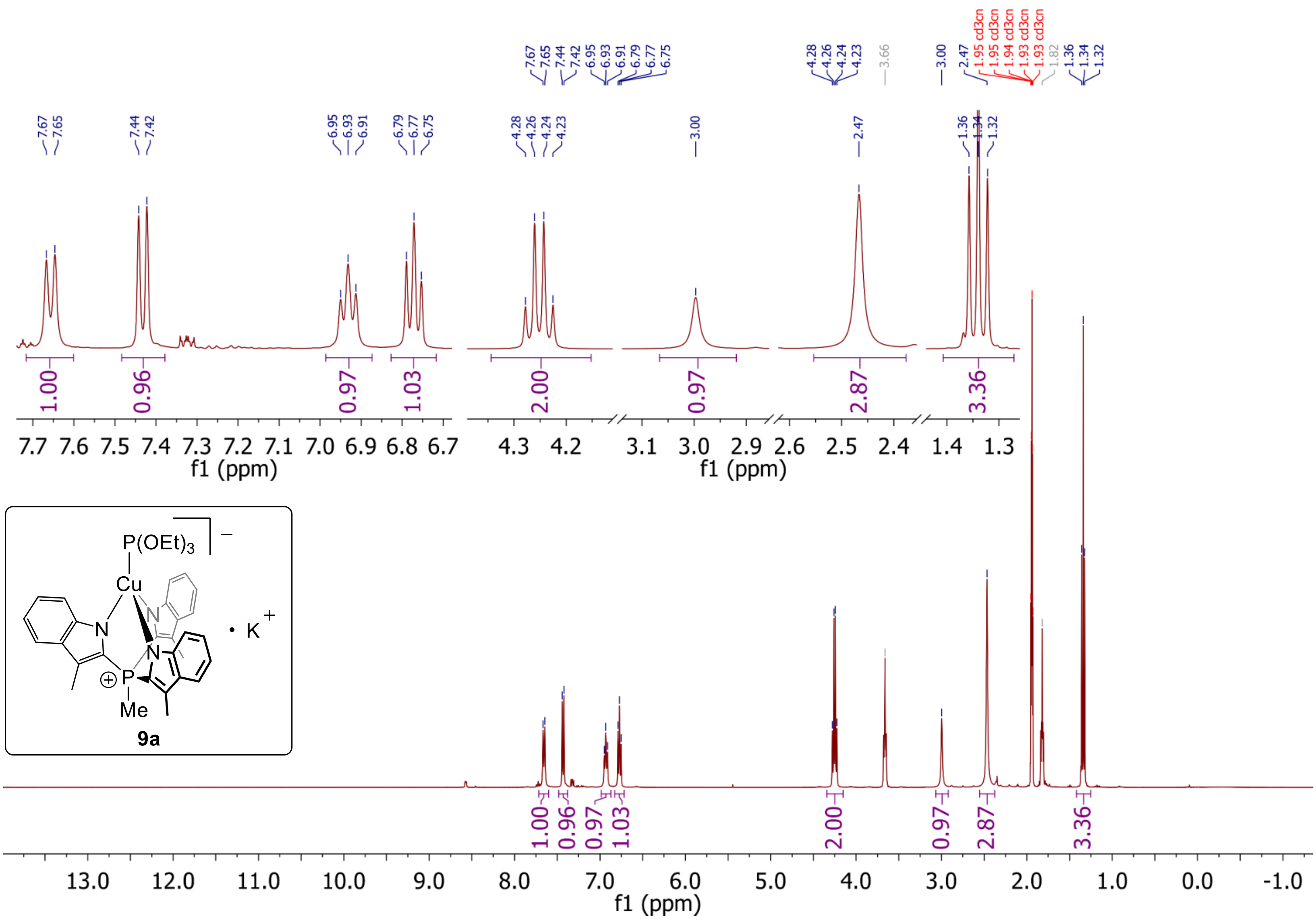

Figure S50. $^{1}H\{^{31}P\}$ NMR spectrum of complex **9a** in acetonitrile-*d*$_3$. Decoupling was achieved by using a bilevel scheme. Impurities: 1.82, 3.66 ppm – THF, other minor peaks are unidentified impurities.

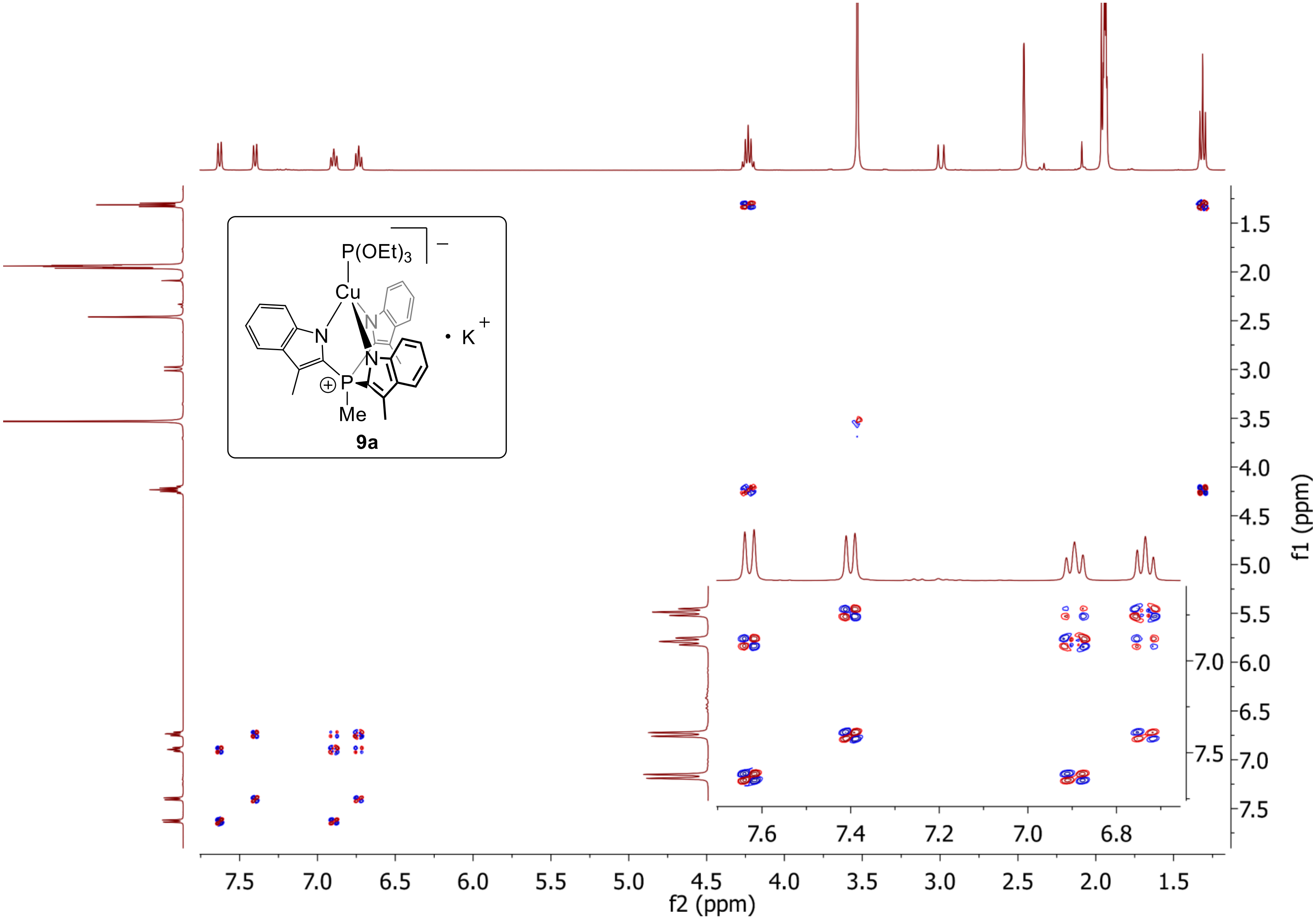

Figure S51. ^{1}H DQF-COSY spectrum of complex **9a** in acetonitrile-d_3.

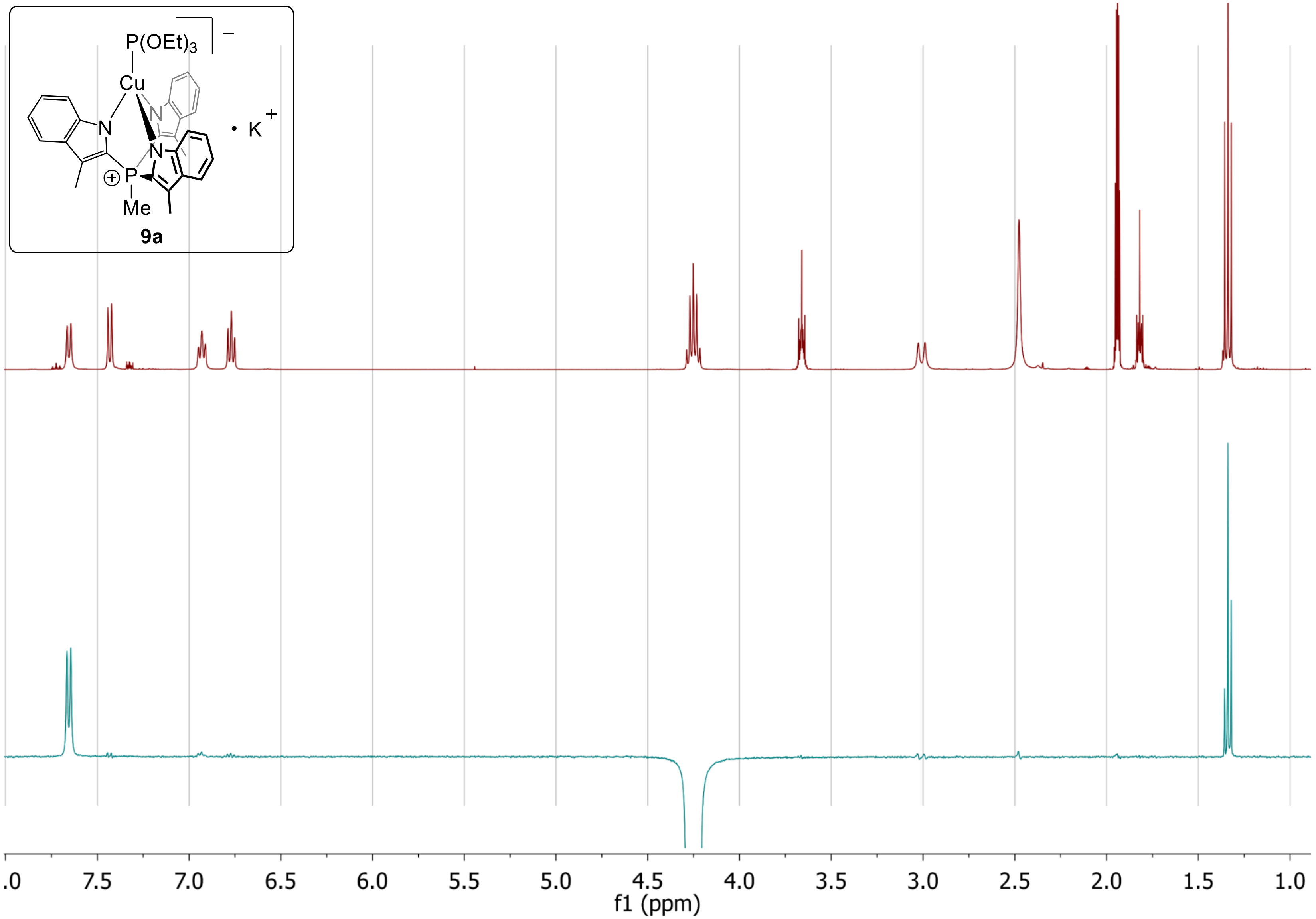

Figure S52. ^{1}H NOE spectrum of compound **9a** in acetonitrile-*d*$_3$ (bottom panel; top panel: regular ^{1}H spectrum for the reference).

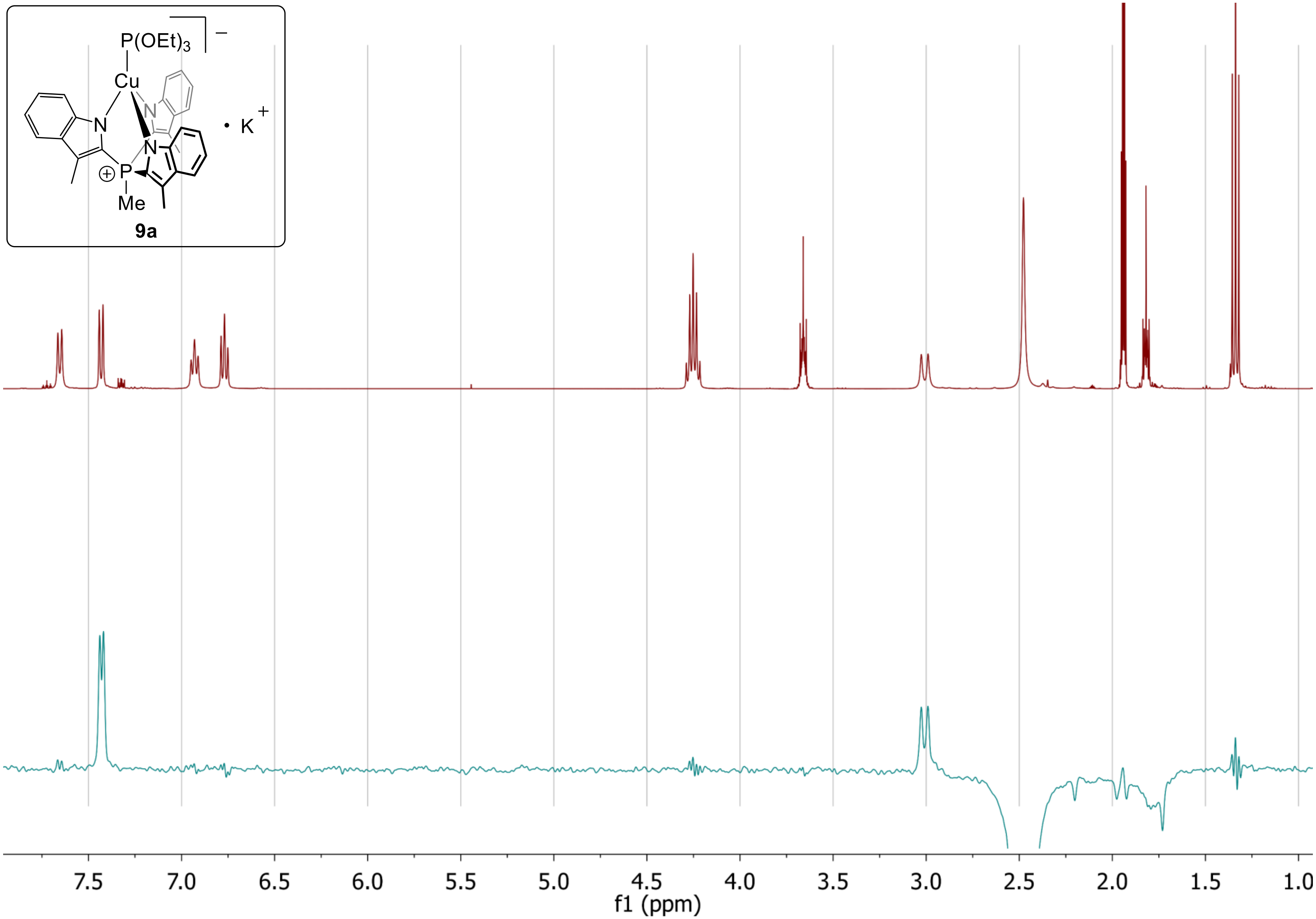

Figure S53. ^{1}H NOE spectrum of compound **9a** in acetonitrile-*d*$_3$ (bottom panel; top panel: regular ^{1}H spectrum for reference).

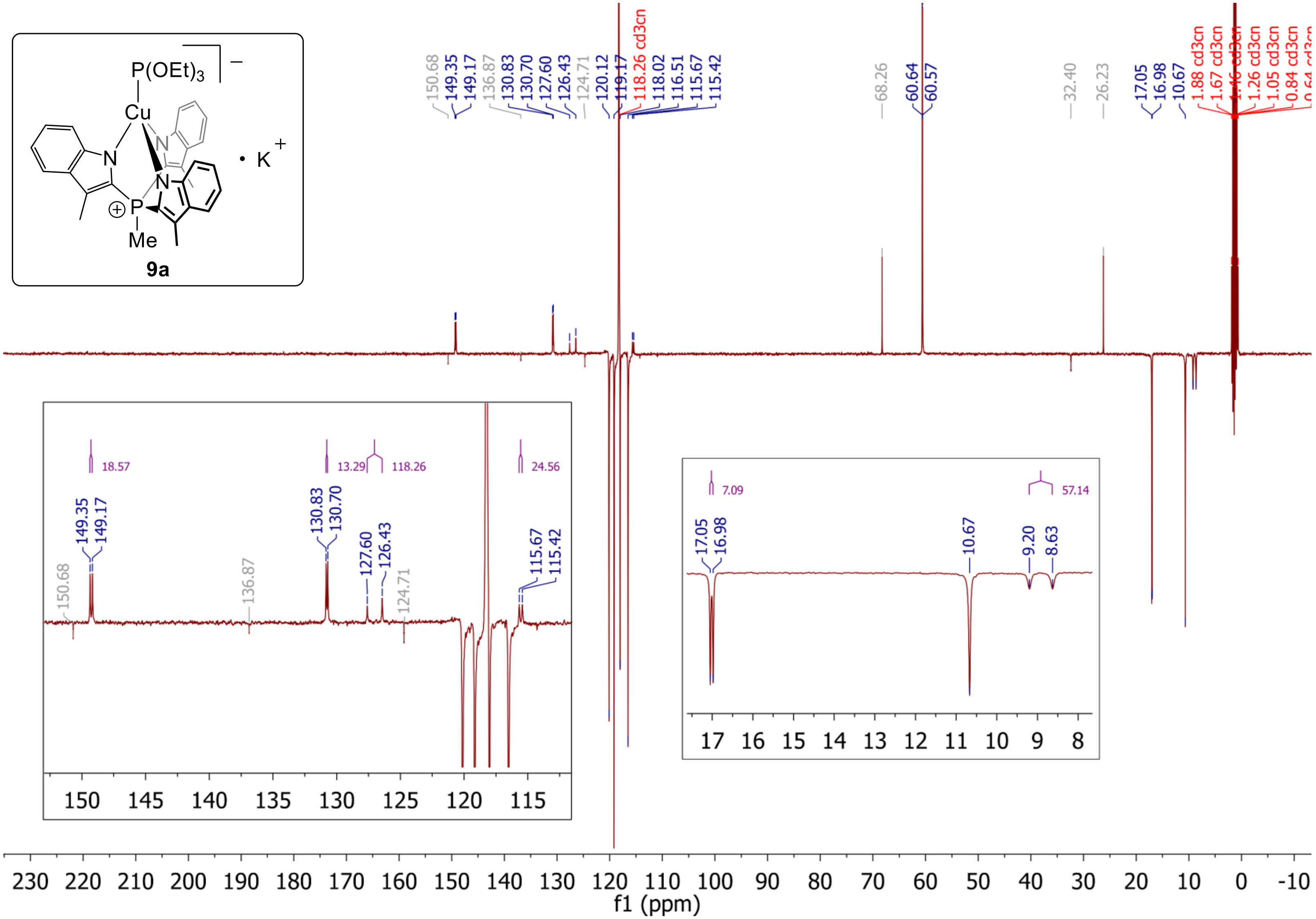

Figure S54. ^{13}C{^{1}H} DEPTQ-135 NMR spectrum of complex **9a** in acetonitrile-d_3. Positive signal phase indicates quaternary and secondary carbons, negative phase is for tertiary and primary carbons. Impurities: 26.33 and 68.26 ppm – THF, other peaks labeled in grey – unidentified.

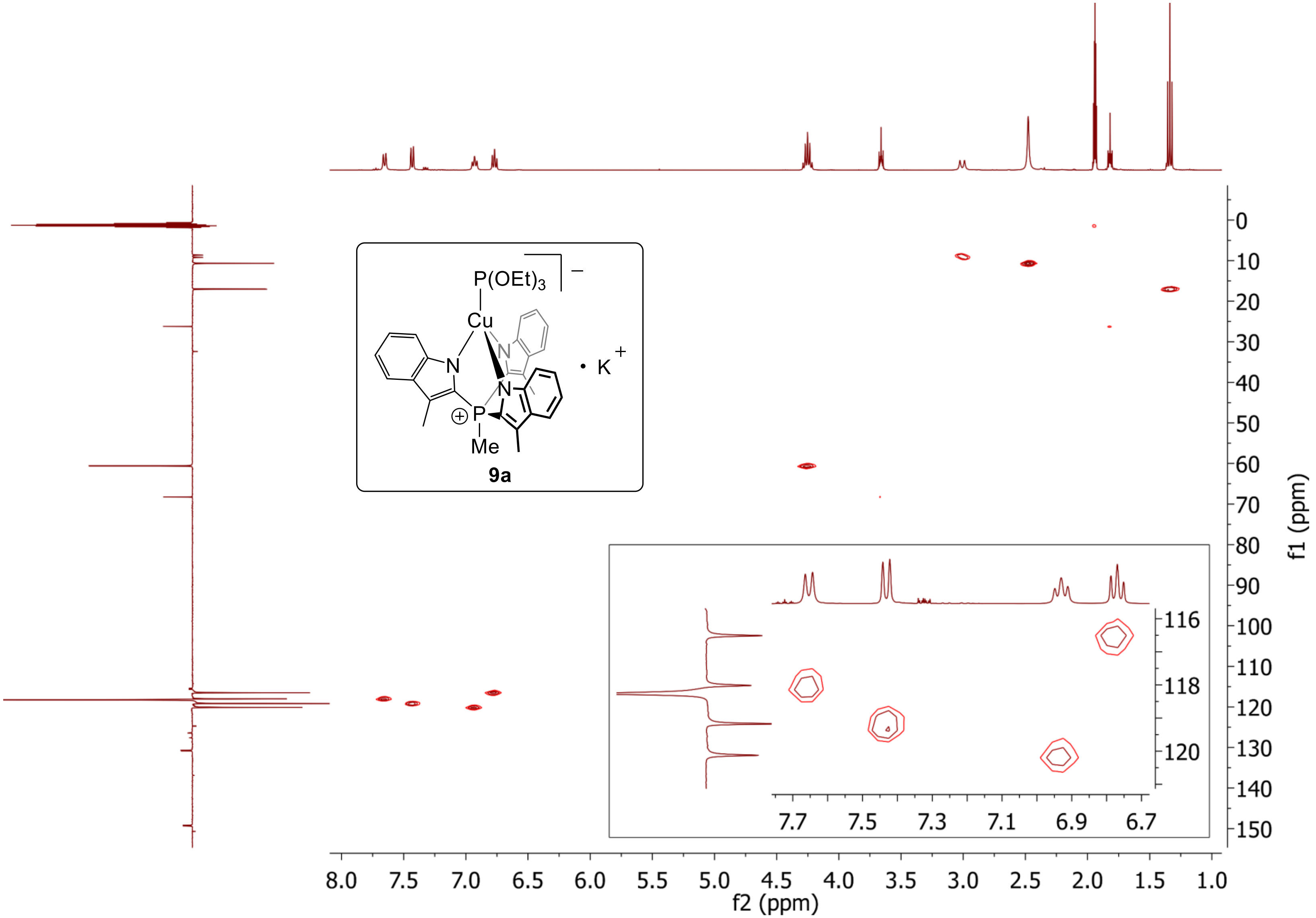

Figure S55. ^{1}H-^{13}C ASAPHMQC spectrum of complex **9a** in acetonitrile-d_3. The vertical trace is the ^{13}C{^{1}H} DEPTQ-135 spectrum from *Figure S54*.

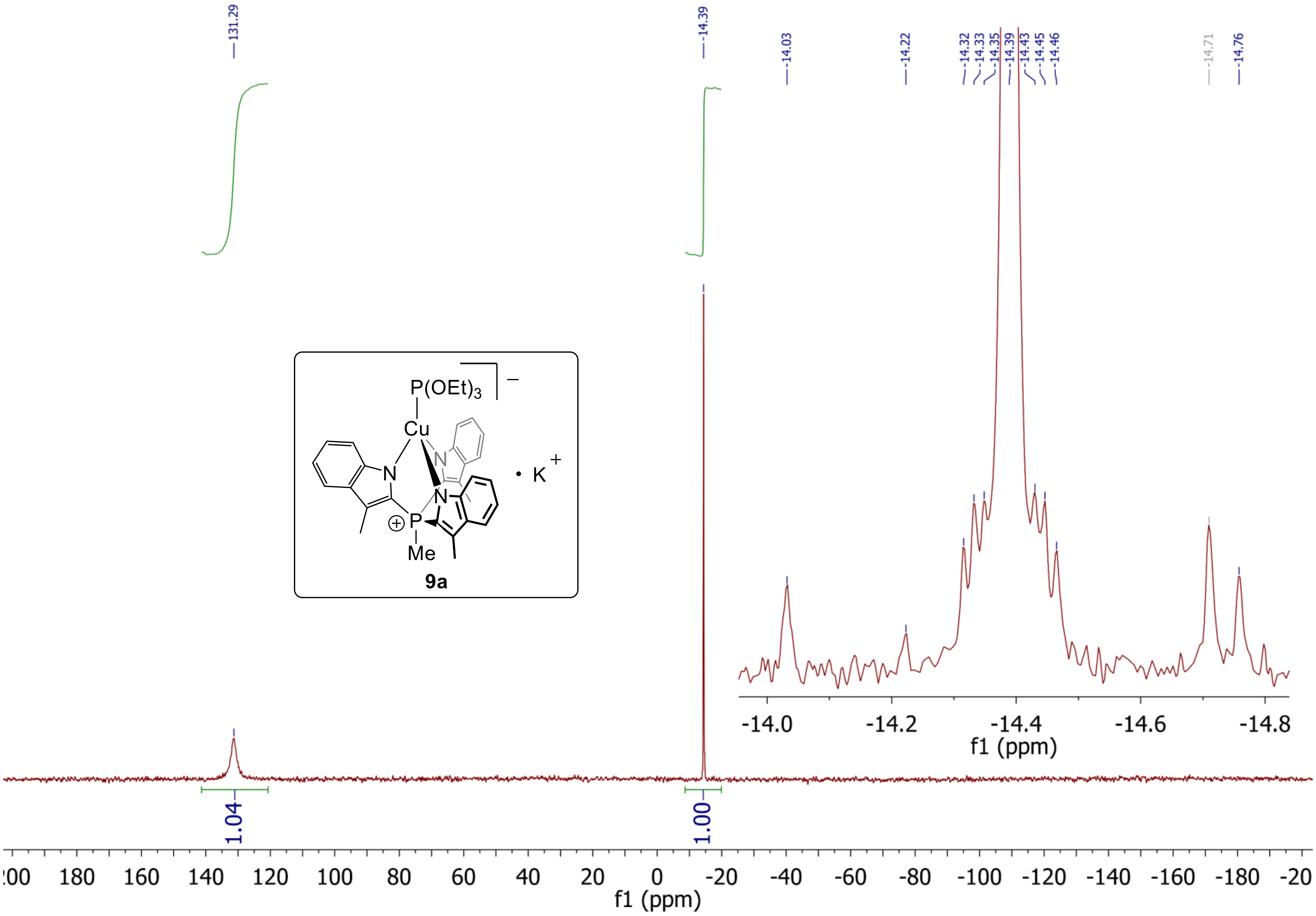

Figure S56. $^{31}P\{^{1}H\}$ NMR spectrum of complex **9a** in acetonitrile-d_3. Impurities: -14.71 ppm – unidentified; -14.22 ppm – a CH_3-P^+ satellite, its counterpart cannot be visualized well because of the low signal-to-noise ratio.

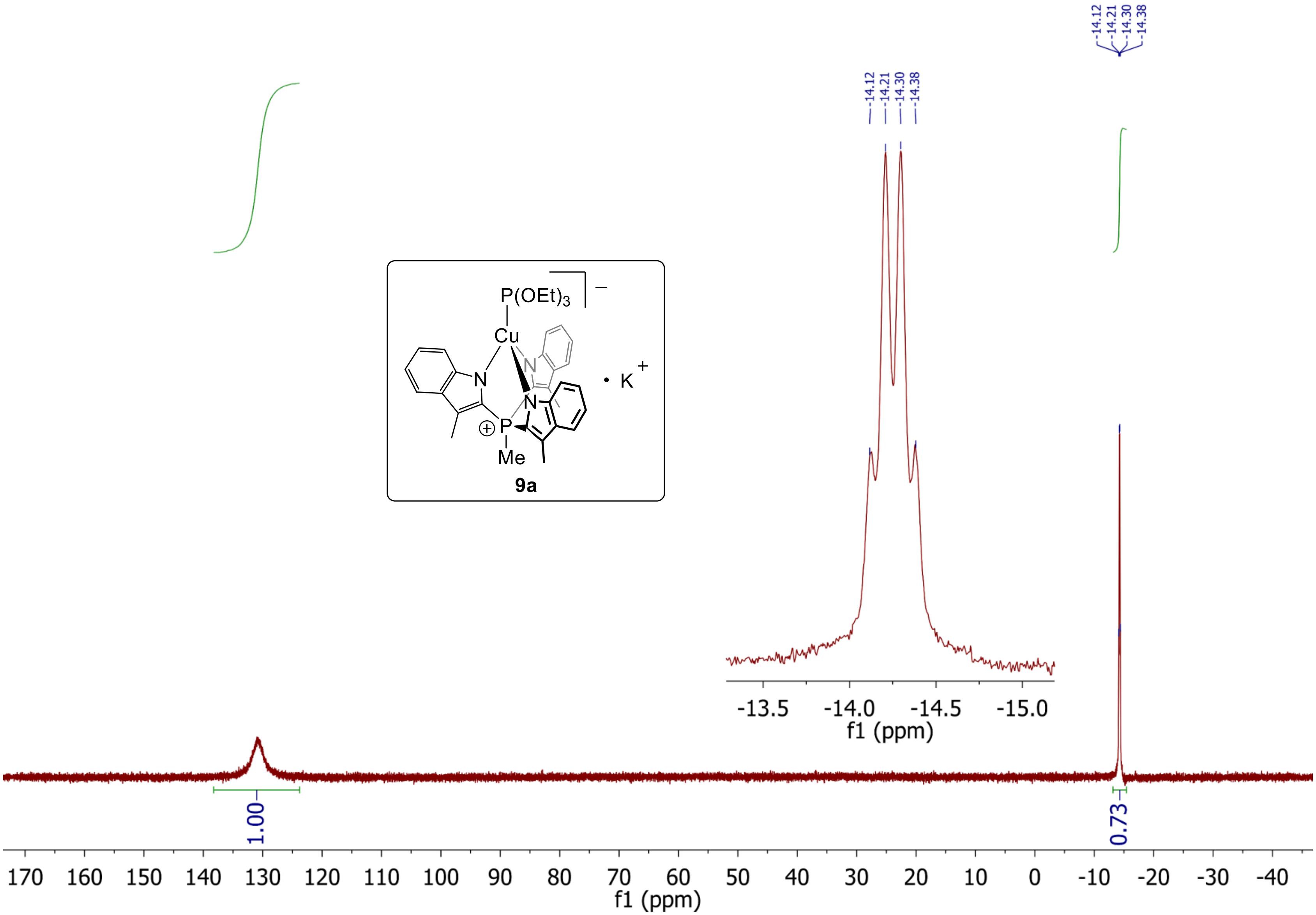

Figure S57. ^{31}P NMR spectrum of complex **9a** in acetonitrile-d_3.

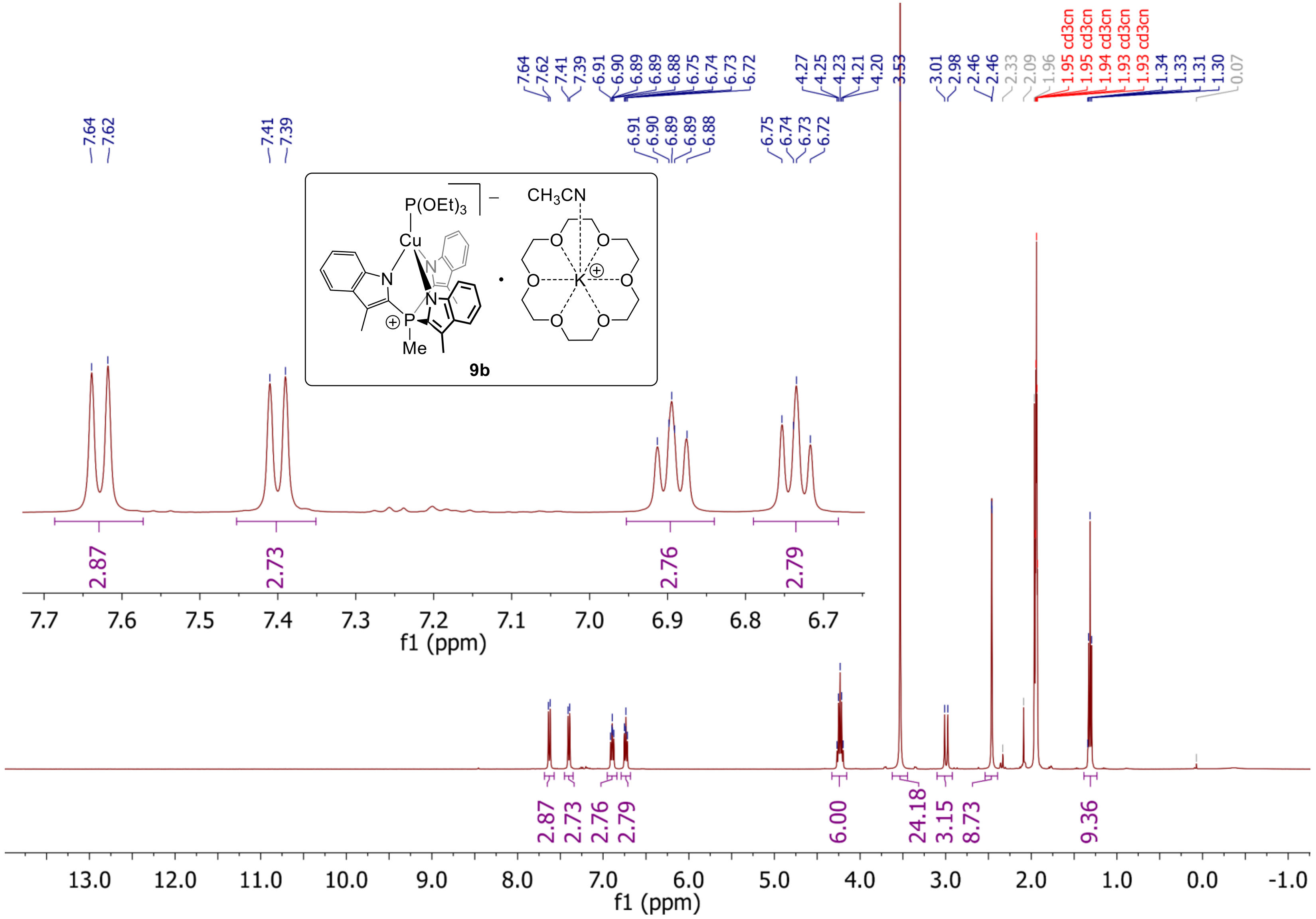

Figure S58. ^{1}H NMR spectrum of complex **9b** in acetonitrile-d_3. Impurities: 0.07 ppm – silicon grease, 1.96 ppm – CH_3CN, 2.09 and 2.33 ppm – unidentified.

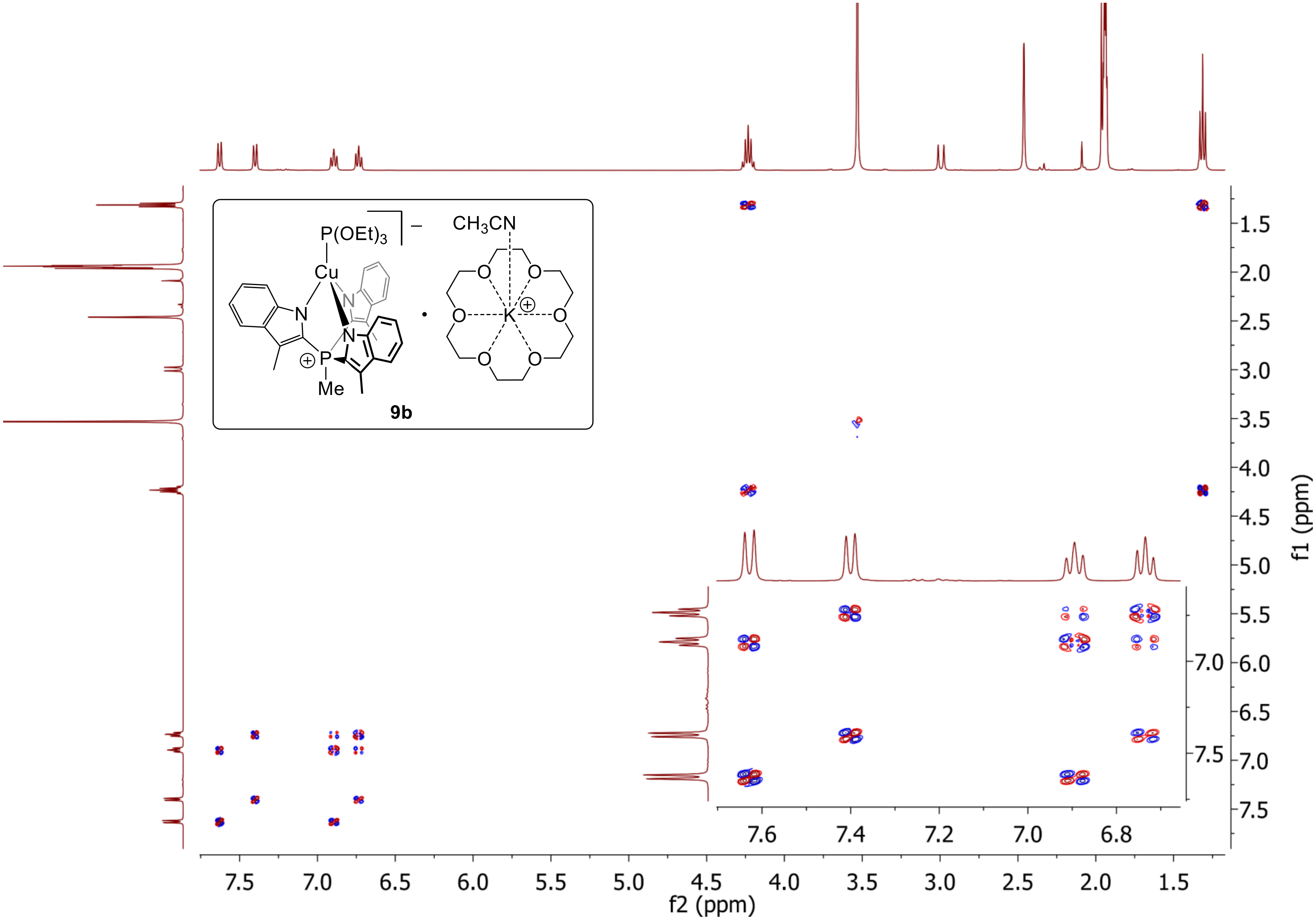

Figure S59. ^{1}H DQF-COSY spectrum of complex **9b** in acetonitrile-d_3.

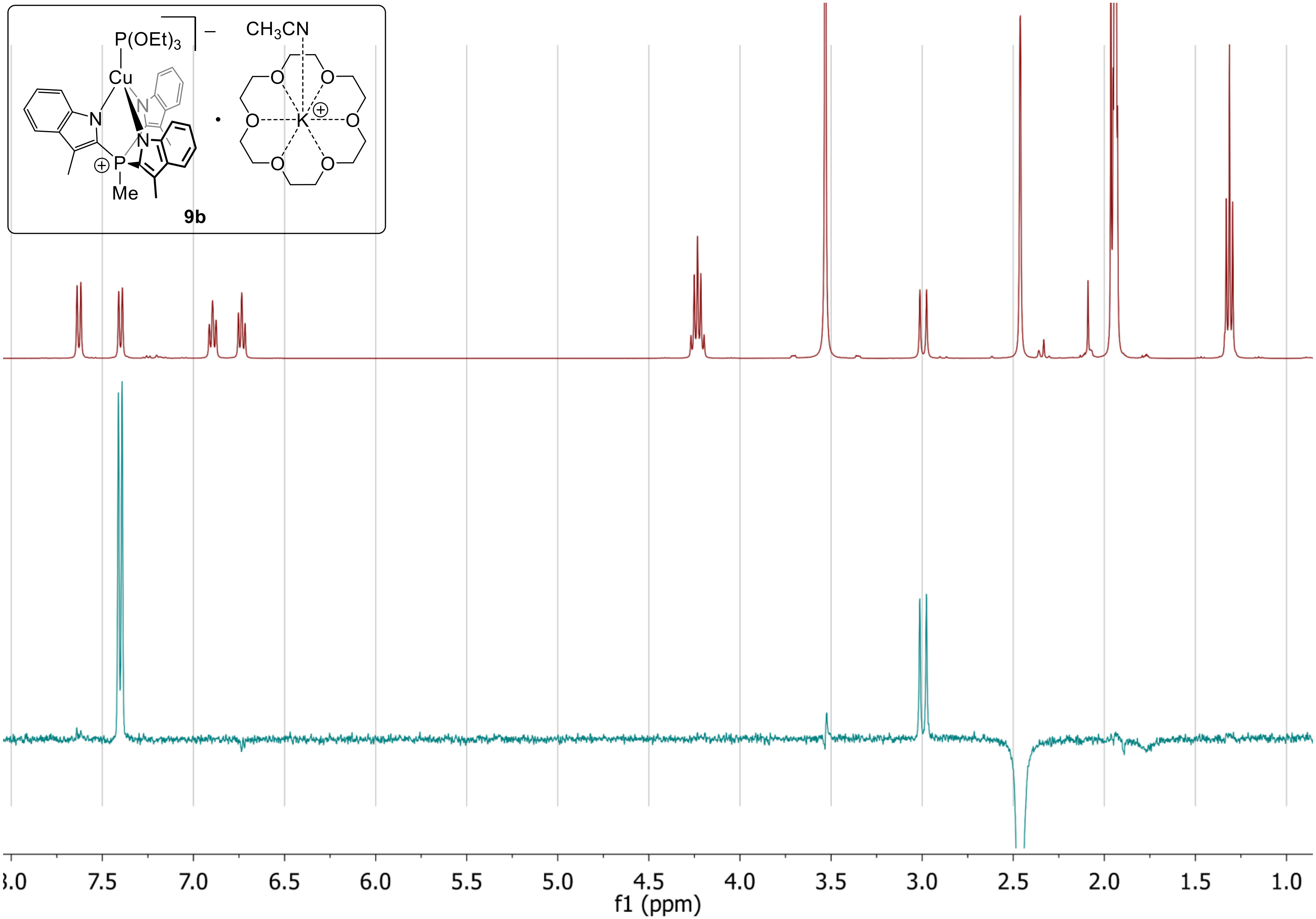

Figure S60. ^{1}H NOE spectrum of compound **9b** in acetonitrile-d_3 (bottom panel; top panel: regular ^{1}H spectrum for reference).

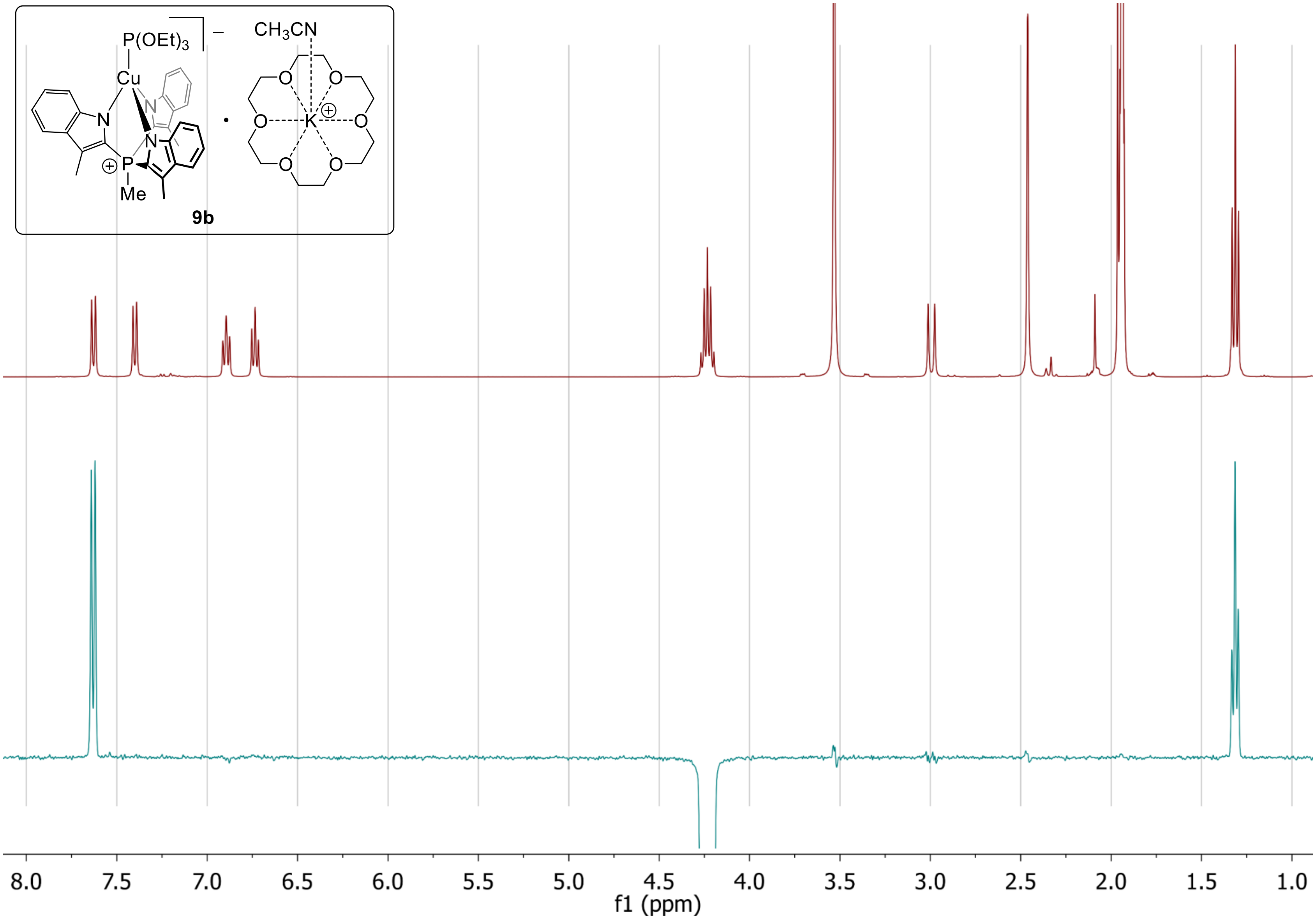

Figure S61. ^{1}H NOE spectrum of compound **9b** in acetonitrile-d_3 (bottom panel; top panel: regular ^{1}H spectrum for reference).

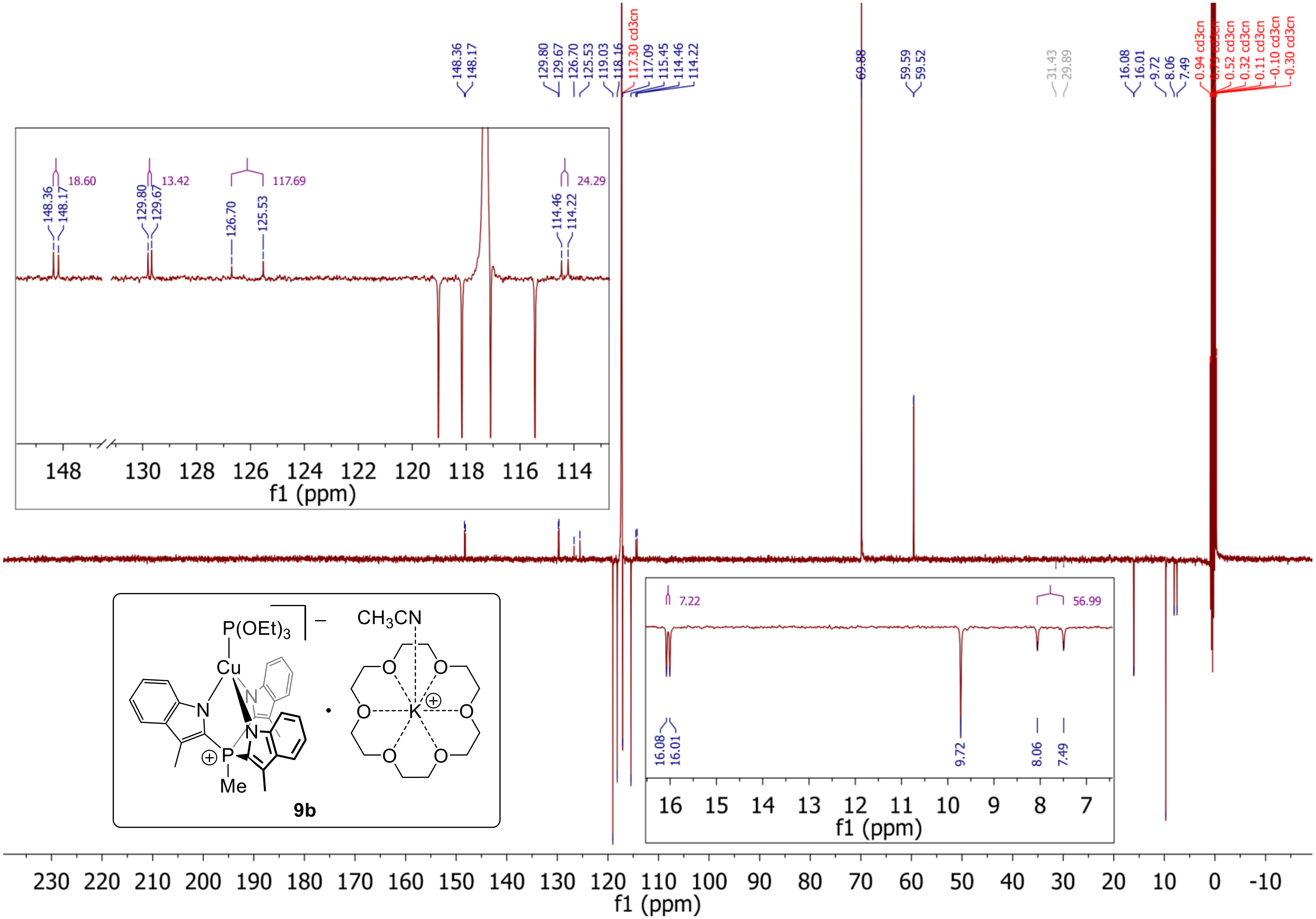

Figure S62. $^{13}C\{^1H\}$ DEPTQ-135 NMR spectrum of complex **9b** in acetonitrile-d_3. Positive signal phase indicates quaternary and secondary carbons, negative phase is for tertiary and primary carbons. Impurities: 29.89 and 31.43 ppm – unidentified.

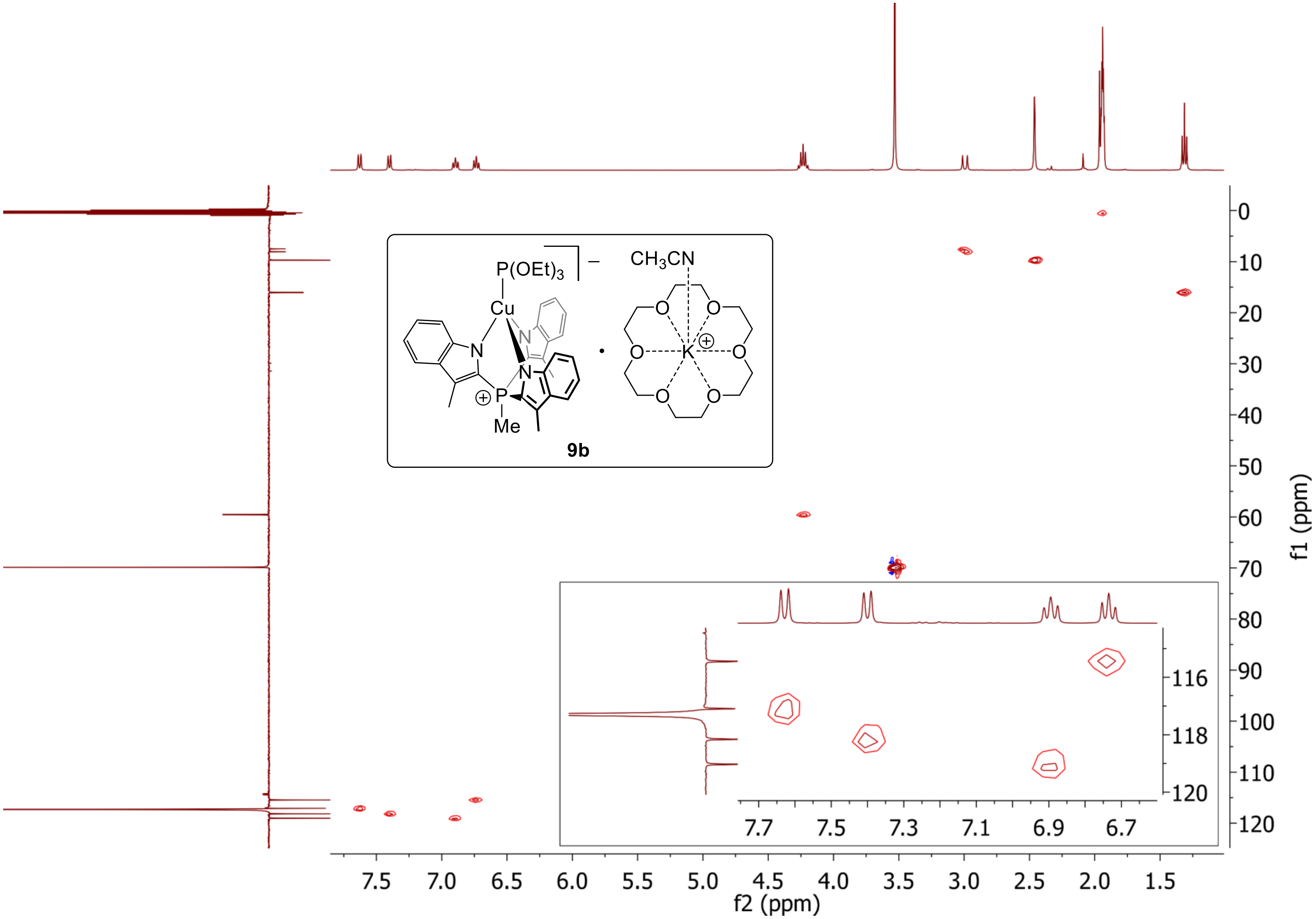

Figure S63. ^{1}H-^{13}C ASAPHMQC spectrum of complex **9b** in acetonitrile-d_3. The vertical trace is the ^{13}C{^{1}H} DEPTQ-135 spectrum from *Figure S62*.

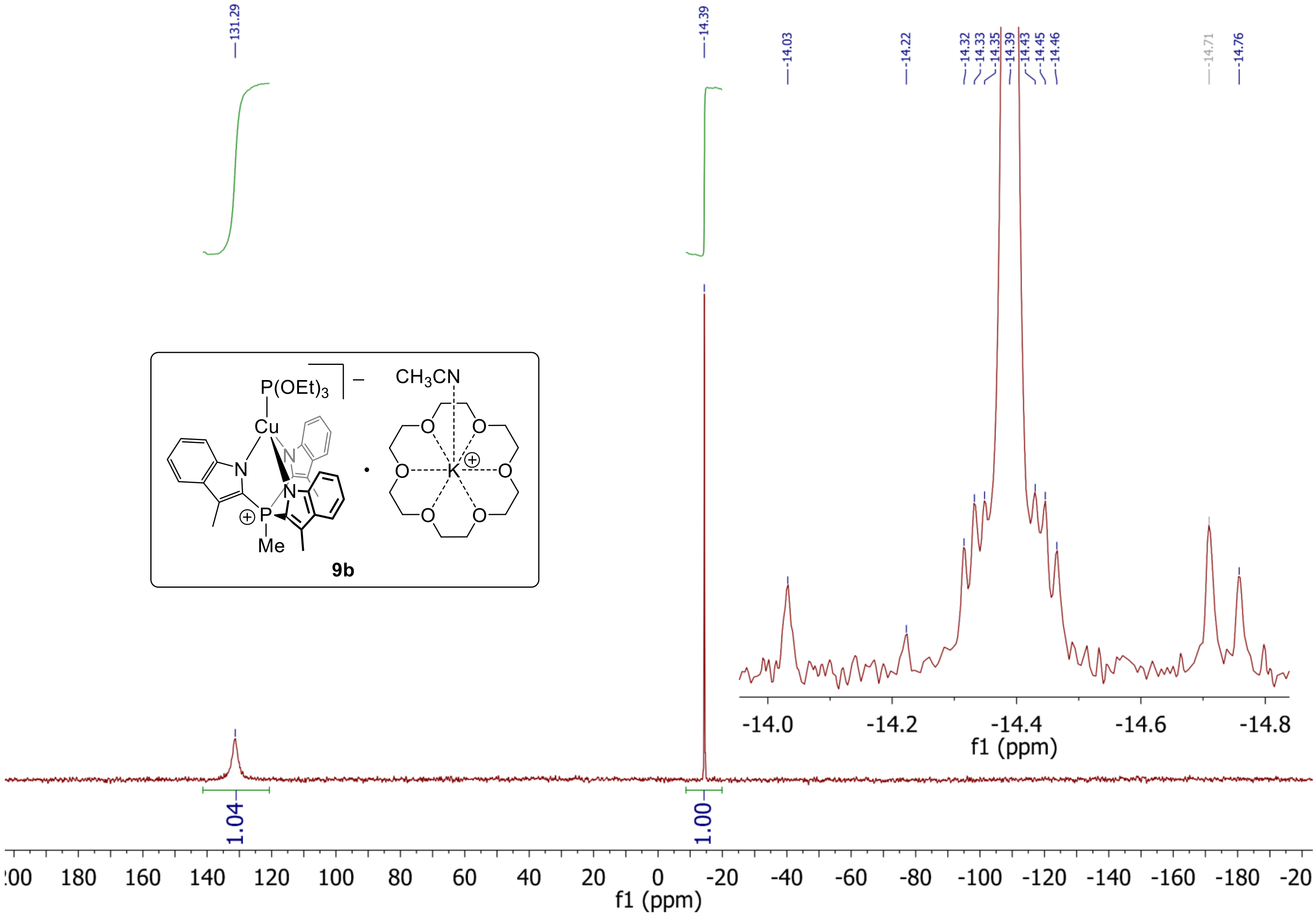

Figure S64. ^{31}P{^{1}H} NMR spectrum of complex **9b** in acetonitrile-d_3. Impurities: -14.71 ppm – unidentified; -14.22 ppm – a CH_3-P^+ satellite, its counterpart cannot be visualized well because of the low signal-to-noise ratio.

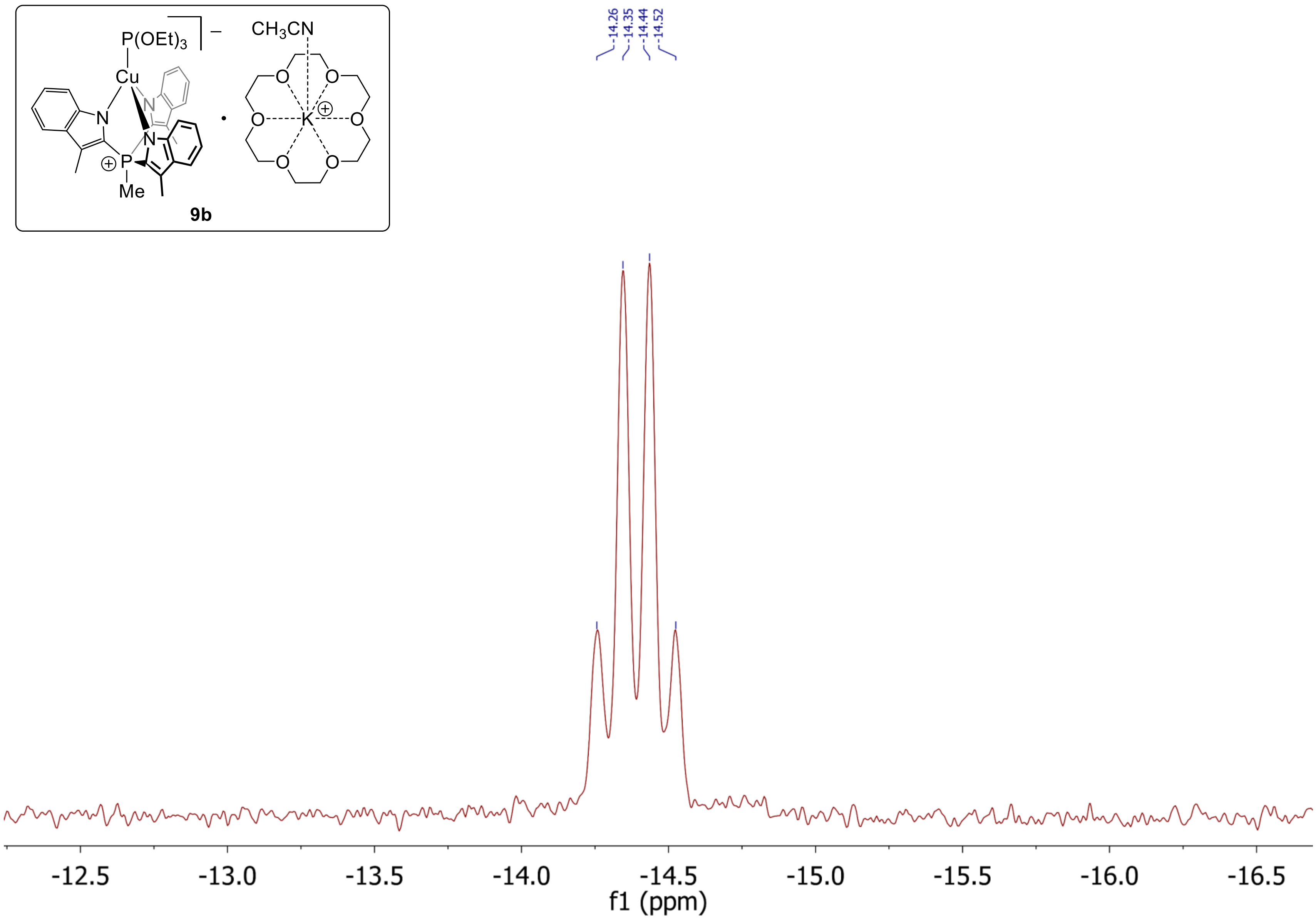

Figure S65. ^{31}P NMR spectrum of complex **9b** in acetonitrile-*d*$_3$.

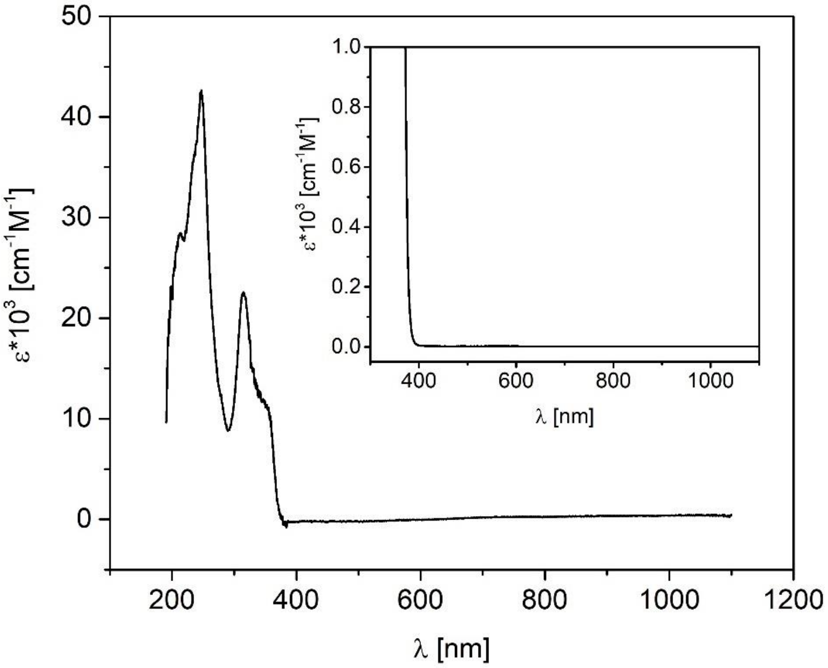

Figure S66. UV-Vis spectrum of compound **9b** in acetonitrile.

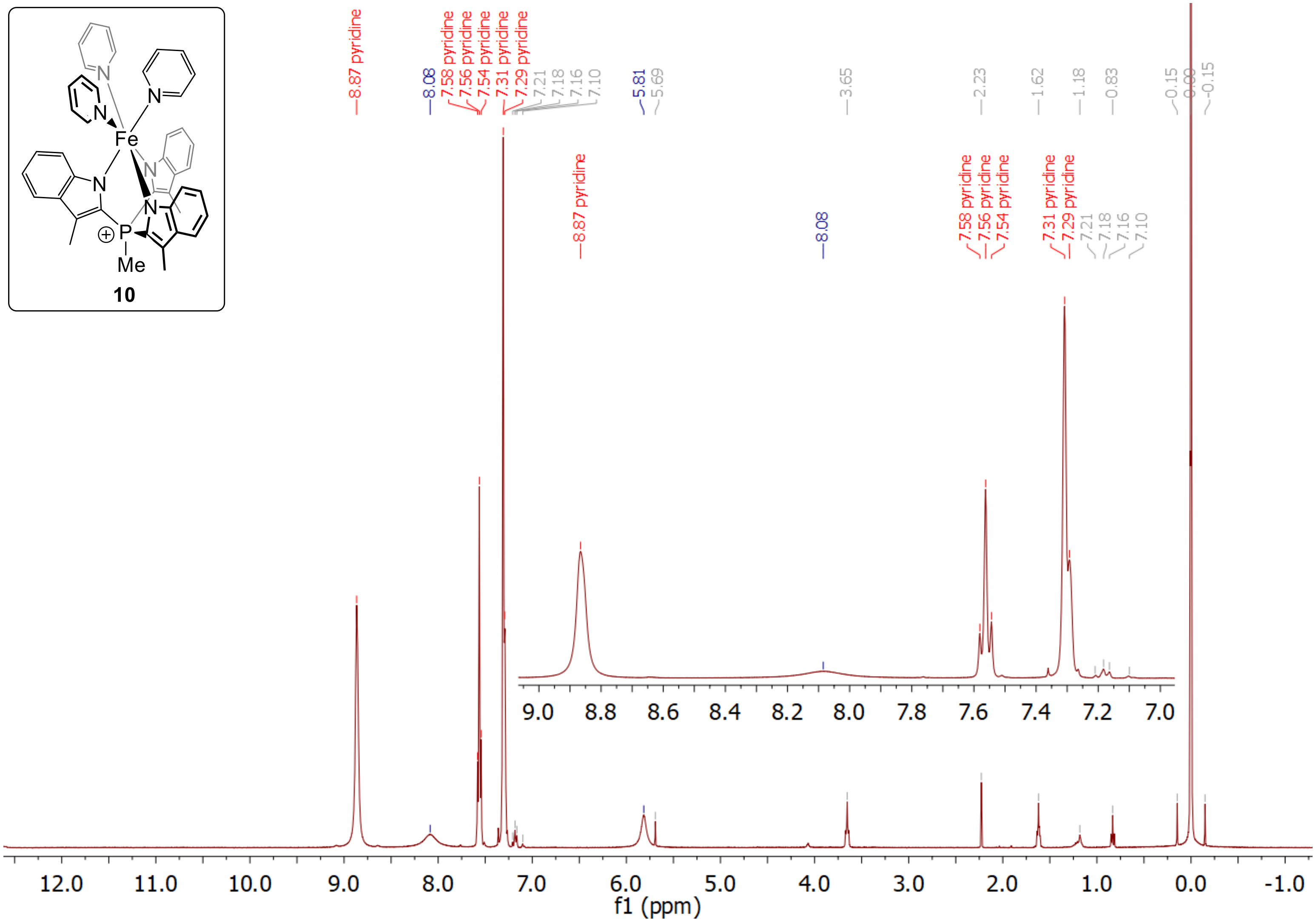

10

Figure S67. ^{1}H NMR spectrum of complex **10** in pyridine-d_5 (diamagnetic range). The peak at 0 ppm is TMS, the signals at ±0.15 ppm are the satellites ($J_{\text{H-C}}$=118.2 Hz). Impurities: 0.83 and 1.18 ppm – hexane, 1.62 and 3.66 ppm – THF, signal at 2.23 ppm – acetonitrile, signal at 5.69 ppm – dichloromethane, 7.10-7.21 ppm – unidentified impurity.

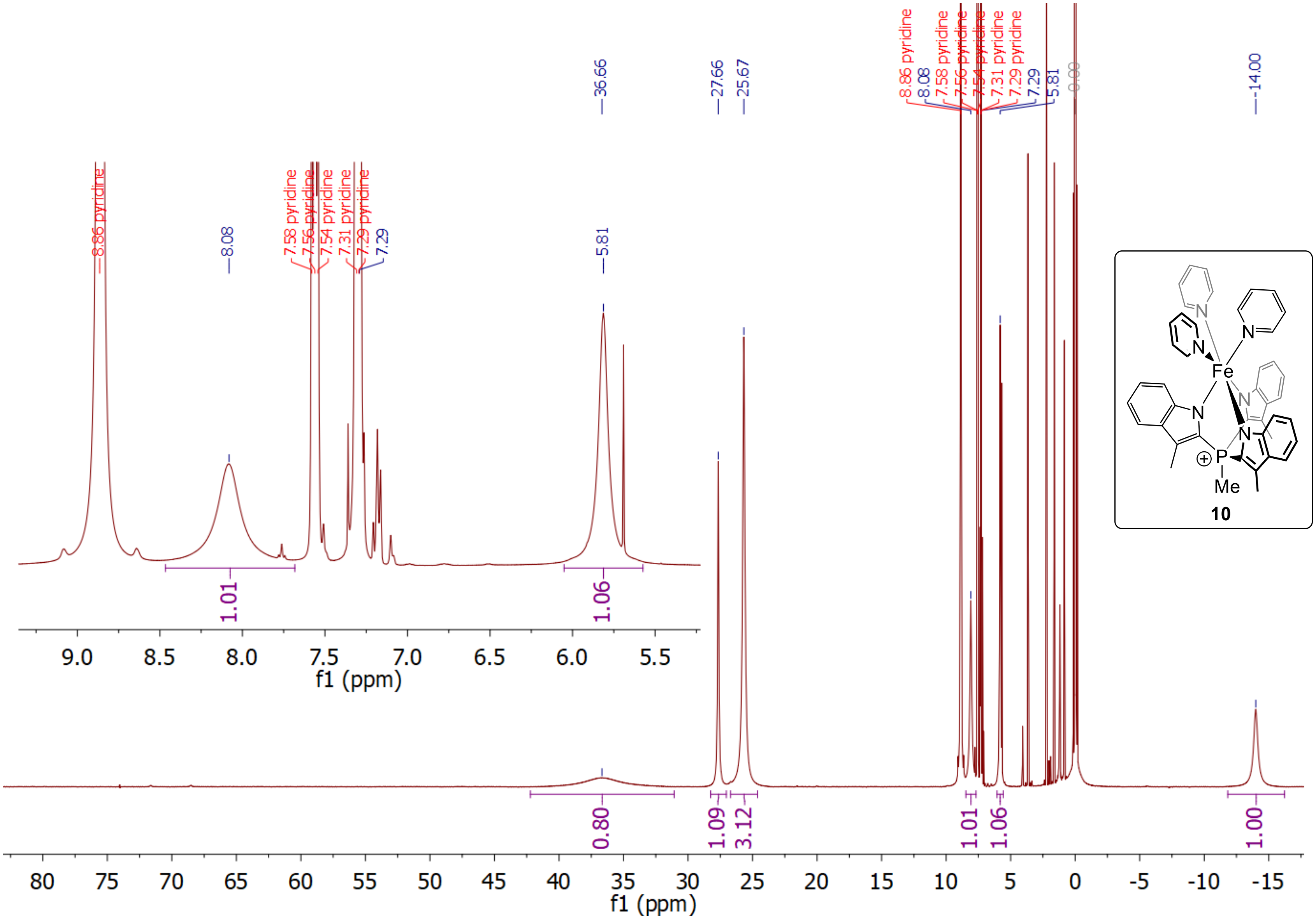

Figure S68. ^{1}H NMR spectrum of complex **10** in pyridine-d_5 (all paramagnetic signals).

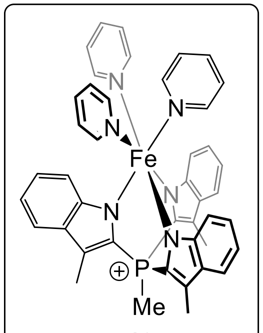

10

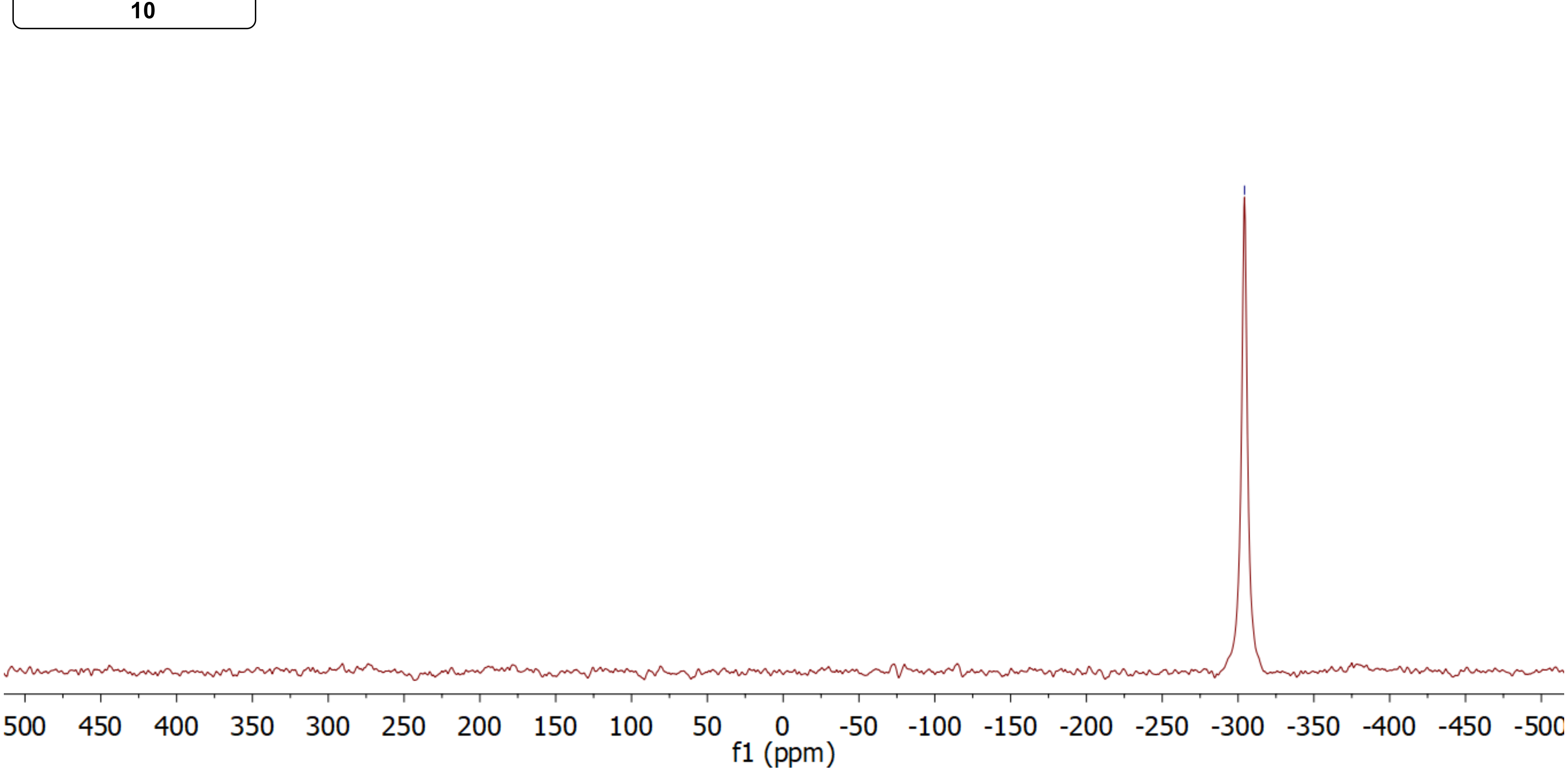

Figure S69. ^{31}P NMR spectrum of complex **10** in pyridine-d_5.

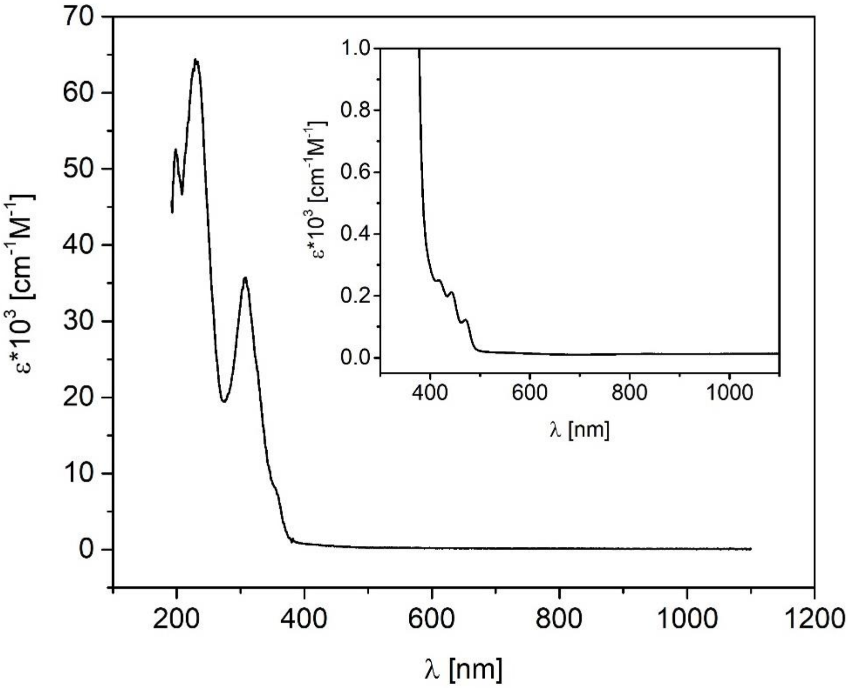

Figure S70. UV-Vis spectrum of compound **10** in acetonitrile.

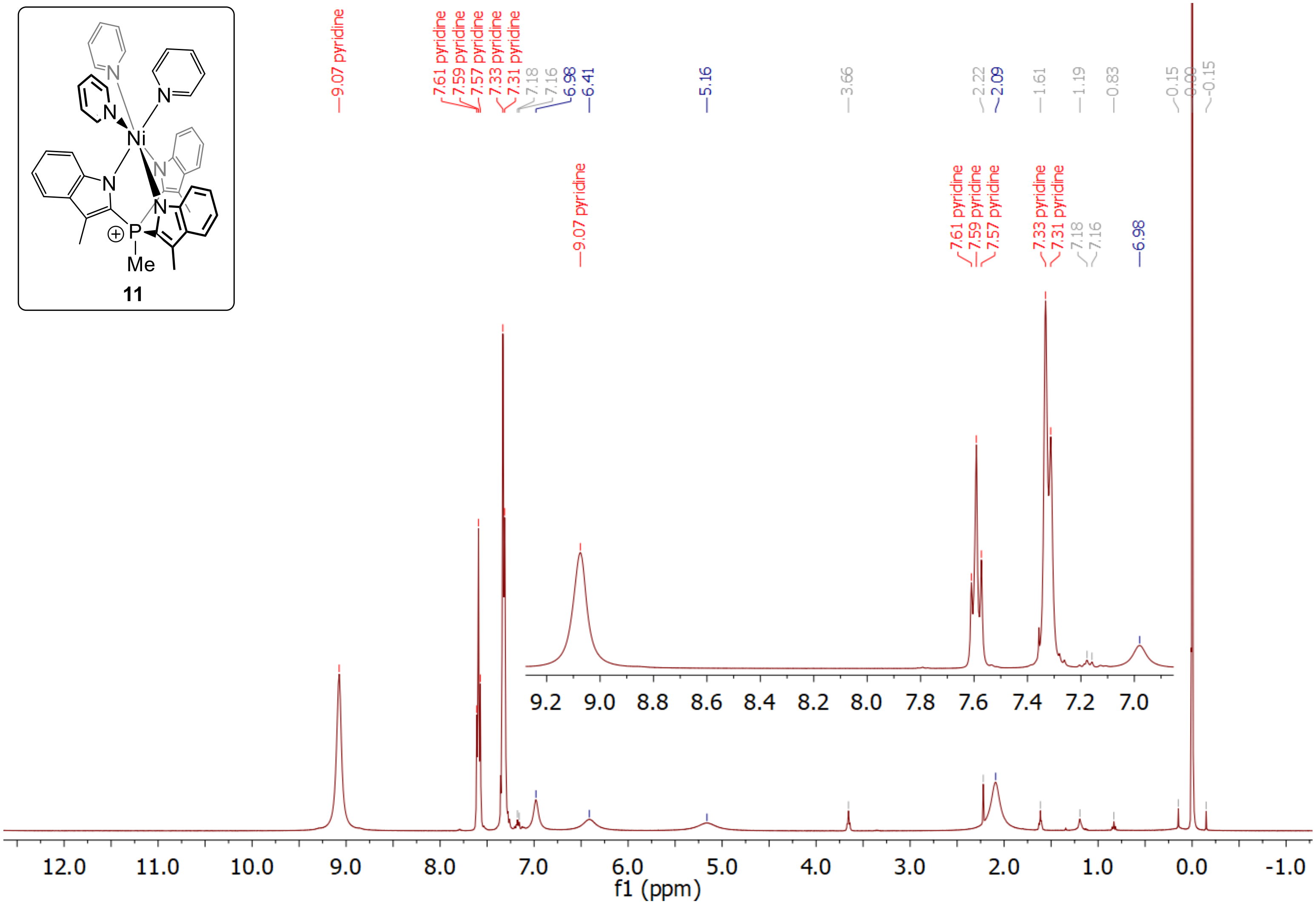

Figure S71. ^{1}H NMR spectrum of complex **11** in pyridine-d_5 (diamagnetic range). The peak at 0 ppm is TMS, the signals at ±0.15 ppm are the satellites ($J_{\text{H-C}}$=118.2 Hz). Impurities: 0.83 and 1.19 ppm – hexane, 1.61 and 3.66 ppm – THF, 2.22 ppm – acetonitrile, 7.16 and 7.18 ppm are unidentified impurities.

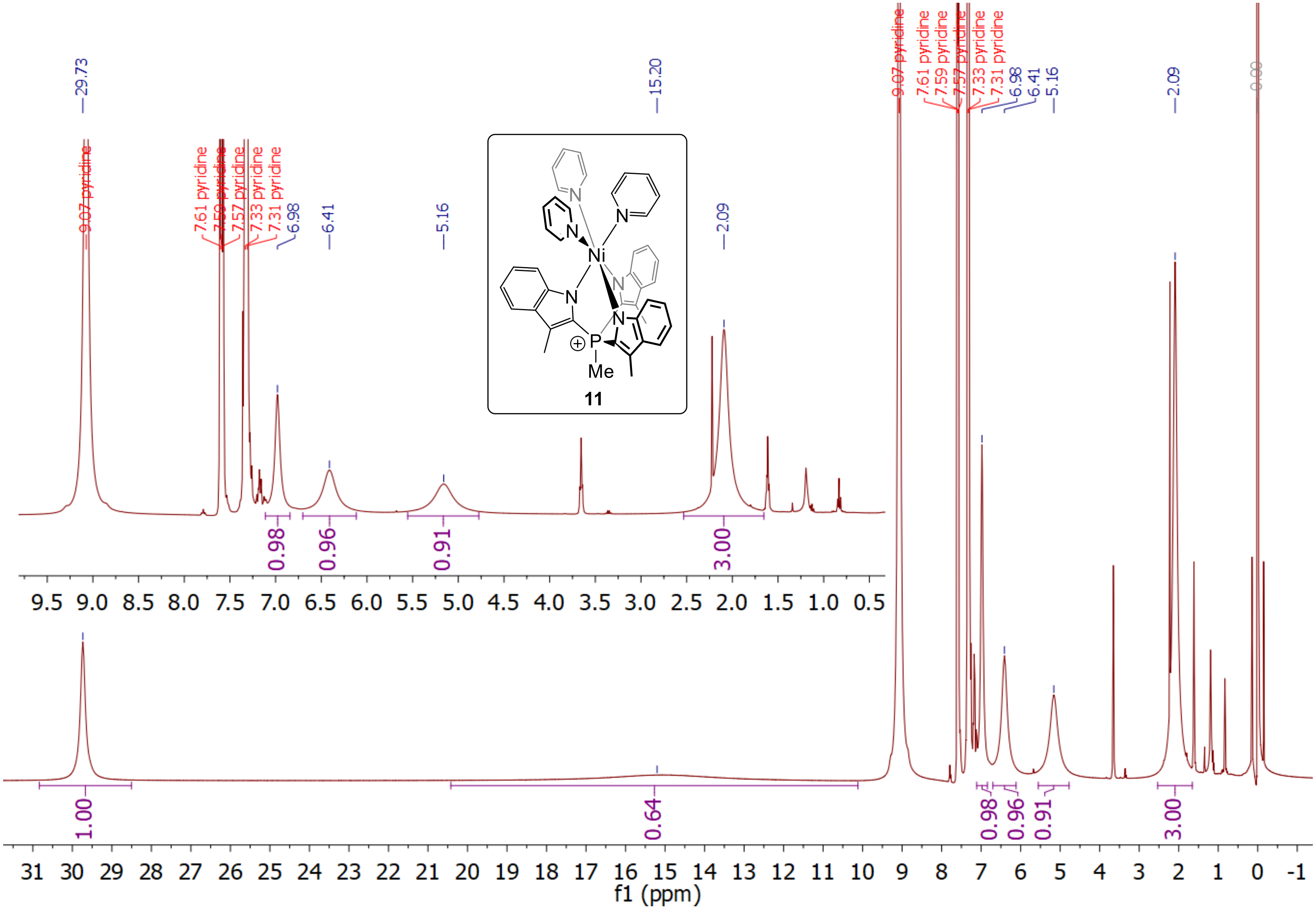

Figure S72. ^{1}H NMR spectrum of complex **11** in pyridine-d_5 (all paramagnetic signals).

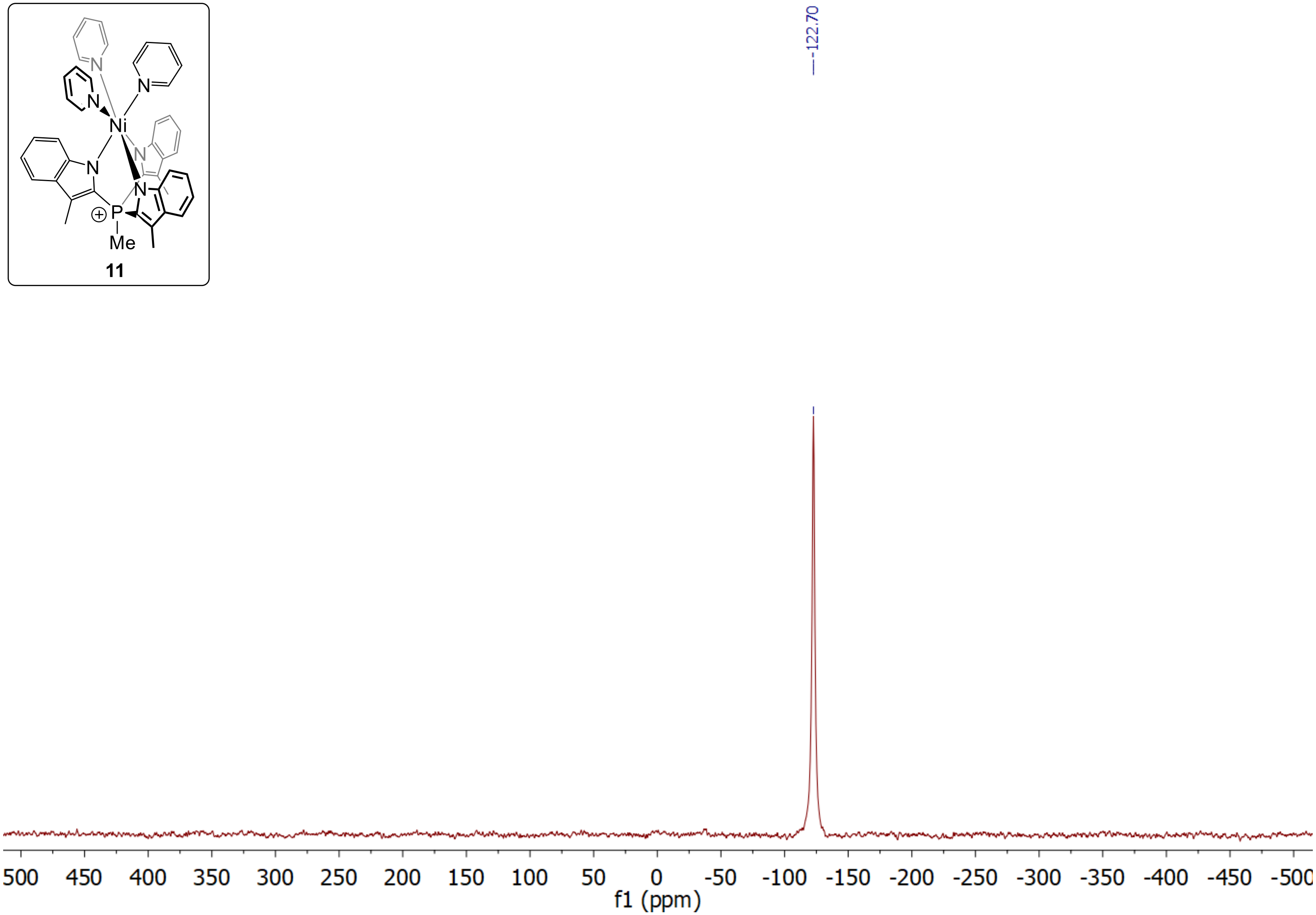

Figure S73. ^{31}P NMR spectrum of complex **11** in pyridine-d_5.

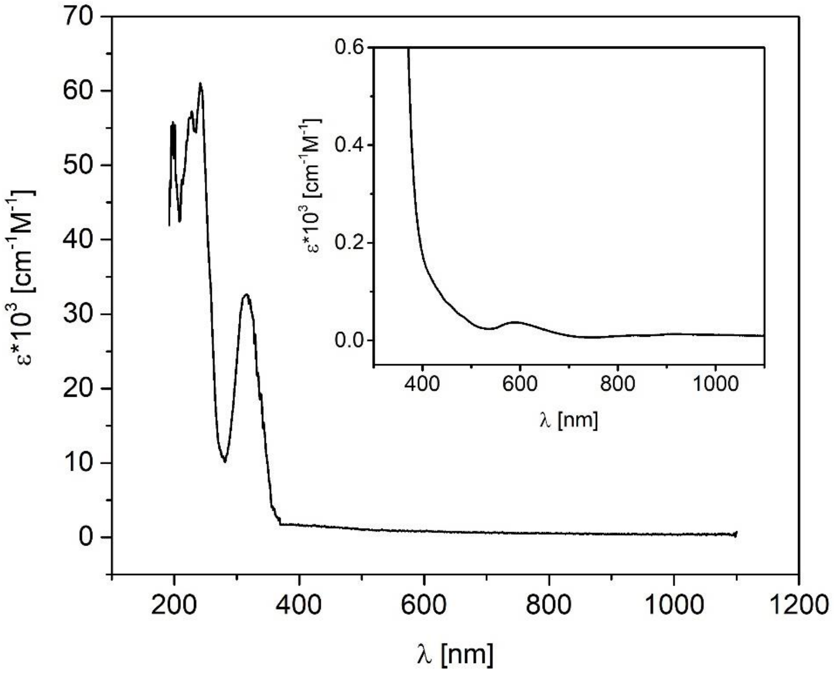

Figure S74. UV-Vis spectrum of compound **11** in acetonitrile.

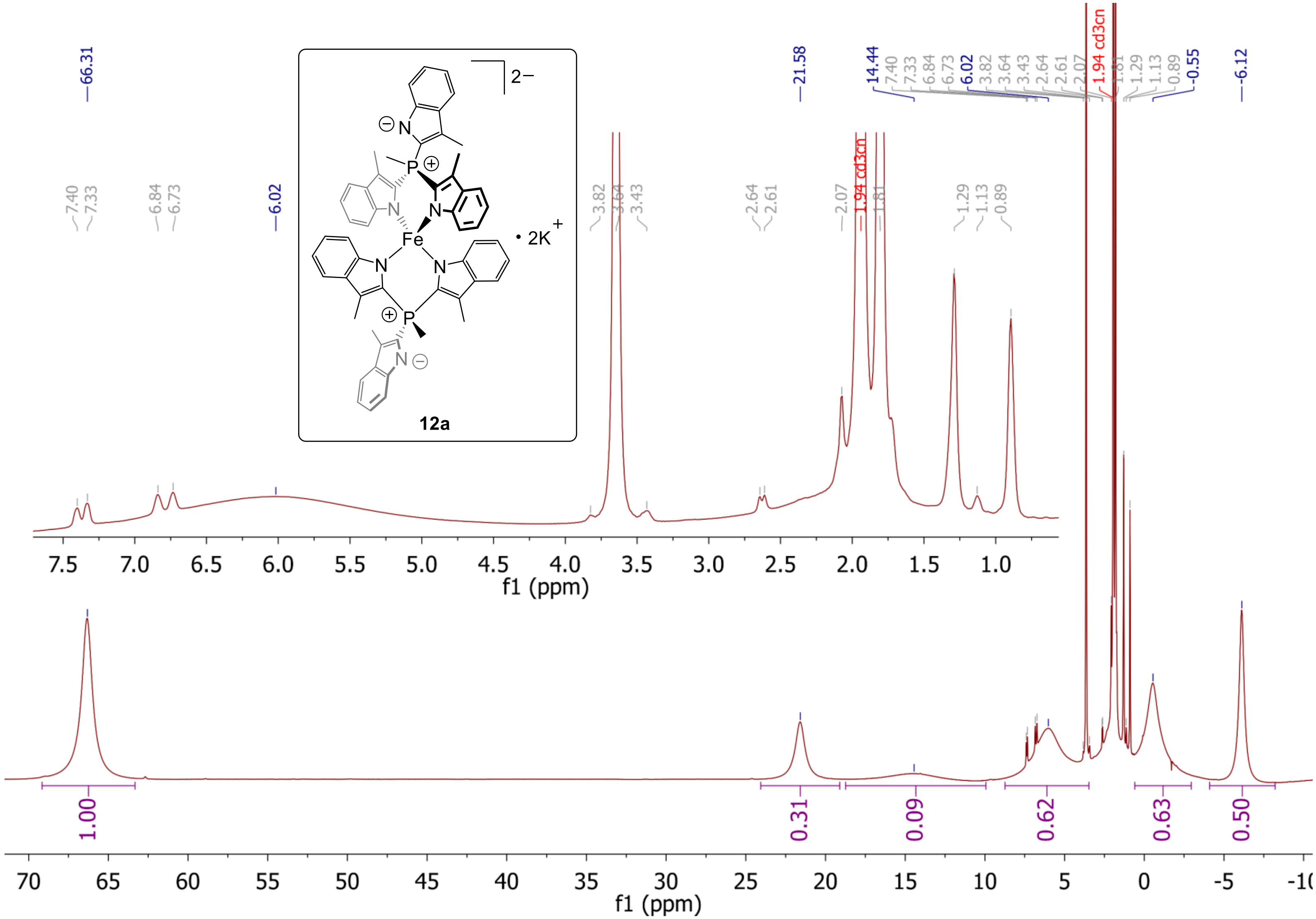

Figure S75. ^{1}H NMR spectrum of complex **12a** in acetonitrile-d_3. Integral intensities were extracted using Mnova[9] peak deconvolution tools. Impurities: 2.07, 2.61, 2.64, 6.73, 6.84, 7.33, 7.40 ppm – traces of the starting TSMPK$_2$ salt (**1**); 0.89 and 1.29 ppm – hexane; 1.81, 3.43, 3.64, 3.82 ppm – THF (main signals and satellites); 1.13 ppm – unknown.

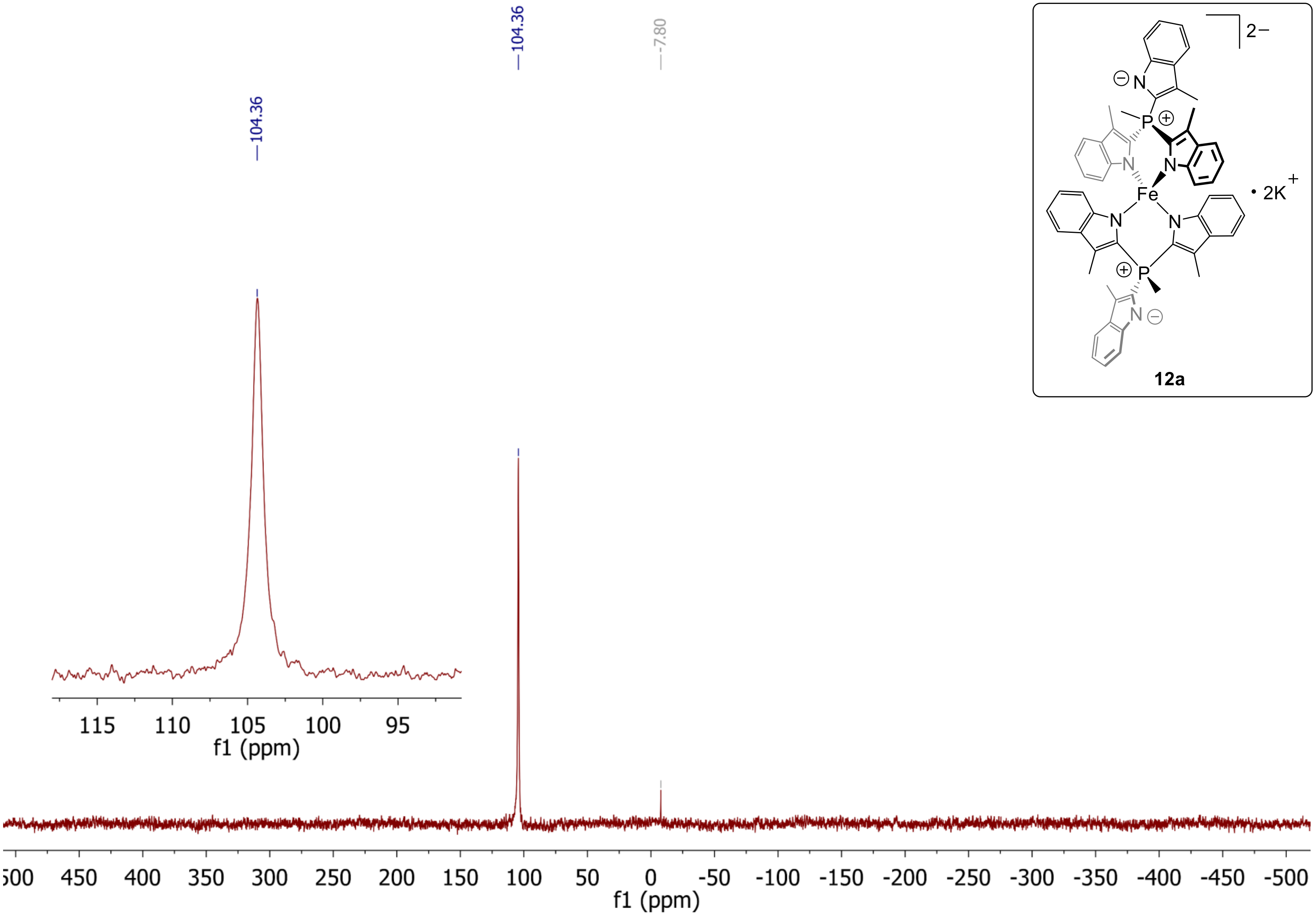

Figure S76. $^{31}P\{^1H\}$ NMR spectrum of complex **12a** in acetonitrile-*d*$_3$. Impurities: -7.80 ppm – traces of the starting TSMPK$_2$ salt (**1**).

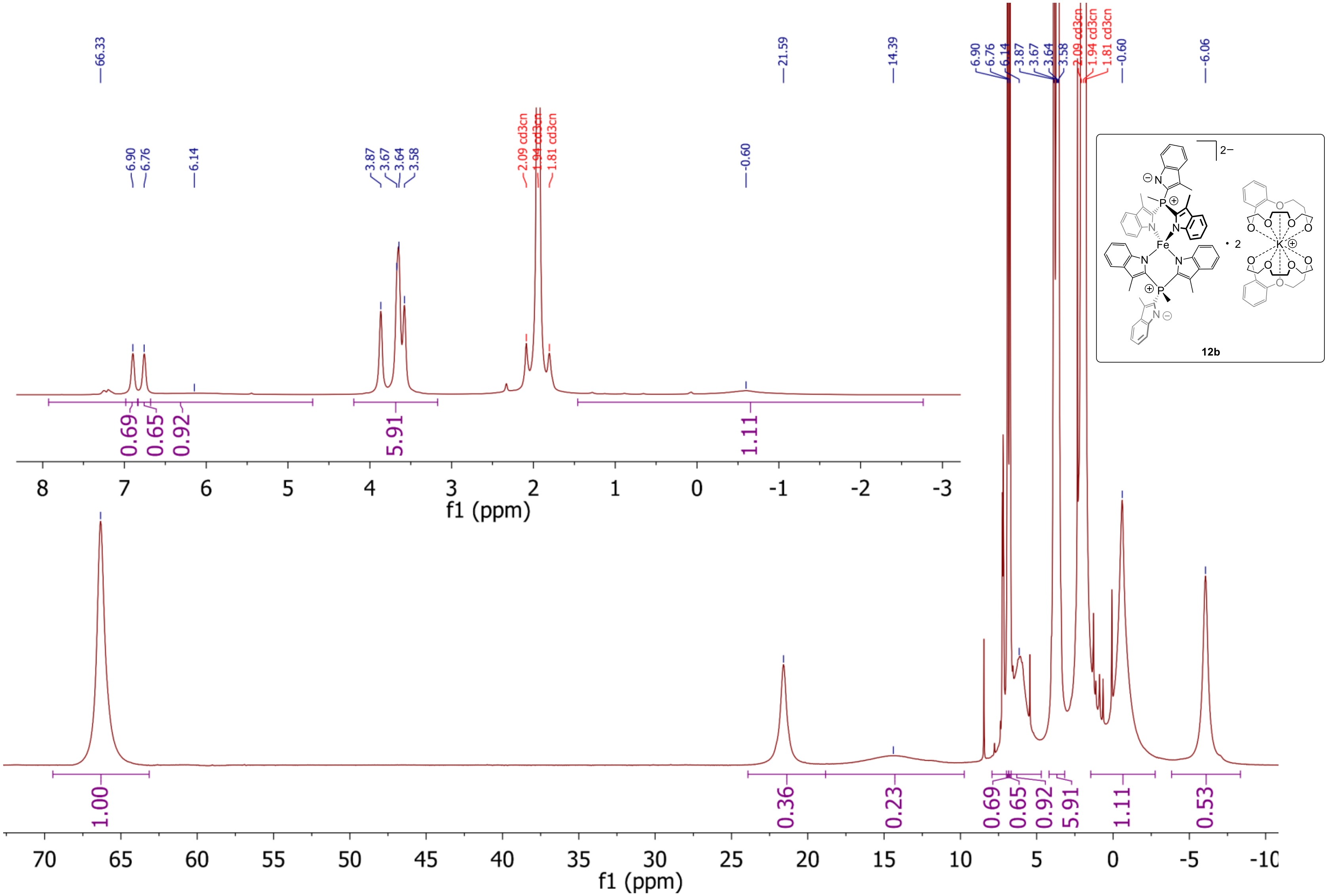

Figure S77. ^{1}H NMR spectrum of complex **12b** in acetonitrile-d_3. Integral intensities were extracted using Mnova[9] peak deconvolution tools. Unlabeled minor peaks are unidentified impurities.

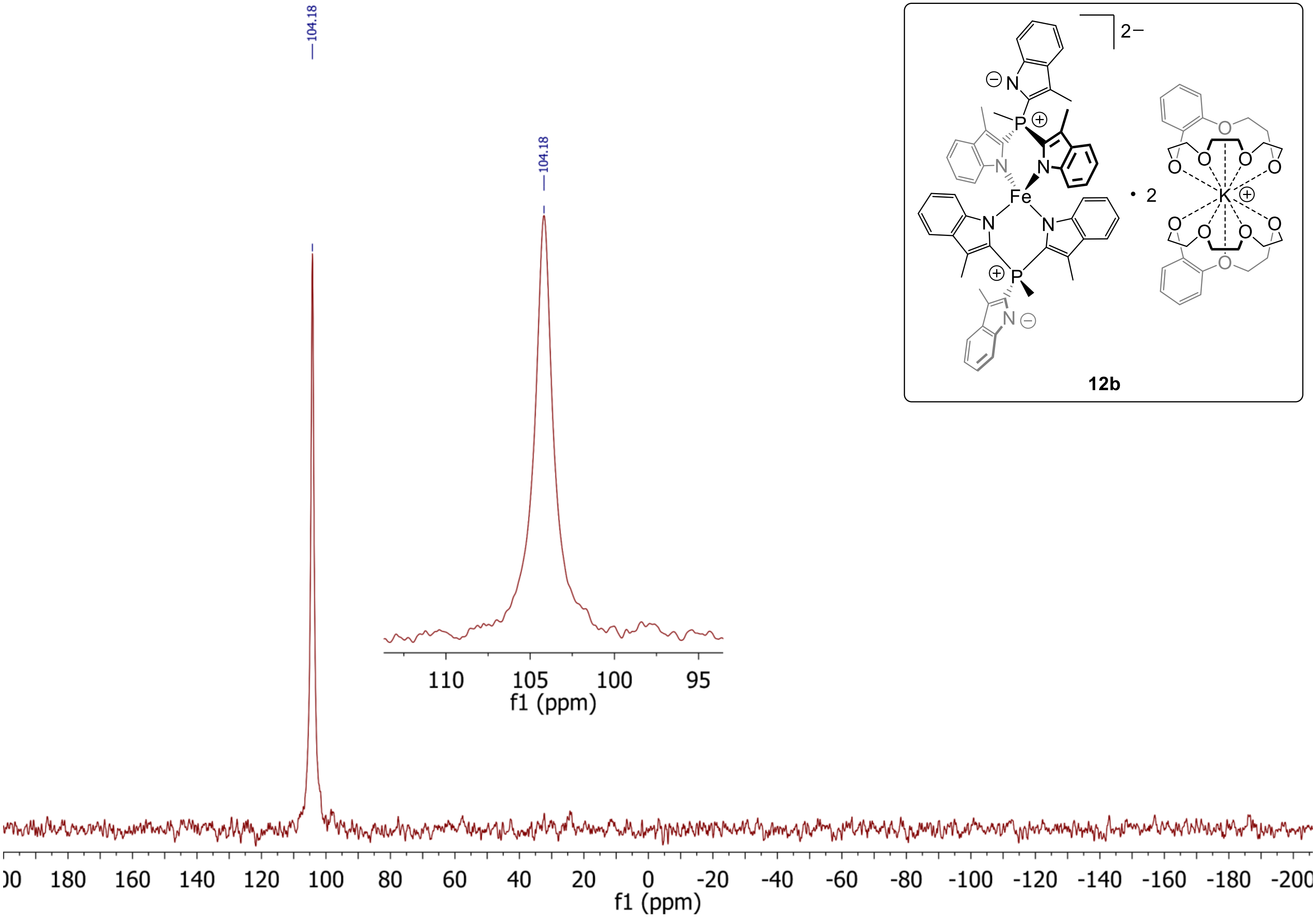

Figure S78. $^{31}P\{^{1}H\}$ NMR spectrum of complex **12b** in acetonitrile-d_3.

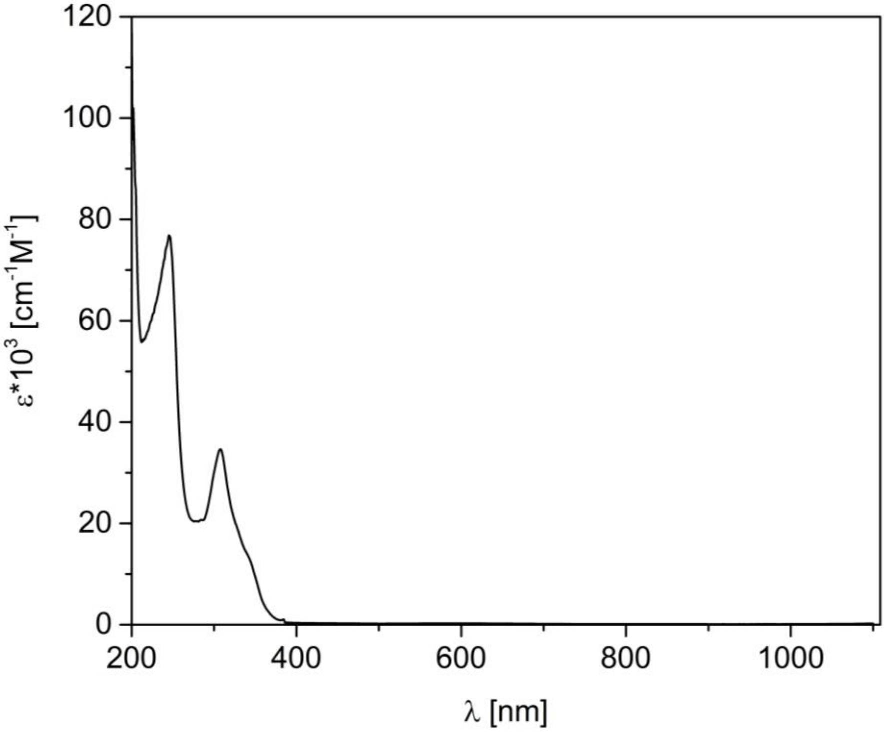

Figure S79. UV-Vis spectrum of compound **12b** in acetonitrile.

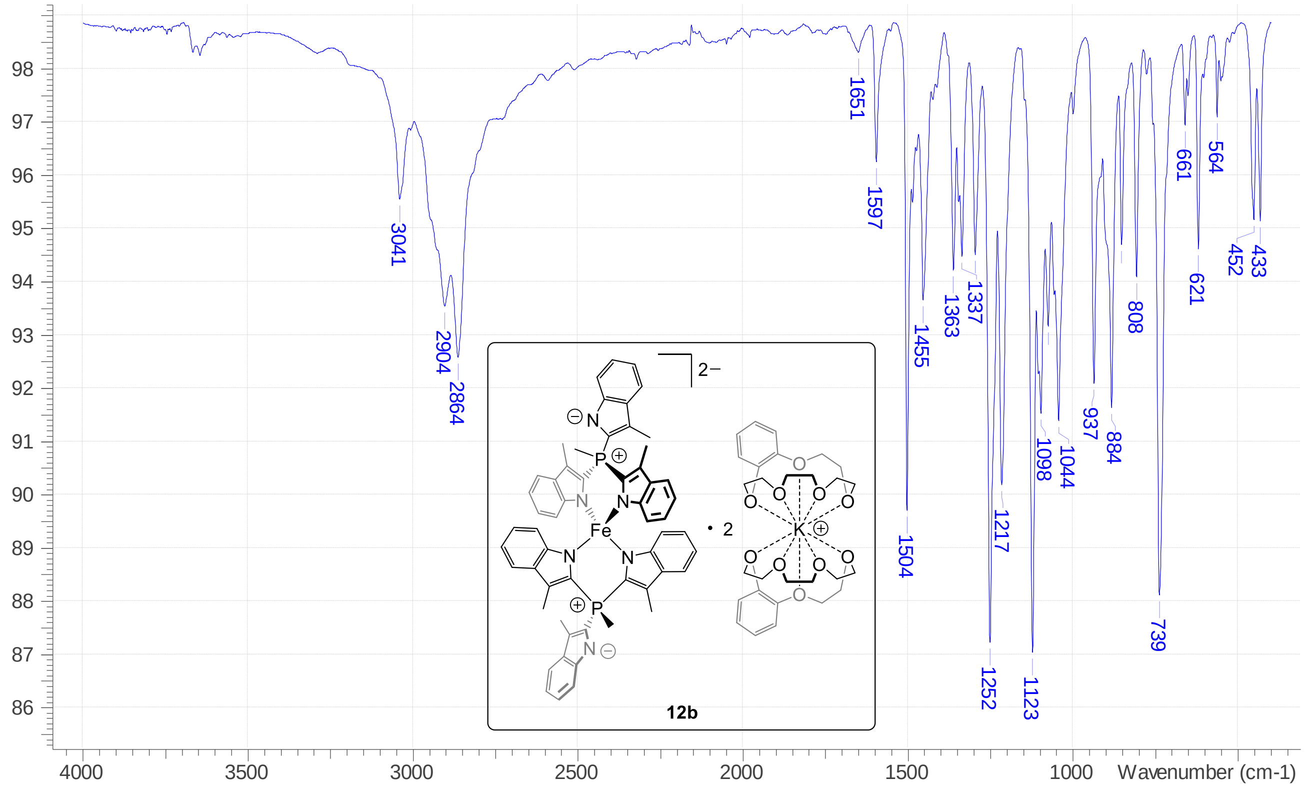

Figure S80. ATR-FTIR (neat) spectrum of compound **12b**.